CANADIAN
THESES

THÈSES
CANADIENNES

WANG, QINGPING

STUDIES OF DISTORTED AMIDES AS ...

ISBN

0-315-73205-9

National Library of Canada
Canadian Theses Service
Ottawa, Canada
K1A 0N4

Bibliothèque nationale du Canada
Service des thèses canadiennes

NOTICE

The quality of this microform is heavily dependent upon the quality of the original thesis submitted for microfilming. Every effort has been made to ensure the highest quality of reproduction possible.

If pages are missing, contact the university which granted the degree.

Some pages may have indistinct print especially if the original pages were typed with a poor typewriter ribbon or if the university sent us an inferior photocopy.

Reproduction in full or in part of this microform is governed by the Canadian Copyright Act, R.S.C. 1970, c. C-30, and subsequent amendments.

AVIS

La qualité de cette microforme dépend grandement de la qualité de la thèse soumise au microfilmage. Nous avons tout fait pour assurer une qualité supérieure de reproduction.

S'il manque des pages, veuillez communiquer avec l'université qui a conféré le grade.

La qualité d'impression de certaines pages peut laisser à désirer, surtout si les pages originales ont été dactylographiées à l'aide d'un ruban usé ou si l'université nous a fait parvenir une photocopie de qualité inférieure.

La reproduction, même partielle, de cette microforme est soumise à la Loi canadienne sur le droit d'auteur, SRC 1970, c. C-30, et ses amendements subséquents.

NL-339 (r. 88/04) c

Canada

UNIVERSITY OF ALBERTA

Studies of Distorted Amides as Models for Activated Peptide N-C(O) Units

BY ©

Qingping Wang

A thesis submitted to the Faculty of Graduate Studies and Research in partial fulfillment of the requirements for the degree of Doctor of Philosophy.

DEPARTMENT OF CHEMISTRY

Edmonton, Alberta

Spring 1992

National Library
of Canada

Bibliothèque nationale
du Canada

Canadian Theses Service

Service des thèses canadiennes

Ottawa, Canada
K1A 0N4

The author has granted an irrevocable non-exclusive licence allowing the National Library of Canada to reproduce, loan, distribute or sell copies of his/her thesis by any means and in any form or format, making this thesis available to interested persons.

The author retains ownership of the copyright in his/her thesis. Neither the thesis nor substantial extracts from it may be printed or otherwise reproduced without his/her permission.

L'auteur a accordé une licence irrévocable et non exclusive permettant à la Bibliothèque nationale du Canada de reproduire, prêter, distribuer ou vendre des copies de sa thèse de quelque manière et sous quelque forme que ce soit pour mettre des exemplaires de cette thèse à la disposition des personnes intéressées.

L'auteur conserve la propriété du droit d'auteur qui protège sa thèse. Ni la thèse ni des extraits substantiels de celle-ci ne doivent être imprimés ou autrement reproduits sans son autorisation.

ISBN 0-315-73205-9

Canadä

UNIVERSITY OF ALBERTA

RELEASE FORM

NAME OF AUTHOR: Qingping Wang

TITLE OF THESIS: Studies of Distorted Amides as Models for Activated Peptide N-C(O) Units

DEGREE: Ph.D.

YEAR THIS DEGREE GRANTED: 1992

Permission is hereby granted to the University of Alberta Library to reproduce single copies of this thesis and to lend or sell such copies for private, scholarly or scientific purposes only.

The author reserves all other publication and other rights, in association with the copyright in the thesis, and except as hereinbefore provided neither the thesis nor any substantial portion thereof may be printed or otherwise reproduced in any material form whatever without the author's prior written permission.

Qingping Wang

Permanent Address:

Nanchang, Jiangxi
P.R. China

Date: October, 1991

UNIVERSITY OF ALBERTA

FACULTY OF GRADUATE STUDIES AND RESEARCH

The undersigned certify that they have read, and recommend to the Faculty of Graduate Studies and Research for acceptance, a thesis entitled Studies of Distorted Amides as Models for Activated Peptide N-C(O) Units submitted by QINGPING WANG in partial fulfillment of the requirements for the degree of Doctor of Philosophy.

RS Brown
Supervisor
R.S. Brown

Dennis Tanner
D.D. Tanner

H.J. Liu

HB Dunford
H.B. Dunford

F.M. Pasutto

External Examiner
O.S. Tee

Date: October, 1991

Dedicated to my family

ABSTRACT

In this work, two distorted model compounds, 3,4-dihydro-2-oxo-propanoquinoline (**III**) and 2,3,4,5-tetrahydro-1,4-propanobenzazepine (**IV**) were synthesized. Studies were made first to determine the structures of **III** and **IV** by x-ray diffraction and then to compare their structures with those of a more distorted amide 2,3,4,5-tetrahydro-2-oxo-1,5-ethanobenzazepine (**II**) and an undistorted amide *p*-bromo-N,2-dimethylacetanilide (**29**). The structural parameters indicate that the distortion manifests itself by lengthening the N-C(O) bond, and a slight shortening of the C=O bond, as well as a twisting about the N-C(O) unit with pyramidalization of the N from sp^2 to sp^3 hybridization. Second, the hydrolysis of distorted amides **III-IV** were studied and the corresponding mechanisms were proposed. Enhanced hydrolytic reactivities were found for distorted amides; ~11 orders of magnitude in the rate constants for acid catalyzed hydrolysis when passing from the undistorted amide N-methyl acetanilide (**31a**) to the most distorted amide 3,4-dihydro-2-oxo-ethanoquinoline (**Ia**); ~7 orders of magnitude in OH^- hydrolysis for the same series. The solvent kinetic isotope effect for hydrolysis of distorted amides **Ia-IV** in both acidic and basic media were measured to further support the mechanism. In order to more fully understand the factors controlling the changes in rate

produced by distortion, the activation parameters for amides **Ia**-**IV** and **31a** in both acid and base were determined. Analysis of these activation parameters implies that the reduction of activation enthalpy ($\Delta H^{\ddagger}$) passing through the series **IV**→**Ia** is probably the major reason of enhanced hydrolytic reactivities. Third, the effect of varying [acetate] in catalyzing the hydrolysis of **II** and **III** in both H_2O and D_2O media was studied and the results were analyzed in terms of a specific acid/general base mechanism in which acetate functions as a general base to deliver L_2O to the protonated amide. Fourth, the position of kinetic methylation (N or O) was studied for amides **III** and **IV**. The results of this study combined with the kinetic pK_a's for amides **Ia**-**IV** were analyzed in terms of a proposed process which involves an equilibrium between $N-H^+$ and $O-H^+$ forms followed by nucleophilic attack of water on the protonated form. Finally, a chiral amide **III** was synthesized and the possible kinetic discrimination of attack by (+) or (-)-ephedrine (**39**,**40**) and (+) or (-)-ψ-ephedrine (**41**,**42**) was studied. This chiral amide **III** does not show any preference with ephedrine enantiomers (**39** vs **40**; or **41** vs [illegible]), but it shows some preference with ephedrine diastereoisomers (**39**,**40** vs **41**,**42**).

Acknowledgments

It is a privilege for the author to sincerely thank Prof. R.S. Brown for his outstanding guidance and assistance during the course of this work. His patience and interest in the preparation of this thesis are really appreciated.

Thanks to my husband, Dr. X. Huang, for his years of helpfulness; supports and the typing of this thesis.

Special thanks are extended to: Dr. A. Bennet for his invaluable helpfulness; J. Keillor and R. Nagorski for proofreading this thesis.

Finally, I would like to thank Alberta Heritage Foundation for Medical Research and the University of Alberta for the financial support.

Table of Contents

page

1. Introduction 1

A. Background 1

B. Studies of Distorted Amides as Models for Activated Peptides 9

C. Objective 30

2. Results 34

A. Syntheses 34

B. Crystal and Molecular Structures 41

C. Kinetics of Hydrolysis 54

D. Effects of Acetate Buffer on the Hydrolysis of **II,III** in H_2O and D_2O 64

E. The Study of the Position of Kinetic Methylation of Distorted Amides **III** and **IV** with MeOTf 70

F. Preparation of the Optically Active Amide **III** 74

G. Kinetic Studies of Chiral Amide **III** with Various Ephedrines 79

3. Discussion 83

A. Molecular Structures of **Ia-IV** and **29** 83

B. Hydrolysis of **Ia-IV** and **31a** 85

C. Activation Parameters for the Hydrolysis of **Ia-IV** and **31a** 90
D. Effect of Acetate on the Hydrolysis Of **II,III** in H_2O and D_2O 92
E. Kinetic Methylation Position (N or O) 96
F. The Attempted Establishment of Kinetic Discrimination of Chirality 99
G. Conclusions 102
4. Experimental 105
A. Syntheses 106
B. Kinetics 115
C. Crystal and Molecular Structures of Amides **III** and **IV** 122
D. Methylation of Amides **III** and **IV** 124
E. Resolution of Chiral Amide **III** 128
5. References 133
Supplementary Material 143

List of Tables

Table		Page
I	pK_a values of conjugated acids of some amides and 2-quinuclidone	13
II	Infrared of $\nu_{C=O}$ 2-quinuclidone and some analogs	13
III	Relative rate constants for hydrolysis of various anilides between pH 12 and 14 at 298 K	16
IV	Activation parameters for the hydrolysis of various amides	16
V	Chemical shifts and coupling constants of the H's in amide **III**	37
VI	Assignment of the ^{1}H-NMR spectrum of amide **IV** on the basis of decoupling experiments	41
VII	Table of selected bond lengths (Å) of the two crystallographically independent molecules of amide **III**	42
VIII	Table of selected interatomic angles of the two crystallographically independent molecules of amide **III**	42
IX	Table of selected bond lengths (Å) of the two crystallographically independent molecules of amide **IV**	46

X Table of selected interatomic angles of the two crystallographically independent molecules of amide **IV** 49

XI Selected structural parameters for anilides **II,III,IV** and **29** 52

XII Calculated structural parameters for amide **30** 54

XIII Pseudo first-order hydrolysis rate constants (k_{hyd}) for **III** extrapolated to [buffer] = 0, $T = 25\ ^0C$, $\mu = 1.0(KCl)$ 56

XIV Pseudo first-order hydrolysis rate constants (k_{hyd}) for amide **IV** at [buffer] = 0, $T = 25\ ^0C$, $\mu = 1.0(KCl)$ 57

XV Rate and dissociation constants for the hydrolysis of amides **Ia-IV** and **31a** in H_2O, $T = 25\ ^0C$, $\mu = 1.0(KCl)$ 61

XVI Solvent kinetic isotope effect for the hydrolysis of amides **Ia-IV** 62

XVII Activation parameters for the hydrolysis of **Ia-IV** and **31a** in aqueous acid and base, $\mu = 1.0(KCl)$ 63

XVIII Acetate buffer catalysis of the hydrolysis of amide **II** in H_2O and D_2O, $T = 25\ ^0C$, $\mu = 1.0(KCl)$ 65

XIX Acetate buffer catalysis of the hydrolysis of amide **III** in H_2O and D_2O, $T = 25\ ^0C$, $\mu = 1.0(KCl)$ 66

XX Rate constant data for the effect of acetate on the hydrolysis of **II** and **III** in H_2O and D_2O, T = 25.0 ^{0}C, μ = 1.0(KCl) 70

XXI Pseudo first-order rate constants for the reaction of chiral amide **III** with (+)-ephedrine and (-)-ephedrine (**39,40**) 80

XXII Pseudo first-order rate constants for the reaction of the chiral amide **III** with (+)-ψ-ephedrine and (-)-ψ-ephedrine (**41,42**) 80

XXIII Rate constant data for the reactions of ephedrine diastereoisomers with chiral amide **III** 81

XXIV ^{18}O-exchange results for amide **31a** 89

XXV Heats of neutralization at 25 ^{0}C in DMSO for various ephedrines and mandelic acid 101

XXVI Experimental Details of Data Collection and Structure Refinement of Amides **III, IV** 122

XXVII Conditions for the attempted separation of various compounds using a chiral HPLC column 130

List of Figures

Figure		Page
1	Schematic representation of the induction of strain or distortion in the substrate to bring it part way along the reaction coordinate toward the transition state.	2
2	The induced-fit mechanism, in which binding of substrate causes a change in the conformation of the enzyme so that the groups H,A,S in the active site, which are required for catalysis, are moved closer to the substrate and each other in order to effect catalysis.	3
3	Wrong-way binding of anilides to chymotrypsin.	4
4	Strain theory of the distorted substrate.	6
5	Binding constants for substrates and lactone transition state analogs with lysozyme.	8
6	pH-rate profile for the hydrolysis of **Ia**.	18
7	pH-rate profile for the hydrolysis of **I-II**.	21
8	Qualitative representation of the distortion of bicyclic anilides in terms of twist (ϕ) and tilt (θ) angles.	24

9a Perspective views of one of the two crystallographically independent molecules of **III** in the unit cell. 43

9b Perspective views of one of the two crystallographically independent molecules of **III** in the unit cell. 44

10 Stereoview of the unit cell of **III**. 45

11a Perspective views of one of the two crystallographically independent molecules of **IV** in the unit cell. 47

11b Perspective views of one of the two crystallographically independent molecules of **IV** in the unit cell. 48

12 Perspective views of **29**. 50

13 pH-rate profile for the hydrolysis of **I-IV** and **31a**. 55

14 Plots of log k_{OAc} (apparent) vs pL for the hydrolysis of **II** (Δ) and **III** (O) in H_2O and D_2O media T = 25 °C, $\mu = 1.0$(KCl), closed symbols, D_2O. 67

15 Plots of log k_{hyd} vs pL for the hydrolysis of **II** (Δ) and **III** (O) derived from the intercepts of plots of k_{hyd} vs $[\text{acetate}]_{total}$ at various pL values in H_2O and D_2O media T = 25 °C, $\mu = 1.0$(KCl), closed symbols, D_2O. 68

16 Kinetic pKa of distorted amides. 98

1. INTRODUCTION

A. Background

All living cells in the world contain peptides. A peptide bond (N-C=O) is the basic component for linking amino acids together to form proteins and enzymes. Therefore, the high stability of the peptide bond (or amide linkage) toward hydrolysis is of crucial importance to biological systems. However, nature has endowed living systems with a series of hydrolytic enzymes (peptidases) which are capable of cleaving the N-C=O linkage extremely rapidly. The digestive enzymes pepsin and trypsin are of this type. Trypsin, from beef pancreas,[1] is a mammalian serine protease with catalytic specificity for basic amino acid substrates, and is kinetically very reactive around pH 7.8.[2]

Normal amides are hydrolyzed very slowly even under harsh conditions and the question of how enzymes accelerate the hydrolysis of peptides has been the subject of many studies.[3,4]

Four mechanisms by which an enzyme might be expected to bring about a rate acceleration have been proposed:[5] 1). approximation or binding together of the reactants; 2). covalent catalysis; 3). general acid-base catalysis and; 4). the introduction of distortion or strain in the substrate, the enzyme, or both.

Although there is no doubt that approximation, covalent catalysis, and general acid-base catalysis are involved in many enzymatic reactions, the available estimates of the rate accelerations to be expected from these factors make it doubtful that they can account for all of the specific rate enhancements that are brought about by enzymes.[5] One is, therefore, led to search for other factors such as the introduction of strain in the substrate, the enzyme, or both as playing a significant role in bringing about the observed specific rate acceleration.

The introduction of strain in the enzyme-substrate complex involves overcoming of part of the energetic and entropic barrier to the reaction by bringing the substrate part of the way along the reaction coordinate toward the transition state thereby decreasing the observed free energy of activation (see Figure 1).

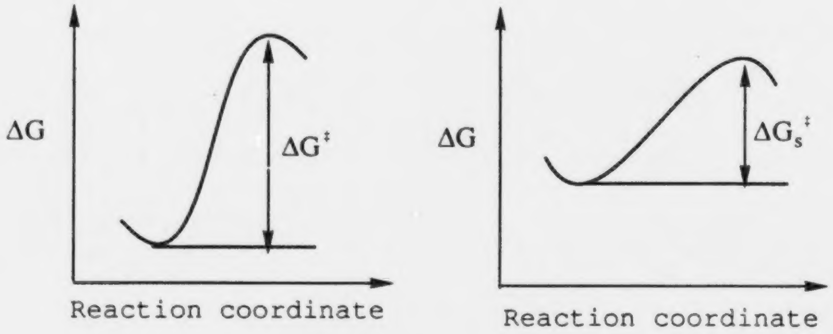

$\Delta G^{\ddagger}$: normal condition $\Delta G_s^{\ddagger}$: after introduced strain

Figure 1. Schematic representation of the induction of strain or distortion in the substrate to bring it part way along the reaction coordinate toward the transition state.

There are three possible explanations for this kind of behavior: induced fit; nonproductive binding; and rate acceleration by the induction of strain.[5]

1) The induced-fit theory:

According to the induced-fit theory as proposed by Koshland,[6] the catalytic groups at the active site of the free enzyme are not in the optimum position where they can exert effective catalytic activity until a good substrate is bound to the enzyme. Then the binding forces between the enzyme and the substrate are utilized to force the enzyme into an energetically less favorable, but catalytically active conformation. This is schematically presented in Figure 2, in which H,S and A represent the active site constituents of the enzyme.

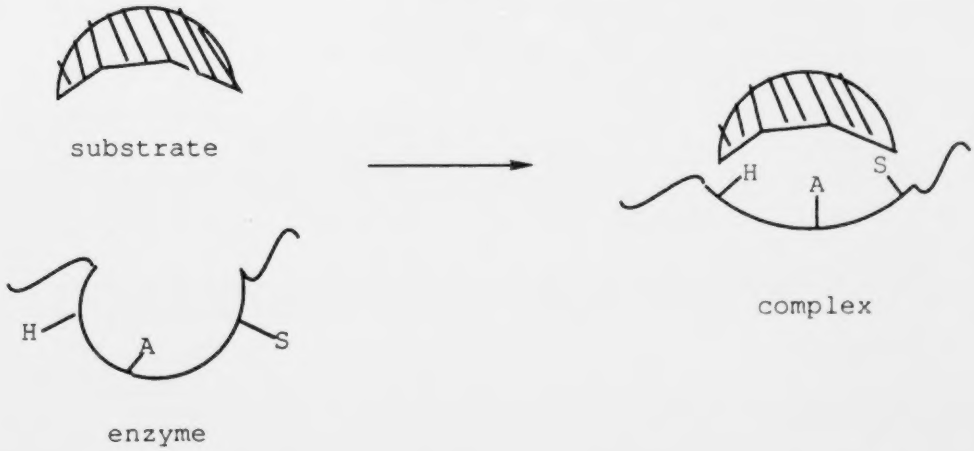

Figure 2. The induced-fit mechanism, in which binding of substrate causes a change in the conformation of the enzyme so that the groups H,A,S in the active site, which are required for catalysis, are moved closer to the substrate and each other in order to effect catalysis.

2). The nonproductive-binding hypothesis:[7]

According to the nonproductive-binding hypothesis, it is the substrate rather than the enzyme that is in a catalytically inactive position in the case of a poor substrate. Suppose that a good specific substrate has several binding sites which are complementary to sites on the enzyme, so that the substrate can only bind in one active position. A poor substrate which lacks one or more of these binding groups or has incorrectly located groups may bind incorrectly to give an inactive enzyme-substrate complex. An example of wrong way binding of anilides to chymotrypsin is shown in Figure 3.[3]

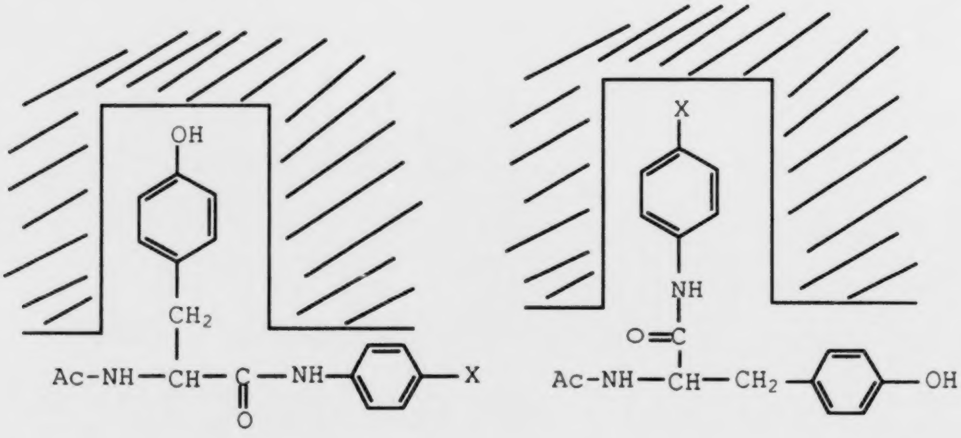

productive binding nonproductive binding

Figure 3. Wrong way binding of anilides to chymotrypsin.

3). The strain or distortion theory:

According to the strain or distortion theory, the binding forces between the substrate and the enzyme are directly utilized to induce strain or distortion which facilitates the reaction. If the enzyme is rigid, the substrate is subjected to distortion in such a way that its structure must approach that of the transition state of the reaction in order that it may undergo binding. The binding forces provide the driving force which allows the substrate to bind in the distorted configuration. Figure 4 shows an example of this kind of situation. If the enzyme is conformationally mobile, but the substrate is relatively rigid, the tendency of the distorted enzyme to return to its undeformed state facilitates the reaction by simply helping to pull apart the bonds of the substrate.

It is apparent that it is not always possible to draw a sharp line between these theories. However, the strain hypothesis[5] seems to us an attractive one in that a share of the exothermicity of substrate binding is utilized in a productive way by the enzyme to destabilize and thereby activate the scissile substrate bond as the transition state for the acyl transfer reaction is approached. It is important to realize that if the induction of strain is an important component of enzyme mediated reactions, it need not to be relegated to peptide hydrolysis and may be applied to any reaction in which bonds are made or broken.

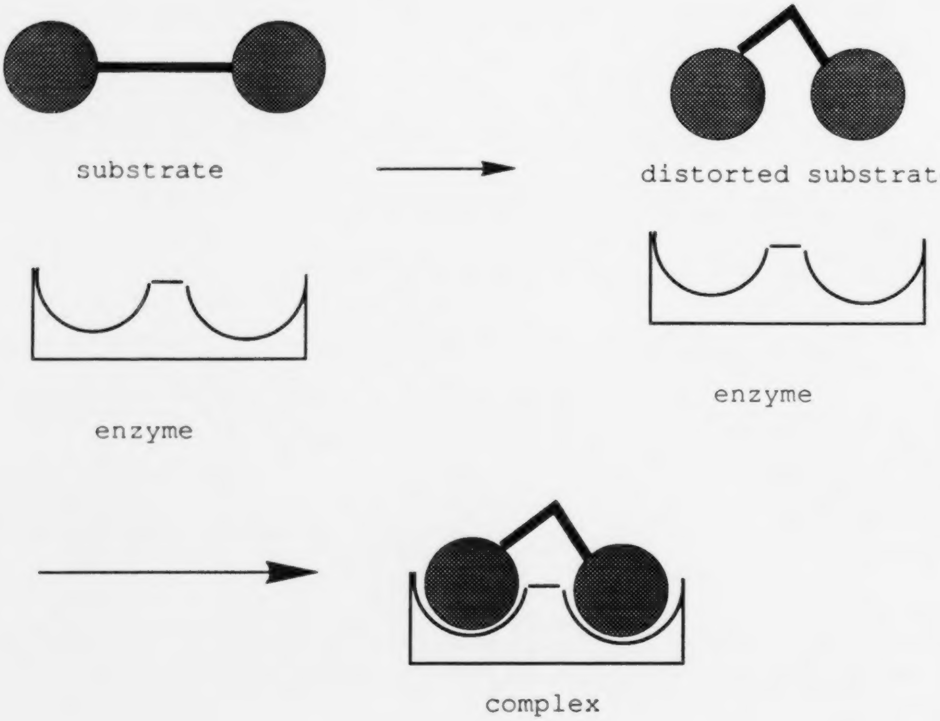

Figure 4. Strain theory of the distorted substrate.

Generally, the strain hypothesis or "Circe effect"[8a] proposed by Jencks[8b] involves a geometric destabilization such as a deformation of bond angles, bond distances and so on to approximate the transition state for the reaction and induce a lower energy of activation. The strain hypothesis suggests that the observed binding energy for a ligand which is distorted on binding, is less than for a ligand that can bind in the same conformation without distortion, the difference being the energy required to cause the distortion.

From the free energy equation (equation 1), an analog that resembles S*, the distorted substrate will be able to

$$\begin{tikzcd} E + S \arrow[r, shift left, "\Delta G_{obs}"] \arrow[d, "\Delta G_s"'] & ES^{\star} \arrow[l, shift left] \arrow[dl, shift left] \\ S^{\star} \arrow[ur, shift left, "\Delta G^{\star}"'] & \end{tikzcd}$$ (1)

$$\Delta G_{obs} = \Delta G_s + \Delta G^{\star}$$

bind to the enzyme without undergoing geometric destabilization. Therefore its binding energy will be more favorable than that of substrate by the amount ΔG_s. The main question is how much energy can be involved in the distortion? Some experiments[9-12] were done to calculate the amount of favorable free energy ΔG_s. Lienhard and coworkers[13,14] have shown that the binding of a lactone tetrasaccharide analog of the substrate to the ABCD subsites of lysozyme is tighter by a factor of approximately 6×10^3 compared to the substrate, corresponding to a free-energy difference of 5.2 kcal/mol. (Figure 5). The C1 atom of the lactone exists in the planar sp^2 structure, similar to the oxocarbonium ion-like transition state, so that the conformation of the lactone ring is expected to be similar to the high energy conformation of the ring in the transition state. Evidently, the oligosaccharide containing this ring structure binds more tightly than does the substrate with a tetrahedral sp^3 C1 atom.

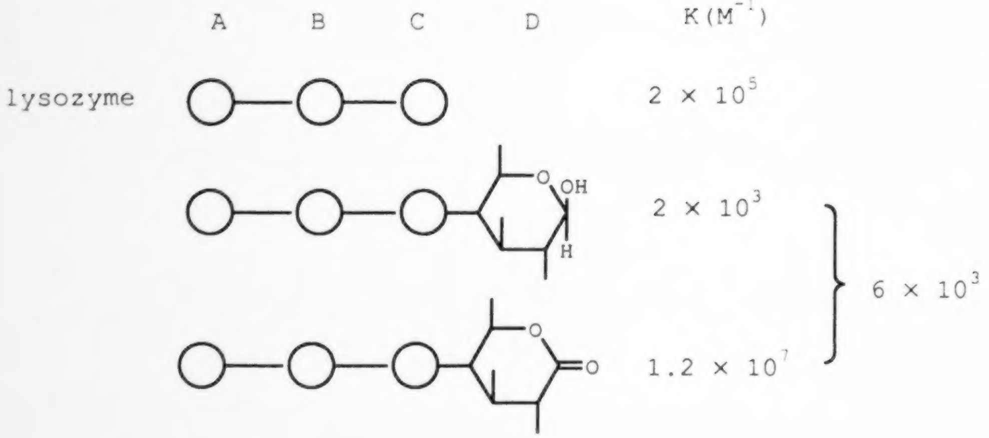

Figure 5. Binding constants for substrates and lactone transition state analogs with lysozyme.

There are many experimental observations which can be satisfactorily explained in terms of the strain theory, although none of them constitute unequivocal proof of the theory. One of the most interesting is Hofstee's finding[15] that the maximal hydrolysis rate of substituted phenyl esters, $CH_3(CH_2)_nCOOC_6H_4COO^-$, by liver esterase and chymotrypsin, increases with increasing chain length of the acyl portion. Within certain limits, this occurs with relatively little change in the value of the Michaelis constant. Thus, a lengthening of the hydrocarbon chain, which has little effect on the chemical reactivity of the esters and would be expected to give only a tighter binding, results in an increase in the rate of attack at the acyl group in the enzymatic reaction. This suggests that the energy of interaction of the hydrocarbon chain with the protein is utilized to activate the acyl position in the enzyme-substrate complex.

Pearl proposed[16] that torsional distortion of the scissile peptide bond in the bound complex decreases the delocalization of the peptide nitrogen lone-pair, making the carbonyl carbon more susceptible to nucleophilic attack and the nitrogen a better proton acceptor. These factors will lower the barrier to formation of the rate limiting transition state and thus promote hydrolysis. Based on this kind of hypothesis, we believed that distorted amides are good models for activated peptides since the molecular structure induces the strain, rather than binding of the peptide by the enzyme.

B. Studies of Distorted Amides as Models for Activated Peptides

Certainly, in order to understand the mechanism of enzyme-catalyzed hydrolysis of peptides, one would first like to understand the mechanism of the nonenzymatic reaction and the means by which this reaction can be accelerated.

The mechanisms of hydrolysis of amides under drastic conditions such as high temperature, low or high pH are well documented.[17] Some species such as **1**[18] or **2**[19] were reported to be subject to hydrolysis under milder conditions approaching physiological ones. It is obvious that those species are activated electronically both toward nucleophilic attack and expulsion of the leaving amino group.

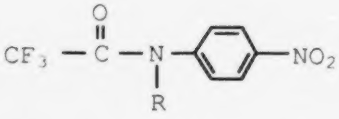

1

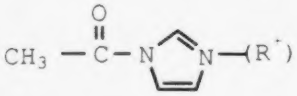

2

The first distorted amide which was noted to be very prone to hydrolysis was penicillin **3**, which contains the

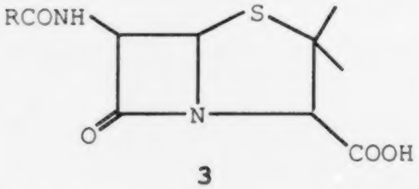

3

β-lactam structure. Holley found a rate increase between 10^3 and 10^6 toward alkaline hydrolysis for β-lactam in **3** relative to N-methyl-β-propiolactam and a normal amide such as acetanilide.[20] He suggested that steric inhibition of amide resonance is the reason for the enhanced rate of hydrolysis.

The biological activity of benzylpenicillin and Δ^3-cephalosporins has been linked to the configuration of the 4-membered ring by crystallographic studies. Sweet and Dahl[21] used single-crystal x-ray diffraction to investigate the structures of penicillins **3**, Δ^3-cephalosporins **4**, Δ^2-cephalosporins **5**. The most striking structural feature is the enhanced pyramidal character of the β-lactam nitrogen

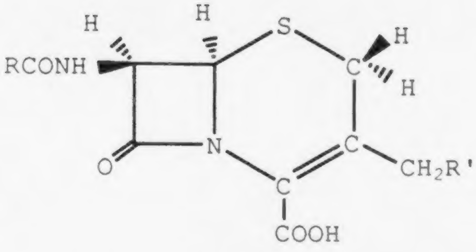

4

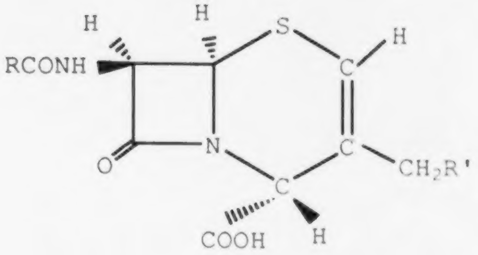

5

atom in **3** and **4** in contrast to the nearly planar lactam nitrogen in the inactive form **5**. The ease of base hydrolysis of the lactam amide bond in these antibiotics correlates with these distorted structures. Sweet's and Dahl's interpretation[21] was that the lability was due to a decrease of the amidic resonance in the antibiotic β-lactam relative to that in free β-lactams and in the biologically inactive Δ^2-cephalosporins.

This kind of structural property that influences the hydrolytic reactivities was also shown by Earle et al[22] for β-lactams having fused rings. They prepared a number of compounds of type **6** and investigated the effect of the size

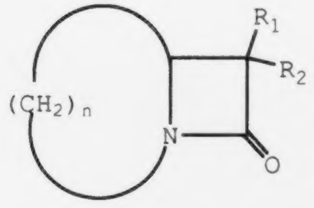

6

	n	R_1	R_2
a	3	H	Ph
b	4	H	H
c	4	H	Ph
d	4	H	$m\text{-}O_2NC_6H_4$
e	4	H	Me
f	4	Me	Me
g	4	Me	Et
h	4	Et	Et
i	5	H	Ph

of a fused homocyclic ring on the rate of hydrolysis of β-lactams. The results showed that in the case of **6a** which has a five-membered homocyclic ring fused to the 1,4-position of the β-lactam ring, there was a very large increase in the hydrolysis rate under acidic conditions relative to **6c** and **6f**, which had β-lactams with fused six-membered rings.

Pracejus and his coworkers^{23} synthesized and studied the mesomerism of a series of bicyclic amides **7** and **8**, and

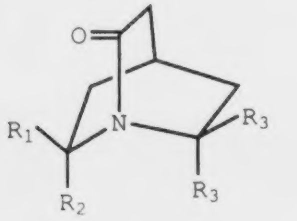

7

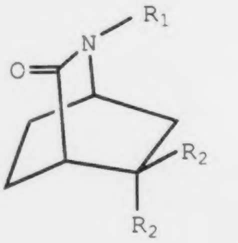

8

7a $R_1=R_2=H$; $R_3=CH_3$
b $R_1=R_3=CH_3$; $R_2=H$
c $R_1=H$; $R_2=R_3=CH_3$
d $R_1=R_2=R_3=H$

8a $R_1=R_2=H$
b $R_1=CH_3$; $R_2=H$
c $R_1=R_2=CH_3$

found that the amides **7a-d** had higher basicities than those of normal amides, and infrared $\nu_{C=O}$ shifted to higher wavenumbers. Listed in Table I and Table II are the pK_a data and $\nu_{C=O}$ data respectively. They also studied the hydrolysis and ethanolysis of compound **7a**-HCl. From the kinetics of hydrolysis and ethanolysis of 0.03-0.06 M *l*-(+)-**7a**-HCl at (20±0.1)^{0}C in CO_2-free water or absolute ethanol, it was found that **7a** followed a pseudo-first order kinetic process

Table I. pK_a values of conjugated acids of some amides and 2-quinuclidone[a]

Compounds	pK_a	temperature
dimethylformamide	0.0[b]	—
N,N-dimethylacetamide	0.1[c]	—
N-acetylpiperidine	0.4[c]	—
8a	0.5	22 °C
8b	1.0	22 °C
7a	5.33	21 °C
7b	5.60	22 °C
7c	5.60	22 °C
quinuclidine	10.65[d]	22 °C
exo-2,2,6-trimethyl-quinuclidine	11.3	22 °C

a. Reference 23b.
b. Huisgen, R.; Brade, H. *Chem. Ber.* **1957**, *90*, 1432.
c. Adelman, R.L. *J. Org. Chem.* **1964**, *29*, 1837.
d. Prelog, V. *Rec. Trav. Chim.* **1952**, *71*, 1171.

Table II. Infrared $\nu_{C=O}$ of 2-quinuclidone and some analogs[a]

Compound	$\nu_{C=O}$ (cm^{-1})
N,N-dimethylacetamide	1674 (iso-octane)[b]
N-methyl-2-piperidine	1658 (CCl_4)
bicyclo[2,2,2]-octan-2-one	1731 (CCl_4)[c]
cyclohexanone	1715 (CCl_4)[d]
8a	1695 (CCl_4)
8b	1678 (CCl_4)
8c	1678 (CCl_4)
7a	1762 (CCl_4)
7a-HCl	1799 (KBr)
7b	1756 (CCl_4)
7b-HCl	1818 ($CHCl_3$)
7c	1764 (CCl_4)
7d	~1750 (CCl_4)

a. Reference 23b.
b. Alelman, R.L. *J. Org. Chem.* **1964**, *29*, 1837.
c. Zbinden, R.; Hall, H.K.Jr. *J. Am. Chem. Soc.* **1960**, *82*, 1215.
d. Hall, H.K.Jr.; Zbinden, R. *J. Am. Chem. Soc.* **1958**, *80*, 6428.

and had a half life of 16±1 min for hydrolysis and about 12 hours for ethanolysis.[23a]

Albertson[24] synthesized distorted amide **9**, but he did not study its kinetic properties.

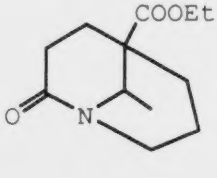

9

In pioneering studies, Blackburn and Plackett[25] have suggested that both bond-angle strain at the carbonyl group and torsional rotation of the amide linkage in the ground state of reactant should exert a profound effect on the rate and the mechanism of its hydrolysis. They synthesized β-lactam **10**, γ-lactam **11**, δ-lactam **12** and *p*-nitro-N-methylacetanilide **13**.[25a]

The kinetic studies of compound **10** with different substituents R on the benzene ring showed that all hydrolyzed in alkaline solution by a mechanism that was first order in $[OH^-]$ at 298 K, $\mu = 1.0$(KCl), between pH 12 and 14: the most reactive **10a**, shows first-order response to $[OH^-]$ to at least pH 10. There was a clear dependence of reactivity on substitution and an excellent linear correlation was found between log k and the Hammett substituent constant σ^- with a slope $\rho = 1.225 \pm 0.013$. They

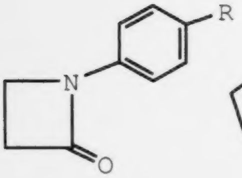

10a $R=NO_2$
b R=H
c R=OMe
d R=Me
e R=Br

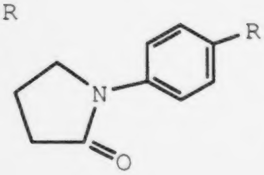

11a $R=NO_2$
b R=H

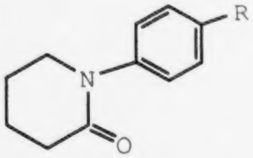

12a $R=NO_2$
b R=H

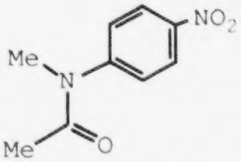

13

concluded that the rate determining step for hydrolysis of β-lactams was hydroxide attack on these amides with the transition state shown in **14**.[25a]

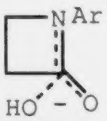

14

Since the same rate law (see below) describes the

$$-d[A]/dt = k_1[OH^-][A]$$

kinetic behavior of all compounds (**10-13**) investigated, a direct comparison of the second order rate constants is valid and shows (Table III) a steady increase in reactivity with ring constraint for *p*-nitroanilides **13, 12a, 11a**, and **10a**.

Table III. Relative rate constants for hydrolysis of various anilides between pH 12 and 14 at 298 K[a]

Compound	k_{rel}	
	N-phenyl	N-p-nitrophenyl
β-lactam (**10a**)	60	2200
γ-lactam (**11a**)	0.1	280
δ-lactam (**12a**)	1.0	30
N-methyl-acetanilide (**13**)	—	20
acetanilide	2.0[b]	110[c]

a.Reference 25a.
b.Bender, M.L.; Thomas, R.J. *J. Am. Chem. Soc.* **1961**, *83*, 4183.
c.Pollack, R.M.; Bender, M.L. *J. Am. Chem. Soc.* **1970**, *92*, 7190 and reference therein.

Crystallographic[26a] and spectroscopic[26b] evidence shows that the N-aryl-β-lactams are effectively planar. Blackburn interpreted the 100-fold acceleration in attack of hydroxide on **10a** over **13** to arise from the acute modification of bond angles in the cyclic transition state. Also the activation

Table IV. Activation parameters for the hydrolysis of various amides[a,b,c]

	$\Delta G^\ddagger$ (298 K) kJ/mol	$\Delta H^\ddagger$ kJ/mol	$\Delta S^\ddagger$ $J\cdot mol^{-1}K^{-1}$
N-methyl-*p* nitroacetanilide (**13**)	92.2±0.8	66.0±6.1	-88.1±5.8
1-*p*-nitrophenyl-azetidine-2-one (**10a**)	80.5±0.5	55.6±5.0	-80.2±5.9

a. Reference 25a.
b. Rate data were collected at temperatures between 298 and 313K, at c = 0.05-1.0 M of $[OH^-]$.
c. The activation parameters for hydrolysis are computed by linear regression analysis of a plot of log k_1 against 1/T.

parameters (Table IV) show that the enhanced reactivity is associated with a decrease in the enthalpy of activation for compound **10a**.

In order to prove that the acceleration of nucleophilic attack on amides that are activated by angular deformation was likely to be even greater for weaker nucleophiles, Blackburn and Plackett studied the aminolysis of compounds **10a** and **11a**.[25b] The results showed that the overall rate of reaction of piperidine with **10a** was at least 10^3 times greater than that with the corresponding γ-lactam **11a**.

Later, Blackburn and coworkers[27] synthesized a bicyclic amide **Ia** having a bridgehead nitrogen and examined its

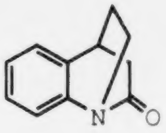

Ia

properties in order to provide an experimental basis for discussion of the effects of torsional strain in amides. The pH-rate profile of amide **Ia** is shown in Figure 6. Analysis of this profile provided rate constants for specific-acid , specific-base, and uncatalyzed terms according to rate equation 2. Thus the specific acid-catalyzed hydrolysis, with an apparent rate constants $k_{H_3O^+}$ = 1.7×10^4 $M^{-1}s^{-1}$, is

$$k_{obs} = 1.7 \times 10^4[H^+] + 7 \times 10^{-4} + 114[OH^-] \qquad (2)$$

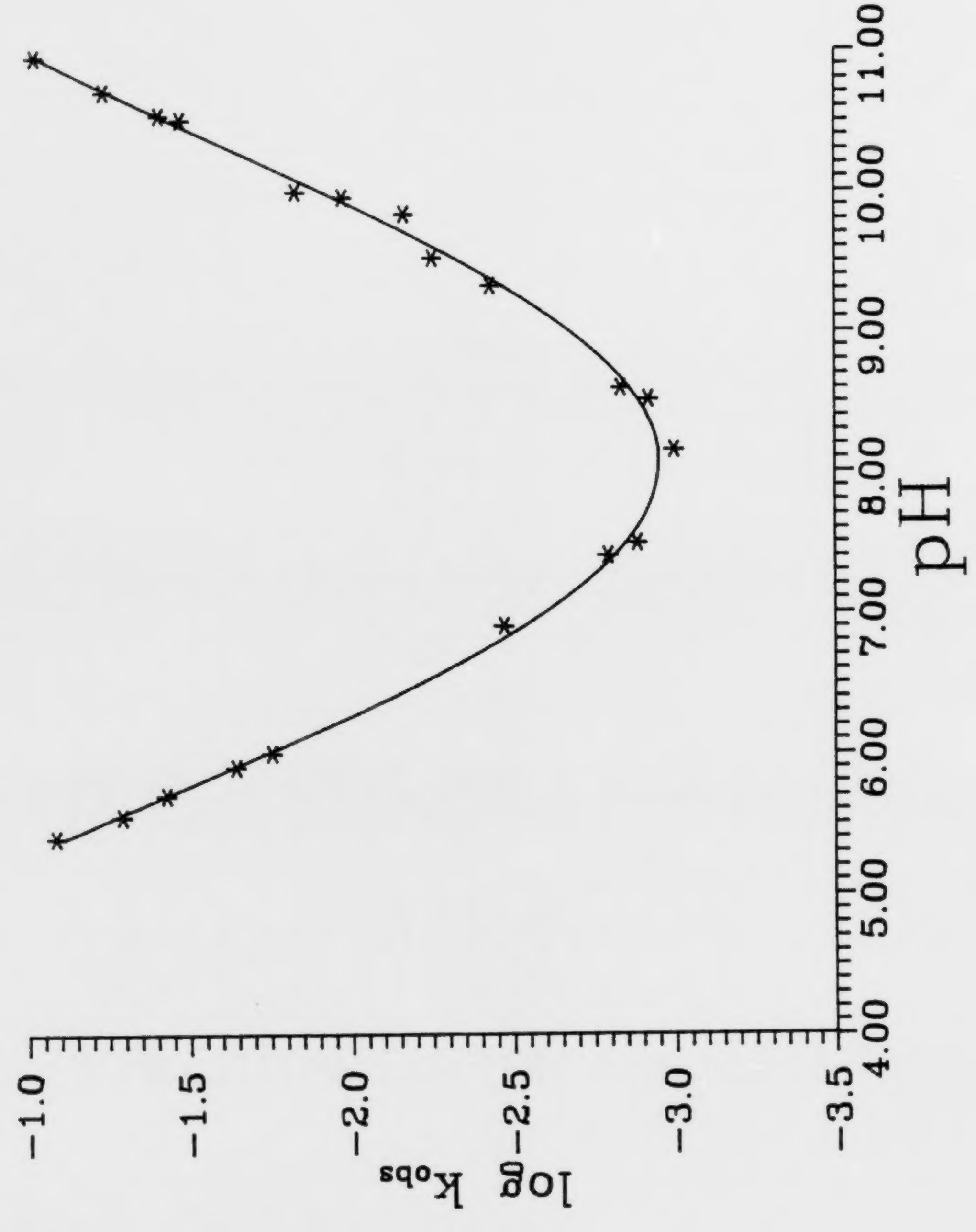

Figure 6. pH-Rate profile for the hydrolysis of **Ia**.

clearly attributable to the attack of a water molecule on the protonated substrate. Also Blackburn and his coworkers estimated the pK_a of **Ia** at ~ 2.5.[27] Therefore the rate constant for water attack on the fully protonated form of **Ia** should be close to 10^2 s^{-1}. The alkaline hydrolysis rate constant, 114 $M^{-1}s^{-1}$, is remarkably high for an amide and is almost ~ 10^7 times faster than that of **12b**, which corresponds to a reduction in activation free energy of 10 kcal/mol.

Blackburn and his coworkers suggested[27] that in the case of alkaline hydrolysis of **Ia**, the rate-determining step is breakdown of the tetrahedral intermediate in a base catalyzed bimolecular process which is most probably well-described by the zwitterionic species (**15a**). Acid catalyzed hydrolysis of **Ia** was suggested to involve N-protonation associated with a transition state (**15b**).[27]

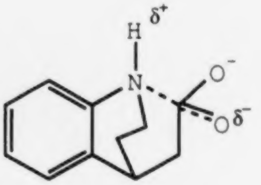

15a

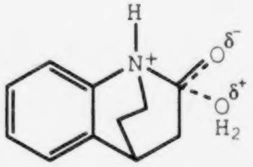

15b

Finally, they suggested that this kind of rate enhancement was due to the torsional inhibition of resonance and a more or less isolated carbonyl group.

Effects of ring substituents on the hydrolysis were not studied nor were ^{18}O-labelling studies done which might probe the reversible formation of tetrahedral intermediates.

Therefore several questions remained with respect to the course of hydrolysis of this type of strained amide. In 1986, our group became interested in studying distorted amides.[28] In order to delineate the response of the various kinetic parameters to substituent effects and determine how a change in N-C=O dihedral angle influences the hydrolysis, Somayaji and Brown[28] synthesized a series of substituted benzoquinuclidones **Ia-d** and the next higher homologue 2,3,4,5-tetrahydro-2-oxo-1,5-ethanobenzazepine **II** and studied their kinetic properties. The results are summarized as follows:

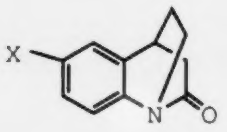

Ia X=H
b X=CH_3
c X=OCH_3
d X=Cl

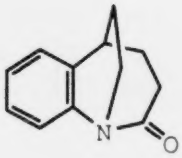

II

a). pH-rate profile for hydrolysis[28]

The buffer-independent pH-rate profiles for hydrolysis of **Ia-d**, and **II** are shown in Figure 7 (with —— —— for **I**; --- for **II**). Since the profiles for amides **Ib-d** were nearly

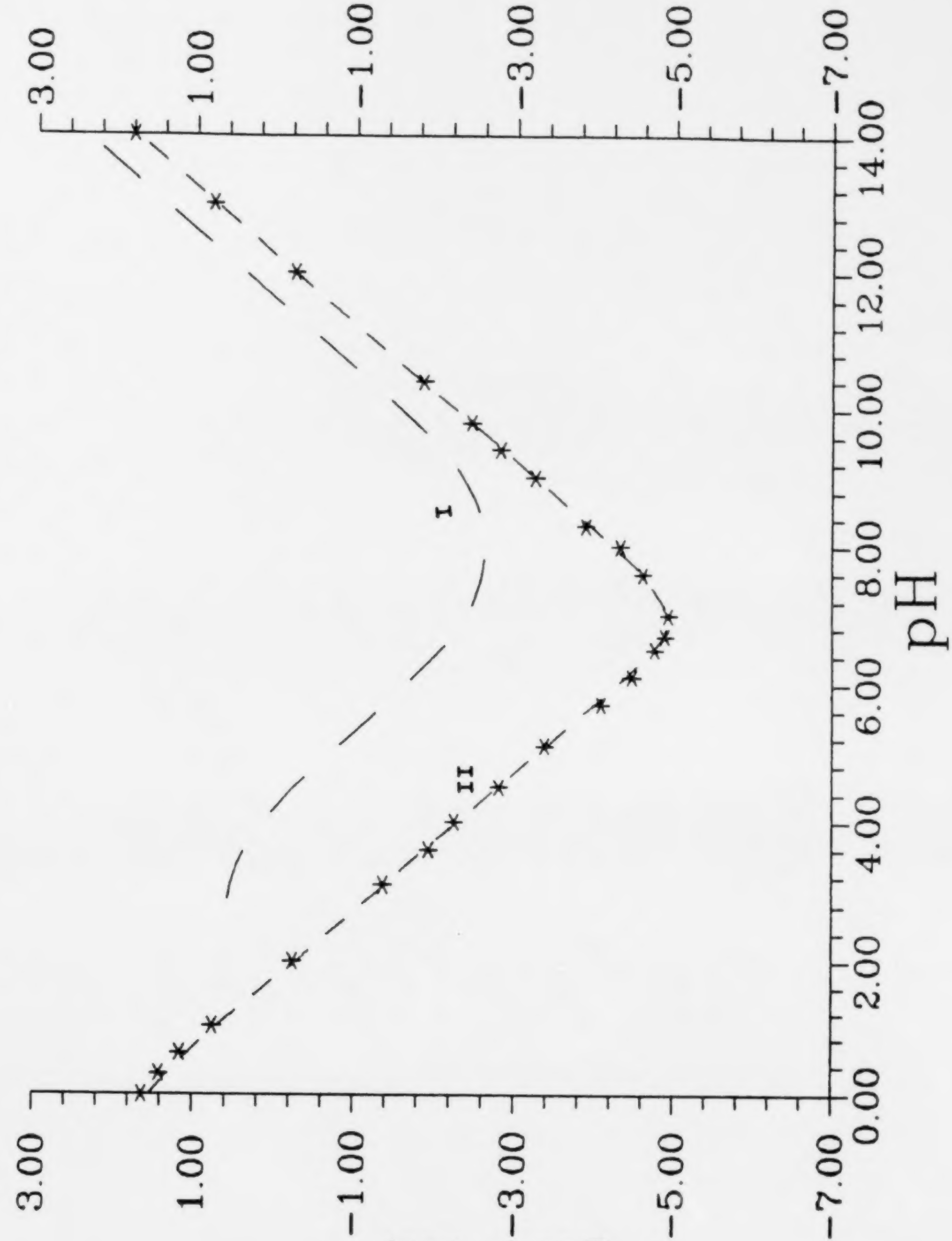

Figure 7. pH-Rate profile for the hydrolysis of I-II.

superimposible on that for **Ia**, for reasons of clarity they are not illustrated in Figure 7.

The profiles for **Ia-d** each exhibited domains involving H_2O attack on a protonated species at pH < 6.3, apparent H_2O attack between pH 6.4-9.0, and OH^- attack on the neutral species at pH > 9.0. At high H_3O^+, the k_{obsd} values tended to become pH independent, indicating a relatively high pK_a (3.5-4) for **I**-H^+. The pH-rate profile for **II** consisted of two domains requiring H_2O attack on **II**-H^+ and OH^- attack on **II** with a rate minimum at pH = 7 showing no evidence of H_2O attack on the neutral form. Also at very low pH (after being reinvestigated)[29], the k_{obsd} values are tend to plateau, and the pK_a for **II**-H^+ was determined to be -0.28. The mechanism and kinetics for hydrolysis of **Ia-d** are shown in equations 3 and 3a. The kinetics for **II** can most simply be accommodated by the processes and expression given in equations 4 and 4a.

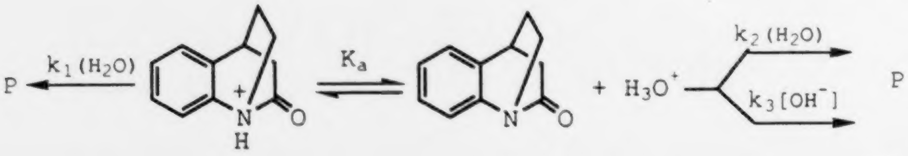

(3)

$$k_{obs} = \frac{k_1[H_3O^+]^2 + k_2K_a[H_3O^+] + k_3K_wK_a}{[H_3O^+]^2 + K_a[H_3O^+]} \qquad (3a)$$

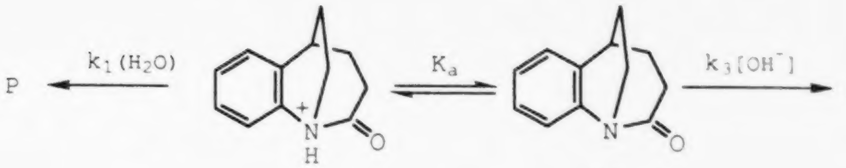

II

(4)

$$k_{obs} = \frac{k_1[H_3O^+]}{K_a + [H_3O^+]} + k_3[OH^-] \qquad (4a)$$

b). Substituent effects on the hydrolysis of **I**

Of all the parameters Somayaji and Brown[28] obtained, only the k_3 term (see equation 3) correlates in a satisfactory way with any Hammett parameter. With σ, a ρ value of 0.720±0.008 (r = 0.987, four data) was obtained. The ρ value for the Hammett plot for OH^- attack on **Ia-d** is consistent with an initial rate-limiting OH^- attack through a transition state with increased (-)charge adjacent to the ring.

c). X-Ray crystal structure for **II**[30]

The increase in reactivity ($10^6 \sim 10^7$ fold) of hydrolysis of **I** and **II** in both acid and base relative to "normal" anilides and amides is believed to be due to the distortion of these amides that reduces the amidic resonance.

Molecular modelling of **Ia** suggested that the bridgehead nitrogen atom is tetrahedral with its sp^3 electron pair oriented nearly coplanar with the C-O internuclear axis (i.e. orthogonal to the C=O π-bond). In **II**, X-ray crystallographic analysis also indicated the relatively localized N lone pair was oriented 55-60^0 from coplanarity with C-O internuclear axis. The distortion in these amides can be visualized qualitatively as in Figure 8 in terms of twist (ϕ)[31] and tilt angles (θ)[31] by considering a planar amide residing in the X-Z plane. Pyramidalization of the N produces a net tilt angle (θ) of the lone pair away from the Y axis in the X direction. Coupled with that motion is a rotation of the C1-C2-O plane about the X axis to produce a twist angle (ϕ) of the p orbital on C away from coplanarity with the N lone pair. Values of θ and ϕ in excess of 0^0 will diminish the

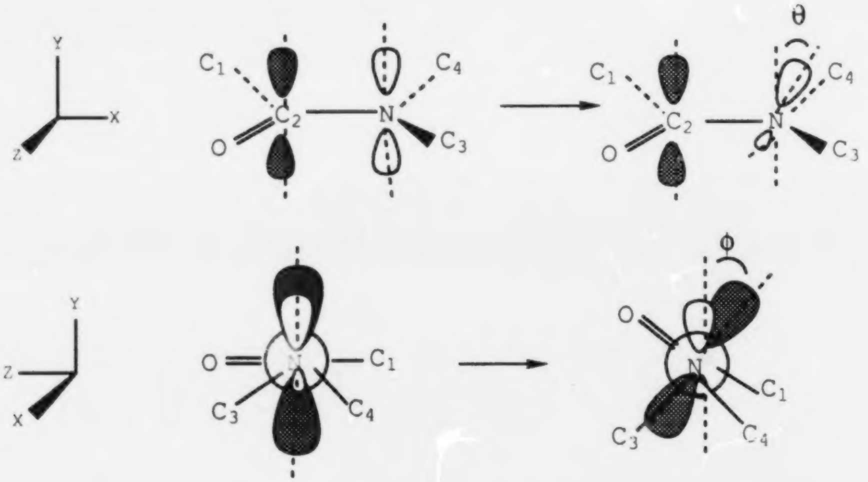

Figure 8. Qualitative representation of the distortion of bicyclic anilides in terms of twist (ϕ) and tilt (θ) angles.

amide resonance. In terms of these angles, θ and ϕ are ~15-20^0 and 90^0, for **Ia-d**, and ~15-20^0 and 30-35^0 for **II**. Assuming that the major difference between **I** and **II** stems from the twist angle, and assuming a (cosine ϕ)^2 relationship for N-C=O overlap, it was concluded that **II** is less torsionally strained than **I**. This is consistent with the lower $\nu_{C=O}$ for **II** than **I**, 1705cm^{-1} vs 1755cm^{-1} respectively.

d). ^{18}O-Exchange experiments for **I** and **II**

In order to determine whether addition of H_2O or OH^- to the C=O unit of the distorted amides under acidic or basic conditions is reversible or not, some ^{18}O-exchange experiments were done.

The results obtained for **I** and **II** showed that contrary to what is observed for substituted acetanilides,[17] neither **I** nor **II** undergo ^{18}O-exchange when attacked by OH^-. But it is notable that the bicyclic anilide structure does not allow the two oxygens O,O* in T_O- (equation 5) to be equivalent even if there is rapid proton transfer between the two oxygens.[32] Nevertheless, due to the ground state destabilization of bicyclic anilide, the rate-limiting step

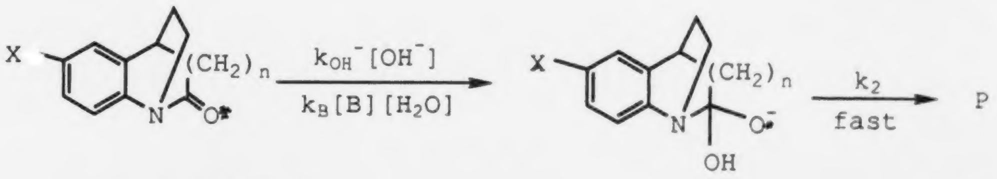

n = 1 (**I;Ia-c**) (5)
n = 2 (**II**) $k_B[B][H_2O]$ is not included

is likely the OH^- attack, and the tetrahedral intermediate is formed irreversibly. The mechanisms of hydrolysis of **I** and **II** under basic or neutral conditions are shown in equation 5.

In the acid domain, ^{16}O-amide was dissolved in 1:1 $CH_3CN:H_2{}^{18}O$ and after hydrolysis, it was shown by ^{18}O-^{13}C NMR that ^{18}O was incorporated in both **I** and **II**. Therefore, apparently the tetrahedral intermediate is formed reversibly for both amides.

e). Attack of bifunctional nucleophiles on bicyclic amide **II**

In the study of reaction of **II** as a model for the acylation step of the serine proteases, Somayaji et al[30] found that β-amino alcohols exhibit large nucleophilic reactivities as their neutral forms by a process involving intramolecular N,O-cooperativity. The proposed mechanism of N-methyl-2-(hydroxymethyl)imidazole attack on **II** is shown in equation 6.

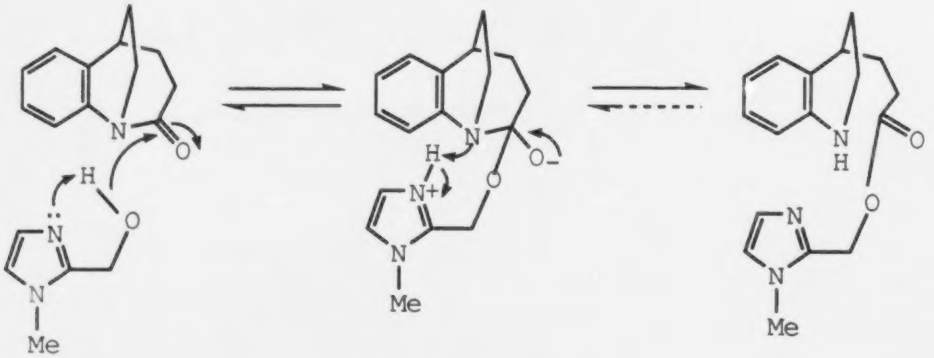

(6)

As a model for the aspartate proteinases, amide **II** also shows a striking reactivity toward hydrolysis promoted by certain dicarboxylic acids,[33] such as compounds **16a,b** and **17a**. The hydrolytic process involves reversible nucleophilic attack to form a linear (open) anhydride. If no second carboxylate is present, or if the remote CO_2H unit is incapable of forming a stable cyclic anhydride, the open anhydride rapidly reverses to re-form **II**. The mechanism of this process is illustrated in Scheme 1. For this process, it is suggested that the inherent distortion in **II** provides the driving force.

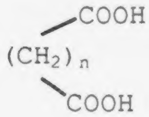

16a n = 3
b n = 2
c n = 1

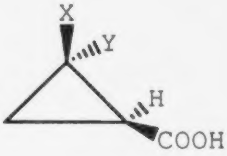

17a X=COOH; Y=H
b X=H; Y=COOH

f). The relative importance of twist vs tilt angle deformation in determining activation

In terms of OH^- attack, the much smaller twist angle of **II** than **Ia** did not lead to the expected large reduction in rate for the former, the difference being only a factor of ~4. Slebocka-Tilk and Brown[34] studied the effect of distortion on the hydrolytic reactivity of amide **18** in which the N is pyramidalized but there is only a slight twist angle. The experimental results showed **18b** (N-benzoylaziridine) was ~200,000 fold more susceptible to OH^- attack ($k_{OH^-} = 1.1\ M^{-1}s^{-1}$ at 25 ^0C) than N,N-dimethylbenzamide ($k_{OH^-} = 6.0\times10^{-6}\ M^{-1}s^{-1}$ at 25 ^0C).

Scheme 1

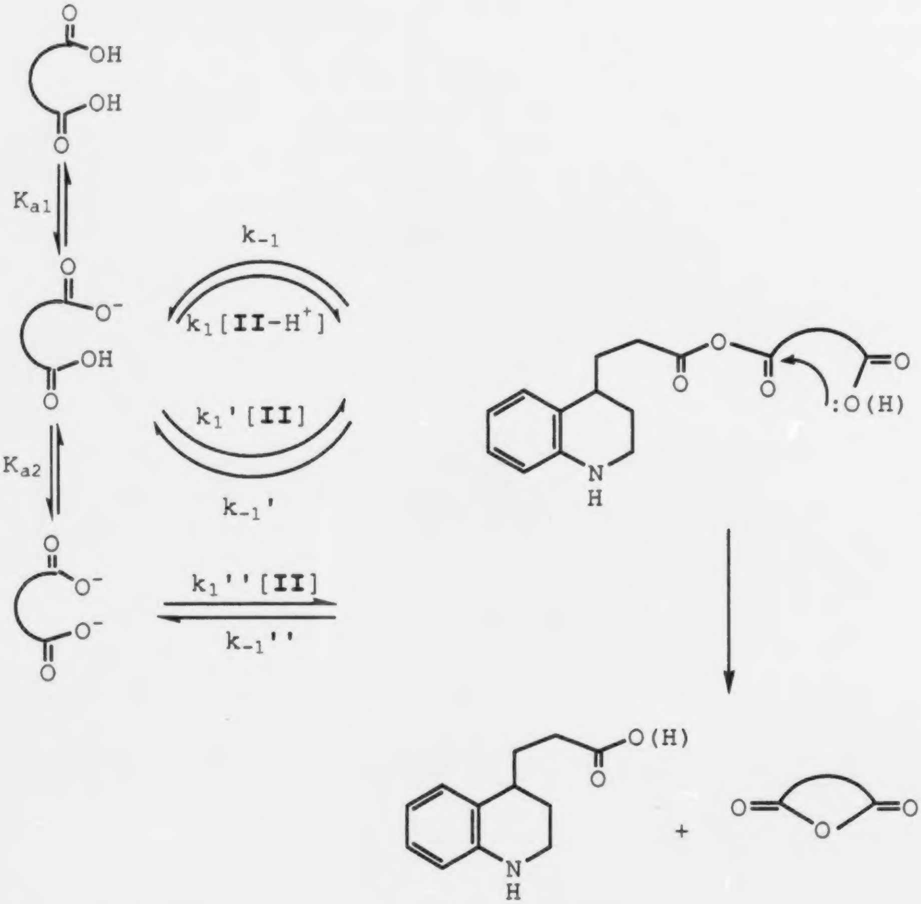
OH
OH
K_{a1}
O^-
OH
K_{a2}
O^-
O^-
k_{-1}
k_1[**II**-H^+]
k_1'[**II**]
k_{-1}'
k_1''[**II**]
k_{-1}''
N
H
:O(H)
O(H)
+

X-Ray crystallographic structures of (*p*-bromobenzoyl)aziridines **18c**[35] and **19**[36] indicated that in both cases the nitrogen was pyramidalized, with tilt angles of

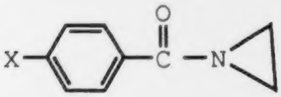

18a X = OCH3
b X = H
c X = Br
d X = NO_2

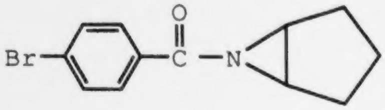

19

34^{0}, and 27^{0} respectively, and twist angles of 0 ± 10^{0}. Therefore the pyramidalization of N in **18** may lead to ~10^5 fold enhancement of the attack of OH^- on the acyl unit. It must be kept in mind, however, that the N-C(O) bond length in **18c** is longer than that in N,N-dimethyl-*p*-bromobenzamide.

The hydrolytic profile for **18** shows three dominant terms: OH^- and H_2O attack on the neutral form and H_2O attack on a protonated form of the amide. In base, the exclusive reaction is the rate-limiting and irreversible attack of OH^- on the C=O unit leading to normal hydrolytic products. This was proved by the first-order dependence on $[OH^-]$ from pH 8 to 14 of the hydrolysis rate and by the fact that ~50% ^{18}O-enriched amide recovered from the hydrolysis medium as a function of time showed no ^{18}O loss. In acid, the products are not the expected hydrolytic ones of benzoic acid and aziridine. Rather, ring opening occurs exclusively to give *p*-X-C_6H_4(C=O)$NHCH_2CH_2OY$ (Y = H and $COCH_3$ if done at pH 4.7 with acetate buffer).

Bennet et al[37] studied the hydrolysis of amide **20**. The

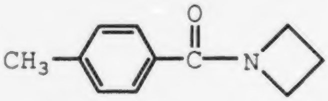

20

results showed that amide **20** hydrolyzes very slowly (k_2 = 4.01 × 10^{-5} $M^{-1}s^{-1}$, 25 °C) compared with **18b** (k_2 = 1.1 $M^{-1}s^{-1}$, 25 °C), although the N in **20** is pyramidalized. The x-ray crystallographic structure of **20** indicated[38] that the N-C bond length (1.339 Å) is much shorter than that of **18b** (1.410 Å); therefore the lengthened N-C in **18b** is probably the major reason for enhanced reactivity.

C. Objective:

The strain hypothesis for enzyme-mediated amide hydrolysis suggests that a share of the exothermicity of substrate binding is utilized in a productive way to induce stress or strain in the substrate, enzyme, or enzyme-substrate complex which is relaxed as the transition state for the acyl transfer reaction is approached.[3-5] Therefore it is important to study the model compounds to determine how the induction of strain modifies the hydrolytic reactivity of amides.

Although there are a few studies[25-28,33-34] for this kind of distorted amide, there is no complete study for the changes in hydrolytic reactivities that accompany a continuous structural change. Also, previous studies have not determined whether chiral amides in aqueous solution have different reactivities toward nucleophilic attack by chiral reagents. In order to probe more completely the manner in which amide hydrolytic reactivity can be influenced by distortion, we need a series of amides such as amides **Ia**-**IV**, which give a continuous variation in the degree of distortion about the amide linkage. In this work, distorted amides of 3,4-dihydro-2-oxo-1,4-propanoquinoline **III** and 2,3,4,5-tetrahydro-2-oxo-1,5-propanobenzazepine **IV** have been prepared and characterized and their hydrolytic profiles determined.

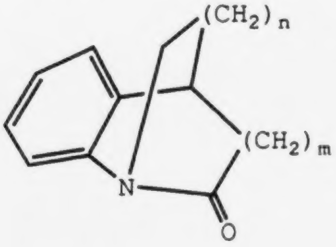

Ia $n = m = 1$

II $n = 1; m = 2$

III $n = 2; m = 1$

IV $n = 2; m = 2$

The structures of both **III** and **IV** have been determined using X-ray diffraction. Those will be compared with a crystal structure of **II** and a model structure of **Ia** in order to establish the relationship between hydrolytic reactivity and amidic distortions that involve rotation about and the lengthening of the N-C(O) bond, and N-pyramidalization. A comparison will be made of distorted and normal amides with respect to the large observed differences in hydrolytic reactivity and molecular structure.

In order to explain the enhanced hydrolytic reactivity, the activation parameters for hydrolysis of this series of amides have been measured. The changes in the activation enthalpy $\Delta H^{\ddagger}$ and activation entropy $\Delta S^{\ddagger}$ are discussed in relationship to the distortion.

The effect of acetate on the hydrolysis of **II** and **III** in H_2O and D_2O was investigated in order to understand the observed catalytic effect of this buffer.

The reactions of **III** and **IV** with methyl trifluoromethane sulfonate (MeOTf) were investigated in order to establish the position of kinetic methylation which may be of relevance to the site of protonation of these amides.

Enzymes have the ability to distinguish between various isomeric structures with different chiralities and are commonly described as highly efficient catalysts showing a high degree of selectivity and specificity. As a model for this, the reaction of the obtained chiral amide, (S) or (R)-3,4-dihydro-2-oxo-1,4-propanoquinoline **III**, with various ephedrine diastereomers was studied in the hopes of establishing a kinetic preference. It was possible to generate optically active 3,4-dihydro-2-oxo-1,4-propano quinoline **III** by resolving the enantiomers of a synthetic precursor, 5-(2-carboxymethyl)-N-tosyl-2,3,4,5-tetrahydro benzazepine, followed by synthetic steps that retain optical activity.

2. RESULTS

A. Synthesis

Distorted amide **III** was synthesized by a route analogous to that presented by Somayaji and Brown[28] for the syntheses of **Ia** and **II**. Modifications of some steps resulted in an overall yield of 24% in six steps from the known ketone **21**[39] to amide **III**. The route of synthesis of **III** is shown in Scheme 2.

5-(Ethoxycarbonylmethyl)-5-hydroxy-N-tosyl-2,3,4,5-tetrahydrobenzazepine **22** was prepared by Reformatsky reaction of **21**. Thus ketone **21** and ethyl β-bromoacetate in dry benzene were dropped into a suspension of zinc powder in diethyl ether heated at reflux. The alcohol was obtained in 86% isolated yield.

The alcohol was dehydrated using a catalytic amount of TsOH in benzene heated at reflux to generate alkene **23**. However, three isomers were produced. Alkene **23a** contains both Z and E isomers, which were identified from the singlet NMR signals for their olefinic protons at δ 5.28 and 5.61 ppm, respectively. The alkene hydrogen of **23b** appears at δ 5.75 ppm as a triplet with a coupling constant of 6 Hz.

5-Ethoxycarbonylmethyl-2,3,4,5-tetrahydrobenzazepine **24** was obtained by catalytic hydrogenation of the mixture of isomeric **23**. During this process, it was found that alkene **23a** was more difficult to hydrogenate than **23b**, probably

Scheme 2

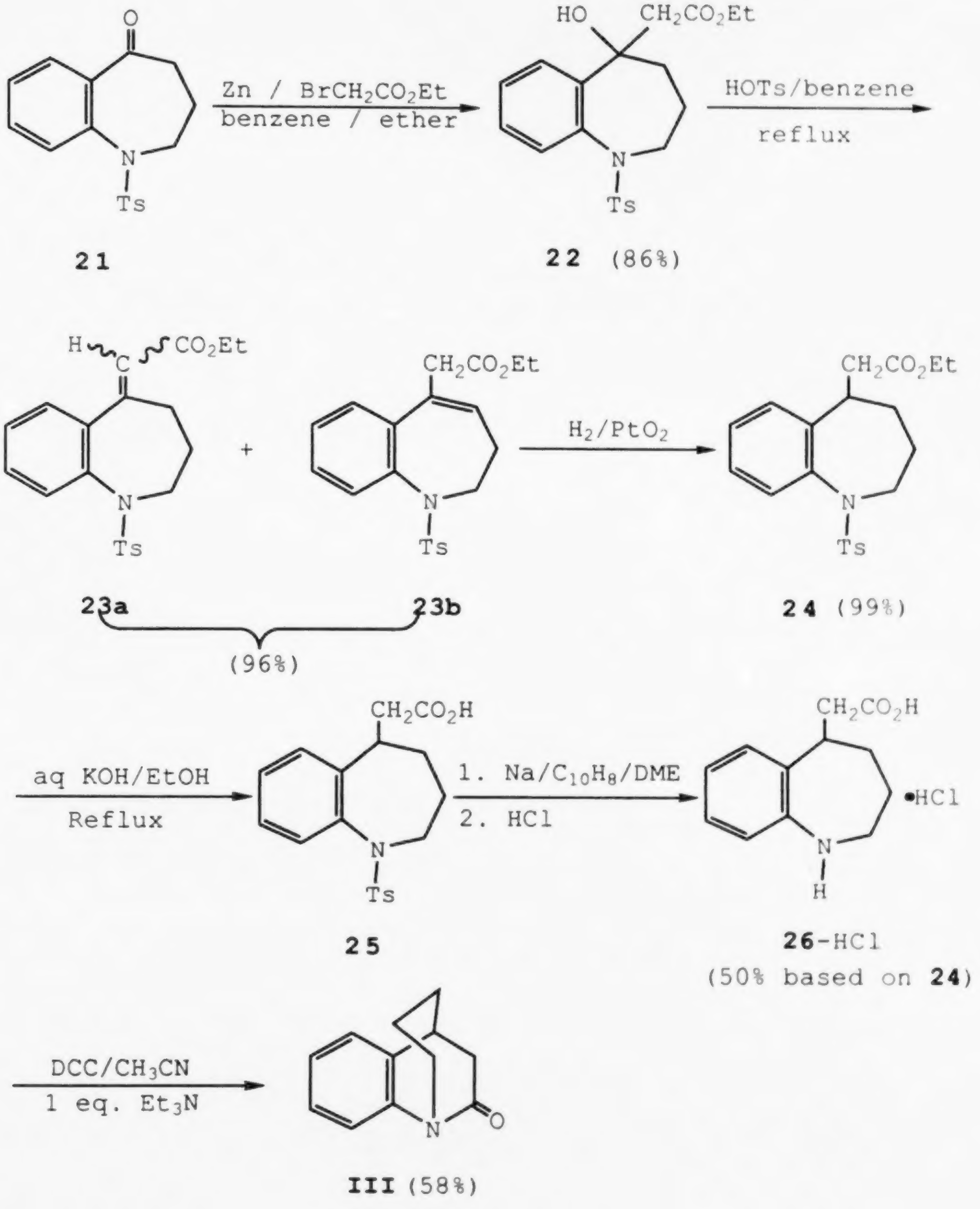

Zn / BrCH₂CO₂Et
benzene / ether
HOTs/benzene
reflux
21
22 (86%)
23a
23b
(96%)
H₂/PtO₂
24 (99%)
aq KOH/EtOH
Reflux
25
1. Na/C₁₀H₈/DME
2. HCl
•HCl
26-HCl
(50% based on 24)
DCC/CH₃CN
1 eq. Et₃N
III (58%)

because of the conjugation of the double bond with the ester group in **23a**. Therefore, a longer reaction time and a higher temperature were required for the completion of the hydrogenation.

Hydrolysis of **24** was carried out in refluxing alcoholic KOH. After acidification, the carboxylic acid was obtained as a syrup-like material. This crude product **25** was dried and directly used for the synthesis of amino acid **26**.

Removal of the N-tosyl group of **25** was the most difficult step for the synthesis of distorted amide **III**. The procedure for the deprotection using $ZnCl_2$-HCl in AcOH described by Blackburn et al[27] was unsuccessful for compound **25**. Finally, a modification of a reported procedure[40], in which the sodium salt of carboxylic acid **25** was treated with sodium-naphthalene in DME (dimethoxyethane) solution at room temperature, was found to be successful. The completion of the reaction was monitored by the formation of a persistent green color in the reaction mixture. After the reaction was complete, the workup process was very difficult because of a large excess of naphthalene. Repeated extractions with benzene followed by sublimation to remove naphthalene were required to give crude amino acid **26**. Further purification was accomplished by converting **26** into its HCl salt. The identity of **26**-HCl was established by mass spectrometry (MS), ^{1}H-NMR spectra and elemental analysis.

3,4-Dihydro-2-oxo-1,4-propanoquinoline **III** was prepared by the reaction of the HCl salt of amino acid **26** with dicyclohexylcarbodiimide (DCC) in dry acetonitrile containing one equivalent of triethylamine that was added first to generate the amino acid. The cyclization was carried out in very dilute acetonitrile solution in order to avoid intermolecular dimerization or polymerization. The product formation was monitored by observing the growth of a $\nu_{C=O}$ band at 1720cm^{-1} periodically during the course of the reaction. Amide **III** was fully characterized by its exact

Table V. Chemical shifts and coupling constants of the H's in **III**

Proton	Chemical shift (ppm)	coupling constant (Hz)
H_3, H_{3a}	2.68	$J_{4,3} = J_{4,3a} = 3$
H_4	3.15	$J_{3a,4} = J_{3,4} = 3$ $J_{5,4} = 8$, $J_{5a,4} = 1$
H_5	2.05	multiplet
H_6, H_{6a}, H_{5a}	1.3-1.7	multiplet
H_7	3.25	$J_{7a,7} = 13$, $J_{6a,7} = 6$ $J_{6,7} = 1$
H_{7a}	3.90	$J_{7,7a} = 13$, $J_{6a,7a} = 5.5$ $J_{6,7a} = 11$, $J_{5,7a} = 2$

a. The experiment was performed in $CDCl_3$ using a 200 MHz spectrometer.

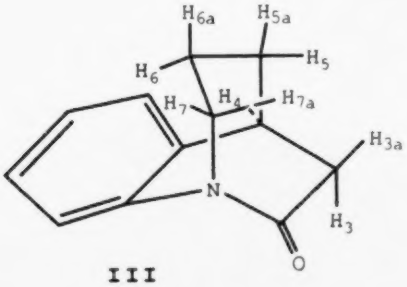

III

mass (187.1001), ^{1}H-NMR and ^{13}C-NMR spectra and elemental analysis.

^{1}H-NMR assignments were made on the basis of decoupling experiments and are listed in Table V. FT-IR indicated a $\nu_{C=O}$ of 1722.23cm^{-1} ($CHCl_3$, cast).

The synthesis of distorted amide **IV** was first attempted through the use of a Grignard reagent to add a three carbon chain at the 5-position of ketone **21** as shown in equation 7; however, that proved unsuccessful.

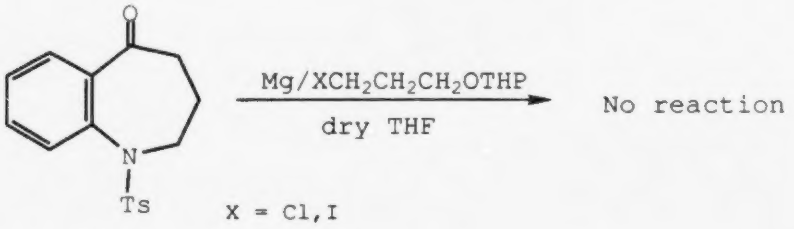

(7)

21

This ketone has been shown to react with Grignard reagents like benzylmagnesium bromide to give a good yield of the expected tertiary alcohols.[41] However, the Grignard reagent $XMgCH_2CH_2CH_2OTHP$ is a stronger base than $PhCH_2MgX$ and probably can enolize ketone **21** first before the addition to the C=O group can occur. Thus the starting material was always recovered after workup.

Therefore, we decided to enlarge the side chain of compound **25** by one carbon through the reaction of the corresponding acyl chloride with CH_2N_2, followed by the modified Wolff rearrangement[42] to yield compound **27**.

Distorted amide **IV** was prepared in 23% yield starting with the carboxylic acid **25** as shown in Scheme 3.

Scheme 3

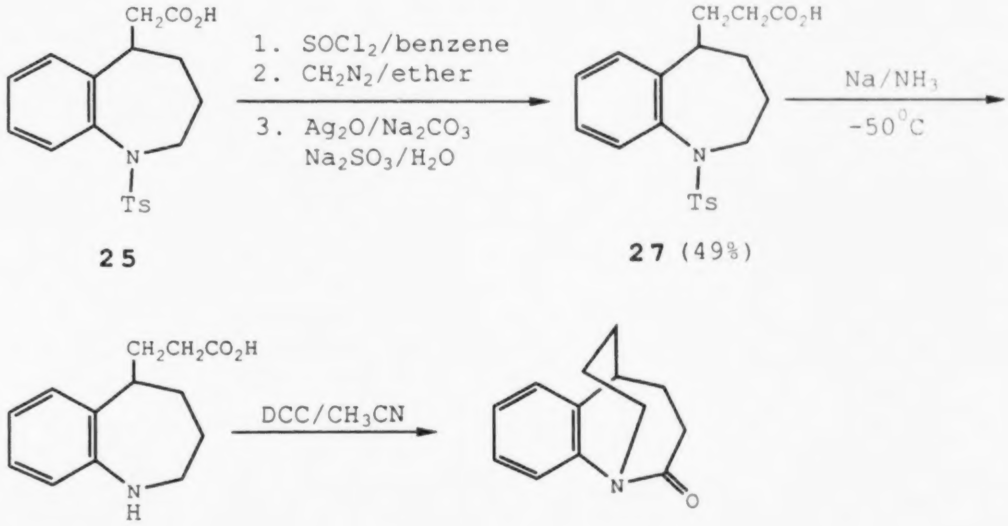
CH₂CO₂H
N
Ts
1. SOCl₂/benzene
2. CH₂N₂/ether
3. Ag₂O/Na₂CO₃
Na₂SO₃/H₂O
CH₂CH₂CO₂H
N
Ts
Na/NH₃
-50°C
CH₂CH₂CO₂H
N
H
DCC/CH₃CN
N
O

25

27 (49%)

28 (52%)

IV (89%)

Carboxylic acid **25** was purified by recrystallization from 50% aqueous EtOH. Dried white crystals of **25** were converted to the acyl chloride by treating with $SOCl_2$ in refluxing benzene. The resulting acyl chloride was directly reacted with CH_2N_2 which was prepared *in situ* according to a standard method.[43] The identity of the diazomethane addition product was confirmed by the diazo stretching frequency at 2120cm^{-1} (film) in the ir spectrum. The diazoketone was subjected to an Arndt-Eistert reaction,[42] in which it was reacted with a mixture of silver oxide, sodium carbonate and sodium thiosulfate in a water/1,4-dioxane mixed solvent. A moderate yield (49%) of pure compound **27** was obtained.

The removal of the N-tosyl protecting group for **27** was accomplished according to the procedure of Schneider[44] since the detosylation procedure for **25** presented some problems in separation and purification. N-Tosyl carboxylic acid **27** was reacted with sodium in liquid ammonia at -50 °C. The reaction was terminated by the addition of solid ammonium chloride about 5 min after the last addition of Na to avoid further reduction. The excess ammonia was then allowed to evaporate slowly at room temperature. The resulting amino acid **28** was purified by recrystallization from EtOH to give a white solid in 52% yield. The compound was identified by MS, ^{1}H-NMR and elemental analysis.

2,3,4,5,-Tetrahydro-2-oxo-1,5-propanobenzazepine **IV** was prepared from amino acid **28** by the same procedure for the preparation of distorted amide **III**. The product formation was monitored by ir spectroscopy by observing the growth of a carbonyl stretch at $1680 cm^{-1}$. The product obtained was recrystallized from octane to give pure amide **IV** in 89% yield. The identity of this compound was confirmed by ^{1}H-NMR, ^{13}C-NMR, MS and elemental analysis.

Based on decoupling experiments, the complete assignment of the ^{1}H-NMR spectrum was made and the results are listed in Table VI.

Table VI. Assignment of the ^{1}H-NMR spectrum of amide **IV** on the basis of decoupling experiments[a]

Proton	chemical shift (ppm)	coupling constant (Hz)
H_3, H_{3a}	2.26	multiplet
H_4, H_{4a}, H_6	2.10	multiplet
H_5	3.16	$J_{6a,5} = 11$, $J_{6,5} = 2$ $J_{4a,5} = 4$, $J_{4,5} = 2.5$
H_{7a}, H_{6a}	1.52-1.68	multiplet
H_7	1.20-1.34	multiplet
H_8	2.90	$J_{8a,8} = 12$, $J_{7a,8} = 2$ $J_{7,8} = 4$
H_{8a}	4.52	$J_{8,8a} = 12$, $J_{7,8a} = 10$ $J_{7a,8a} = 5$, $J_{6,8a} = 2.5$

a. The experiment was performed in $CDCl_3$ on a 400 MHz spectrometer.

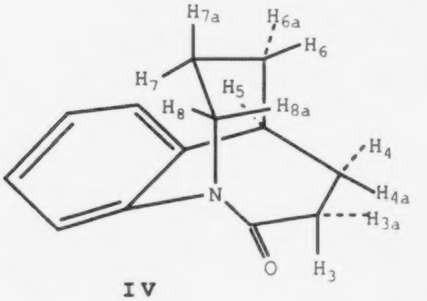

IV

B. Crystal and Molecular Structures

Suitable crystals of amides **III** and **IV**[45a] were submitted for structure determination by X-ray diffraction.

The molecular structures were determined by B.D. Santarsiero in the Department of Chemistry, University of Alberta. The experimental details are reported in the experimental part of this thesis.

For amide **III**, there are two crystallographically independent molecules in the unit cell and the ORTEP drawings for them are given in Figures 9a,9b.

Given in Tables VII,VIII are selected bond distances and angles for each structure.

Table VII. Table of selected bond lengths (Å)[a,b] of the two crystallographically independent molecules of amide **III**

Atom1	Atom2	length	Atom1	atom2	length	Average
N1	C1	1.413(10)	N2	C21	1.419(11)	1.416(3)
N1	C9	1.459(7)	N2	C29	1.467(10)	1.462(4)
N1	C12	1.482(9)	N2	C32	1.488(9)	1.485(3)
C1	O1	1.225(7)	C21	O2	1.233(10)	1.228(4)
C1	C2	1.521(10)	C21	C22	1.500(11)	1.511(11)

a. Numbers in parentheses represent standard deviations of the least significant digit.
b. Atom numbering from Figure 9a,9b.

Table VIII. Table of selected interatomic angles (degree) of the two crystallographically independent molecules of amide **III**[a,b]

Atom1	Atom2	Atom3	Angle	Atom1	Atom2	Atom3	Angle
C1	N1	C9	116.2(5)	C21	N2	C29	115.8(6)
C1	N1	C12	110.0(5)	C21	N2	C32	108.9(6)
C9	N1	C12	110.9(5)	C29	N2	C32	110.3(6)
N1	C1	O1	119.2(6)	N2	C21	O2	119.1(7)
N1	C1	C2	116.9(5)	N2	C21	C22	117.0(7)
O1	C1	C2	122.9(7)	O2	C21	C22	123.6(8)

a. Numbers in parentheses represent standard deviations of the least significant digit.
b. Atom numbering from Figure 9a,9b.

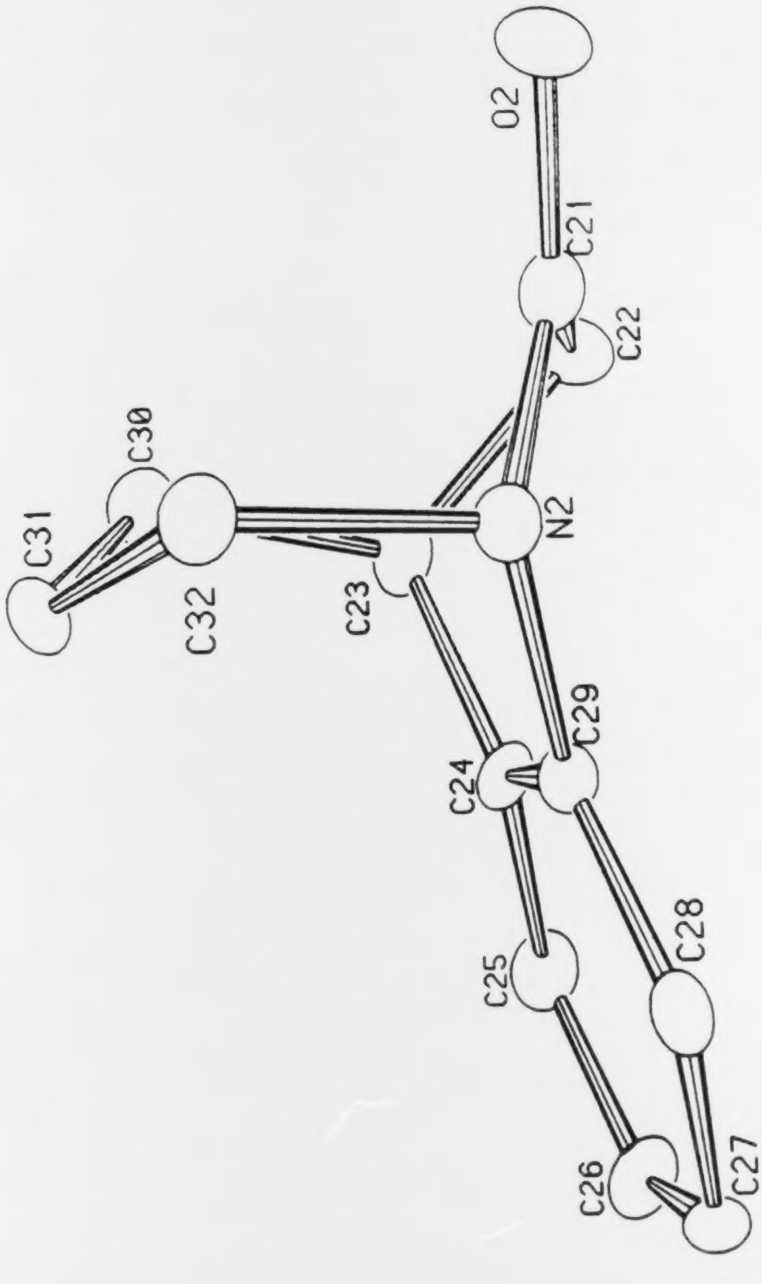
O2
C21
C22
C30
C31
C32
C23
N2
C29
C24
C28
C25
C27
C26

Figure 9a. Perspective views of one of the two crystallographically independent molecules of **III** in the unit cell.

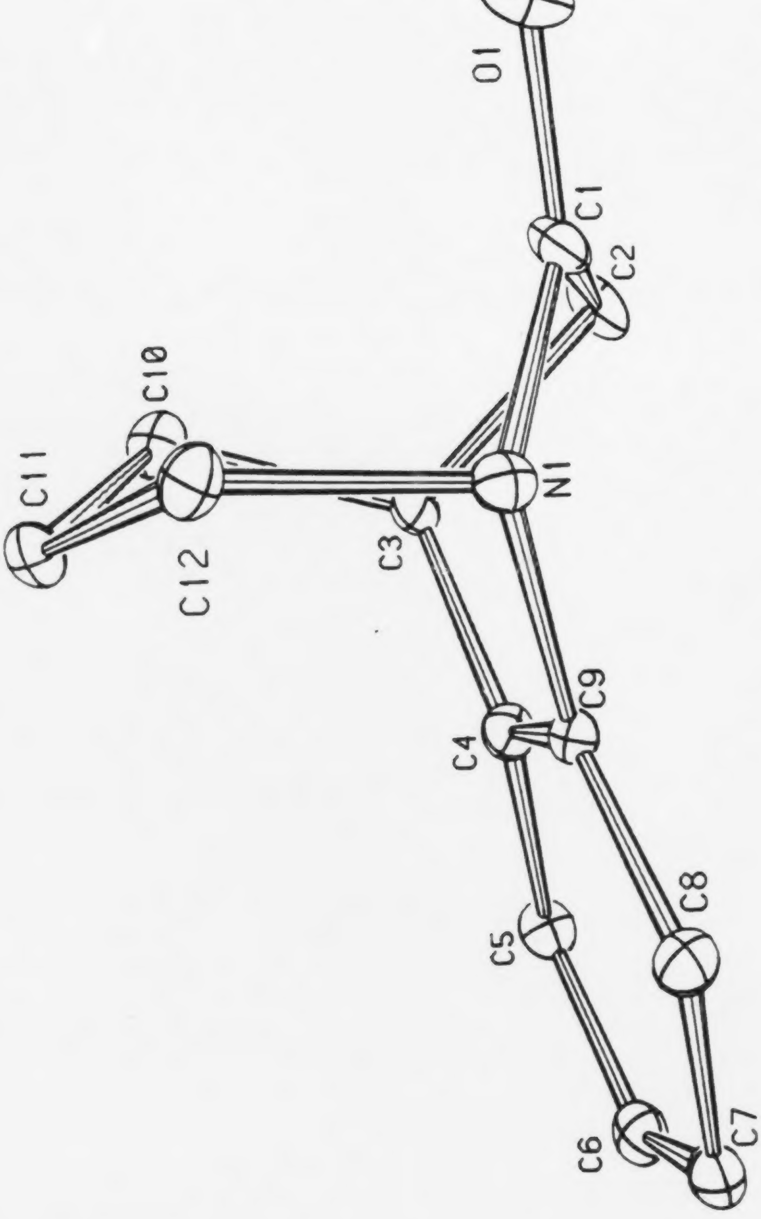
O1
C1
C2
C10
C11
C12
N1
C3
C4
C9
C5
C8
C6
C7

Figure 9b. Perspective views of one of the two crystallographically independent molecules of **III** in the unit cell.

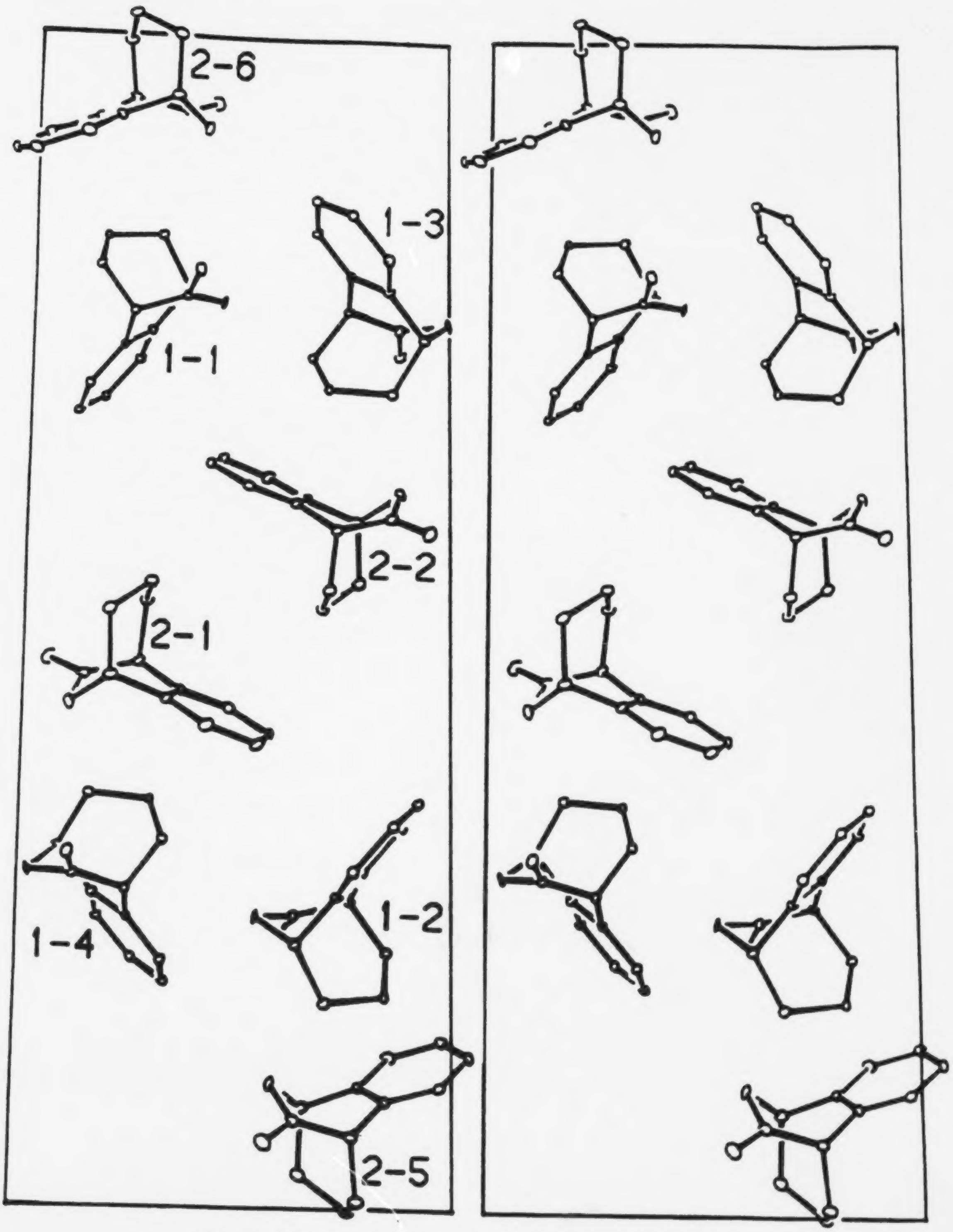
2-6
1-3
1-1
2-2
2-1
1-4
1-2
2-5

Figure 10. Stereoview of the unit cell of III.

Shown in Figure 10 is the stereoview of the unit cell projection for both crystallographically independent molecules. Although the two crystallographically independent molecules have different environments involving different packing arrangements (judged from $U_{eq} = 1/3 \Sigma^{3}_{i=1} r_i^2$, where r_i are the root-mean-square amplitudes of the Gaussian ellipsoids), the conformations of the two molecules are not significantly different. This probably suggests that the observed conformation in each represents a ground state configuration unperturbed by crystal packing forces.

For amide **IV**, the unit cell of **IV** was also found to contain two crytallographically independent molecules. Given in Figures 11a,11b are the perspective views and atom numberings of the two forms of **IV**.

Given in Table IX and Table X are selected bond distances and bond angles for each structure.

Table IX. Table of selected bond lengths (Å)[a,b] of the two crystallographically independent molecules of amide **IV**

Atom1	Atom2	length	Atom1	atom2	length
O1	C1	1.232(5)	O2	C21	1.241(6)
C1	N1	1.369(6)	C21	N2	1.374(6)
C1	C2	1.497(7)	C21	C22	1.497(7)
N1	C10	1.459(6)	N2	C30	1.448(6)
N1	C13	1.493(6)	N2	C33	1.477(6)

---

a. Numbers in parentheses represent standard deviations of the least significant digit.

b. Atom numbering from Figures 11a,b.

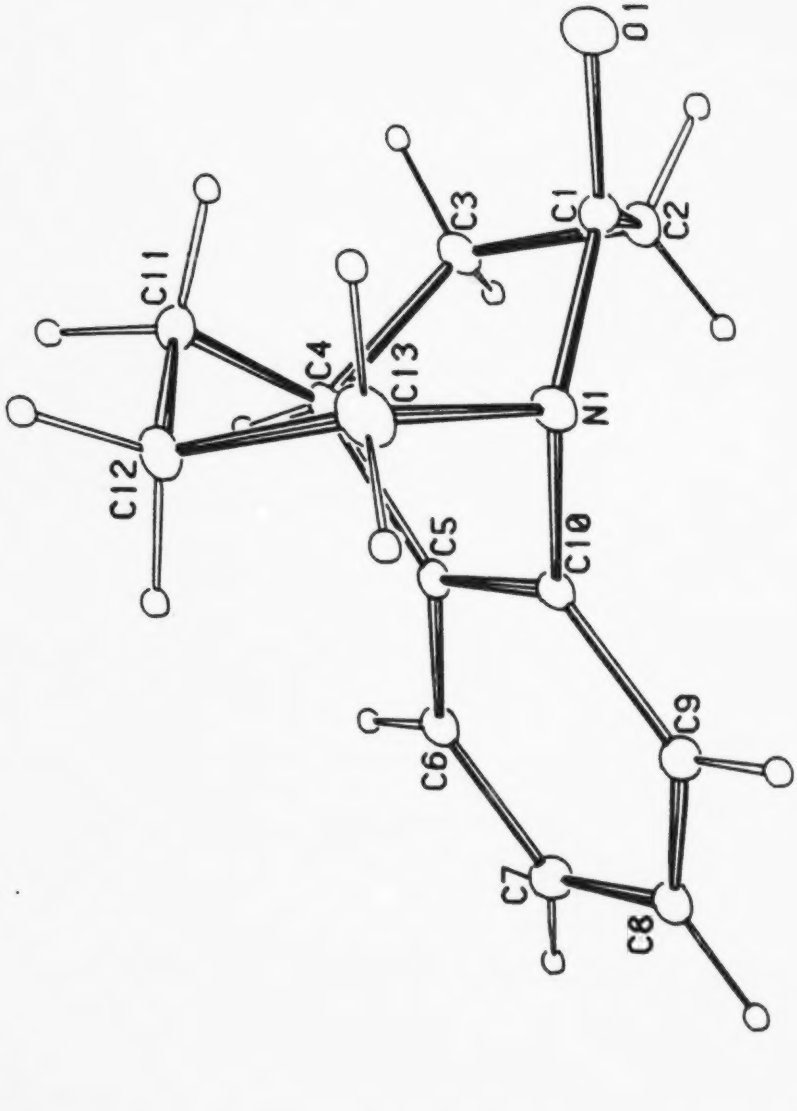
O1
C1
C2
C3
C11
C4
C13
N1
C12
C5
C10
C9
C6
C7
C8

Figure 11a. Prespective views of one of the two crystallographically independent molecules of **IV** in the unit cell.

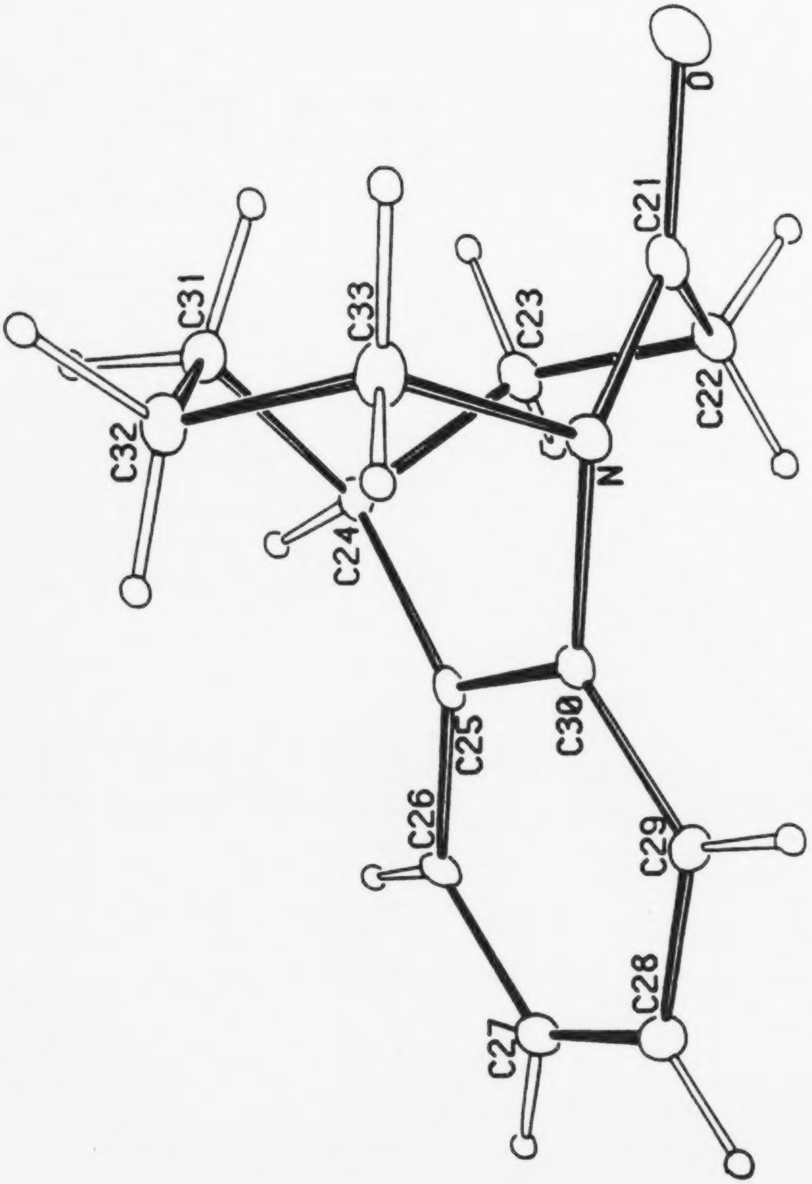
O
C21
C22
C23
C33
C31
C32
C24
N
C25
C30
C26
C29
C27
C28

Figure 11b. Perspective views of one of the two crystallographically independent molecules of **IV** in the unit cell.

Table X. Table of selected interatomic angles (degrees) of the two crystallographically independent molecules of amide **IV**

Atom1	Atom2	Atom3	Angle	Atom1	Atom2	Atom3	Angle
O1	C1	N1	121.8(5)	O2	C21	N2	120.7(5)
O1	C1	C2	121.8(5)	O2	C21	C22	122.4(5)
N1	C1	C2	116.3(4)	N2	C21	C22	116.9(5)
C1	N1	C10	120.2(5)	C21	N2	C30	118.8(4)
C1	N1	C13	116.1(5)	C21	N2	C33	116.8(4)
C10	N1	C13	112.7(4)	C30	N2	C33	113.3(4)

a. Numbers in parentheses represent standard deviations of the least significant digit.
b. Atom numbering from Figures 11a,b.

The distortion imposed by the bridged structure on the amidic N-C=O unit is the unique feature of interest in these molecules. In order to understand the relationship between structural distortion and reactivity, a comparison of structural parameters should be made within this series of amides from the most distorted amide **Ia** to an undistorted amide.

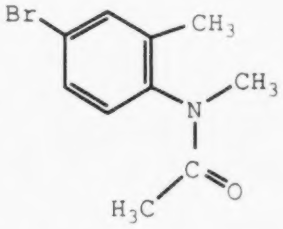

29

p-Bromo-N,2-dimethylacetanilide **29**[45b] was chosen for comparison with the bicyclic amides **Ia,II,III,IV** because it was anticipated to have a planar amidic unit, but the plane

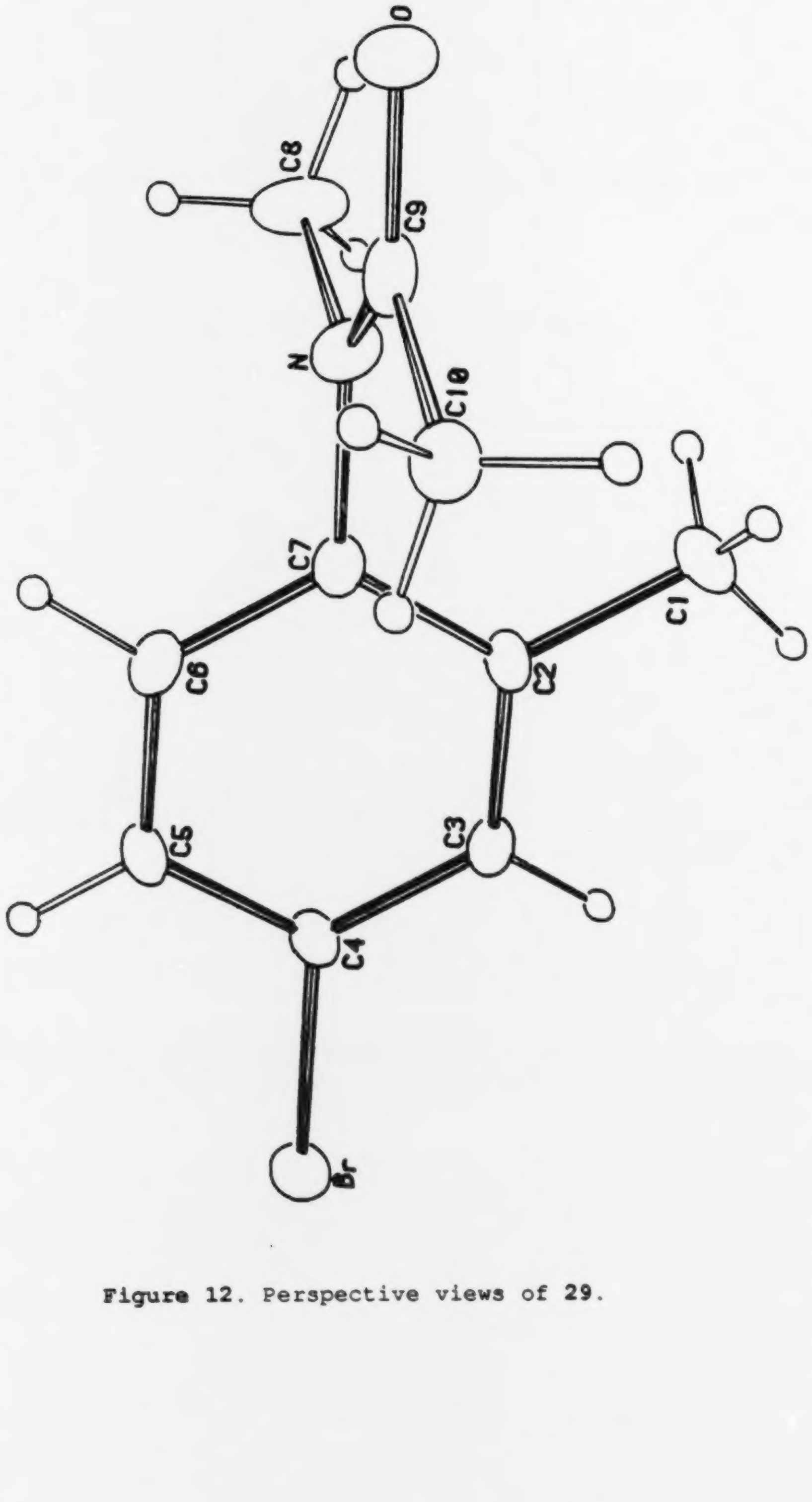
O
C8
C9
N
C10
C1
C7
C6
C2
C5
C3
C4
Br

Figure 12. Perspective views of **29**.

of the amide should be rotated ~ 90° relative to the aromatic ring by virtue of buttressing with the ortho-CH_3 group. Its structure was determined by B.D. Santarsiero (Department of Chemistry, University of Alberta) and is shown in Figure 12.

For the most distorted amide **I**, we have been unable to obtain qualified crystals. Even the obtained crystals of the *p*-chloro-derivative of **I** are not of sufficient quality for X-ray analysis.[46] Therefore, we will discuss the structures of **II-IV** and **29**.

In general, each of these amides **II**, **III**, **IV**, and **29** displays bond distances and angles within normal limits. The fragments of interest in each are those containing the heavy atoms of the amide linkage. Dunitz parameters[47] (χ_C, χ_N, τ') are introduced here to describe the deformations of the amide group. The definition of these parameters is shown in equations 8,8a and 8b, which $\omega_1 = \omega(C_\alpha CNC_\beta)$, $\omega_2 = \omega(OCNC_\gamma)$, $\omega_3 = \omega(OCNC_\beta)$ and $\omega_4 = \omega(C_\alpha CNC_\gamma)$. The values of ω_1-ω_4 are the four linearly dependent torsion angles about the C-N bond.

$$\chi_C = \omega_1 - \omega_3 + \pi = -\omega_2 + \omega_4 + \pi \qquad (8)$$

$$\chi_N = \omega_2 - \omega_3 + \pi = -\omega_1 + \omega_4 + \pi \qquad (8a)$$

$$\tau' = \omega_1 + \omega_2 \qquad (8b)$$

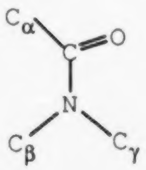

Thus, χ_C indicates the pyramidalization of the carbonyl carbon, χ_N, the pyramidalization of nitrogen, and τ', the twisting of N-C(O) bond. The summary of selected bond distances and angles, Dunitz parameters (χ_C χ_N τ')[47] and twist, tilt angles[31] for these amides is given in Table XI.

Table XI. Selected structural parameters for anilides **II,III,IV** and **29**

Amide	r(N-C(O))	r(C=O)	N-C(O)-C	Dunitz parameters[a]			Twist[b]	Tilt[b]
	Å	Å	angle(^{0})	χ_C	χ_N	τ'	angle(^{0})	(^{0})
II[c]	1.401(2)	1.216(2)	116.5(1)	9.0	57.2	71.2	30.7	15.2
III[d]	1.413(10)	1.225(10)	116.9(5)	11.0	52.8	75.6	33.2	16.0
	1.419(11)	1.233(10)	117.0(7)	6.7	55.1	82.4	38.9	16.8
IV[d]	1.370(6)	1.233(6)	116.3(4)	4.3	38.6	34.4	15.3	10.5
	1.374(6)	1.241(6)	116.9(5)	3.8	38.3	37.8	17.1	10.6
29	1.338(7)	1.235(6)	118.1(5)	~1.5	3.7	1.3	1.5	1.0

a. Reference 47.
b. defined as in Figure 8.
c. Reference 30.
d. Two crystallographically independent molecules in unit cell.

The data (see Table XI) shows that there is an increase of ~0.06-0.08 Å in the N-C(O) bond length in passing from essentially undistorted amide **29** to progressively more distorted **IV→III≈II**, but only about 0.02 Å shortening of C=O bond. The angles of the N-C(O)-C unit remain unchanged for all those amides. The Dunitz parameter,[47] χ_C, changes slightly in passing from **29** through **IV→III→II**, which indicates that each of the carbonyl carbons is only slightly pyramidalized. However, the Dunitz parameters[47] χ_N and τ', twist angle[31] and tilt angle[31] are steady increasing through the series from **29→IV→III≈II**. This suggests that the molecular distortion manifests itself mainly in terms of N pyramidalization (χ_N, tilt angle), rotation about the N-C(O) bond (τ', twist angle), and a lengthening of the N-C(O) bond.

Generally, it is believed that any distortion in an amidic unit causes a reduction in resonance, which should shorten the C=O bond at the same time as lengthening the N-C(O) bond. However, recently Wiberg and Laidig[48] have reported high level *ab initio* calculations on formamides of a planar (**30a**) and orthogonal (**30b**) configuration, as well as atomic population analyses calculated by the method of Bader.[49] It is obvious that the N of **30a** is sp^2 hybridized and that of **30b** approaches sp^3 hybridization. The lone pair electron on N of **30b** cannot delocalize into the p orbital of the carbonyl group. The calculated structural parameters for **30a** and **30b** (shown in Table XII) indicate that there is an increase in the length of N-C(O) bond in passing from **30a** to **30b**, and only slight shortening of the C=O bond. Comparison of calculated data for **30** with the experimental data for distorted amides **II-IV** and **29**

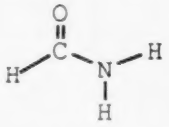

30a

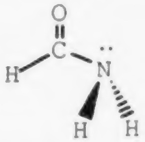

30b

distorted amides **II-IV** and **29** confirms the lengthening of the N-C(O) bond and apparent insensitivity of the C=O length to rotation.

Table XII. Calculated structural parameters for amide **30**

Amide	r(N-C(O))[a]	r(C=O)[a]	Dunitz parameters[b]			Twist[c]	Tilt[c]
	Å	Å	χ_C	χ_N	τ'	(°)	(°)
30a	1.349	1.193	0.0	0.0	0.0	0.0	0.0
30b	1.423	1.179	0.0	63.4	180	90.0	19.5

a. Reference 48.
b. Reference 47.
c. Defined as in reference 31.

C. Kinetics of Hydrolysis

1). pH-Rate profile of amides **III** and **IV**

The rates of hydrolysis were followed spectrophotometrically using a Cary 210 UV-vis spectrophotometer interfaced to an Apple II computer for data collection. Buffers were prepared at 4 different concentrations from 0.05 to 0.20M with μ = 1.0 M (KCl) in triply distilled water.

Given in Table XIII are the pseudo-first order rate constants (k_{hyd}) for the hydrolysis of amide **III** at 25 °C, μ = 1.0 (KCl) extrapolated to zero buffer concentration. The pH/rate profile for **III** given in Figure 13 (O-O-O) shows three domains; one which is first order in [OH^-], and a second which is first order in [H_3O^+], which gives way at

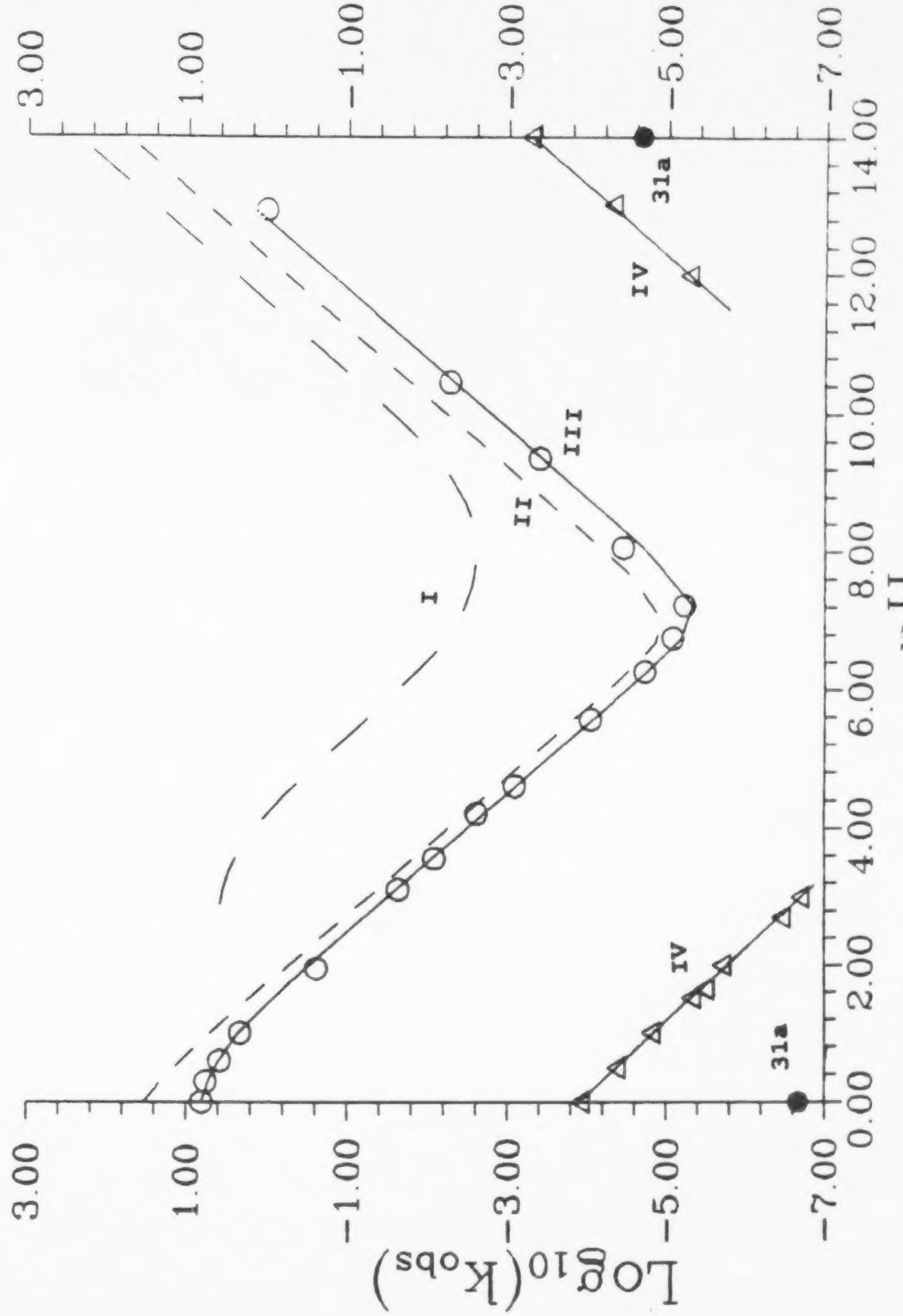

Figure 13. pH-Rate profile for the hydrolysis of I-IV and 31a.

low pH to a pH independent domain. The appearance of the profile is consistent with the mechanism given in equation 9

Table XIII. Pseudo first-order hydrolysis rate constants (k_{hyd}) for **III**, extrapolated to [buffer] = 0, T = 25 °C, μ = 1.0(KCl)[a]

pH	Buffer	$k_{hyd}(s^{-1})$[b]
0.01	HCl	6.5(0.2)
0.30	HCl	5.71(0.06)
0.60	HCl	3.86(0.02)
1.00	HCl	2.14(0.09)
1.95	HCl	0.23(0.01)[c]
3.10	formate	$2.33(0.05)\times10^{-2}$
3.55	formate	$8.3(0.2)\times10^{-3}$
4.20	acetate	$2.44(0.03)\times10^{-3}$
4.60	acetate	$8.21(0.05)\times10^{-4}$
5.56	MES	$9.18(0.08)\times10^{-5}$
6.25	MES	$1.19(0.03)\times10^{-5}$
6.75	MOPS	$8.26(0.09)\times10^{-6}$
7.22	MOPS	$5.87(0.04)\times10^{-6}$
7.60	MOPS	$7.9(0.2)\times10^{-6}$
8.06	EPPS	$3.6(0.3)\times10^{-5}$
9.35	CHES	$4.0(0.1)\times10^{-4}$
10.45	CAPS	$5.40(0.05)\times10^{-3}$
12.94	NaOH	1.08(0.04)[c]

a. pH 0.01-4.60, kinetics followed at 260 nm; pH 5.56-12.94, kinetics followed at 280 nm.

b. Numbers in parentheses are standard deviations of the mean of at least three separate determinations.

c. Calculated from Eyring plot of k_{obsd} vs T ($5^{0}C<T<48^{0}C$) at pH indicated.

$$\mathrm{P} \xleftarrow[\mathrm{H_2O}]{k_1} \mathbf{III}\text{-}\mathrm{H}^+ \underset{}{\overset{K_a'}{\rightleftharpoons}} \mathrm{H_3O^+} + \mathbf{III} \xrightarrow{k_3[\mathrm{OH}^-]} \mathrm{P} \qquad (9)$$

$$k_{hyd} = k_1\,[\mathrm{H_3O^+}]/(K_a' + [\mathrm{H_3O^+}]) \quad + \quad k_3K_w/[\mathrm{H_3O^+}] \qquad (10)$$

where P represents the amino acid product; and **III**-H^+, the protonated amide. From equation 9, the kinetic expression in equation 10 can be derived.

Non-linear least squares (NLLSQ) fitting of the k_{hyd} and $[H_3O^+]$ data of Table XIII to equation 10 yields values of $k_1 = 8\ (2)\ s^{-1}$, $k_3 = 17.2(0.6)\ M^{-1}s^{-1}$ and $K_a' = 0.28\ (0.07)$ ($pK_a = 0.56$) by assuming $K_w = 10^{-14}$; the line drawn through the data points in Figure 13 (see pg 55) is that computed on the basis of the NLLSQ fit.

Table XIV. Pseudo first-order hydrolysis rate constants (k_{hyd}) for amide **IV** at [buffer] = 0, T = 25 °C, μ = 1.0(KCl)[a,b]

pH	Buffer	$k_{hyd}(s^{-1})$
0.00	HCl	$1.207(0.003)\times10^{-4}$
0.51	HCl	$4.28(0.01)\times10^{-5}$
1.00	HCl	$1.556(0.002)\times10^{-5}$
1.50	HCl	$4.82(0.04)\times10^{-6}$
1.63	HCl	$3.3(0.2)\times10^{-6}$
2.00	HCl	$2.00(0.04)\times10^{-6}$
2.70	HCl	$3.55(0.06)\times10^{-7}$
3.00[c]	HCl	$2.056(0.004)\times10^{-7}$
12.00	NaOH	$5.3(0.1)\times10^{-6}$
13.01	NaOH	$5.12(0.02)\times10^{-5}$
13.95	NaOH	$4.94(0.05)\times10^{-4}$

---

a. pH 0.00-3.00, kinetics followed at 230 nm; pH 12.00-14.00 kinetics followed at 240 nm.
b. Numbers in parentheses are standard deviations of the mean of at least three separate determinations.
c. At pH 3.00 the kinetics were only followed to $1/2t_{1/2}$; the end point was measured as the absorbance of authentic amino acid under the same conditions.

Given in Table XIV are pseudo-first order rate constants (k_{hyd}) for hydrolysis of amide **IV** at 25 ^{0}C, $\mu = 1.0$ (KCl). Due to the slow rate of the reaction at 25 ^{0}C, the hydrolysis could only be conveniently monitored between pH 0-3, and 12-14. The data are shown on Figure 13 (see pg 55) as the triangular symbols. Attempts to follow the reaction at pH 6.20(MES), 7.12(MOPS) and 7.98(EPPS) by measuring the absorption change at $\lambda = 240$ nm every two weeks (total 97 days) were unsuccessful.

The pH/rate profile for **IV** shows two domains, one first order in [OH^-] and another, first order in [H_3O^+]. The appearance of the profile is consistent with the mechanism in equation 11 and the corresponding rate expression is given in equation 11a.

$$\begin{array}{l} \mathbf{IV}\text{-}H^+ \xrightarrow{k_1/K_a',\ H_2O} P \\ \mathbf{IV} \xrightarrow{k_3[OH^-]} P \end{array} \qquad (11)$$

$$k_{hyd} = k_1\,[H_3O^+]/K_a' + k_3K_w/[H_3O^+] \qquad (11a)$$

Linear least squares fitting of k_{hyd} of Table XIV to equation 11a gives $k_1/K_a' = 1.21(0.02)\times10^{-4}$ $M^{-1}s^{-1}$, $k_3 = 5.12(0.02)\times10^{-4}$ $M^{-1}s^{-1}$. The lines drawn through the data points in Figure 13 (see pg 55) is that computed on the basis of linear fitting.

In order to make a more complete comparison, an undistorted amide, N-methylacetanilide **31a**, was subjected to hydrolysis under acidic and basic conditions. The rates of hydrolysis of **31a** were followed by observing the rate of

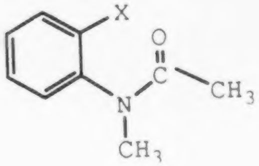

31a X = H
b X = CH_3

appearance of N-methylaniline at 255 nm at ~ pH 14 (1.077M NaOH) at five different temperatures (82.6, 74.0, 65.4, 56.8, 47.7 °C) and by observing the rate of disappearance of N-methylacetanilide at 240 nm at pH 0 (1M HCl) at four different temperatures (82.6, 73.8, 65.6, 56.5 °C). We can obtain the hydrolytic rate constants for **31a** by extrapolating from higher temperature data to 25 °C. The results are shown as the closed circles on Figure 13 (see pg 55) at pH 0 and 14.

Since the kinetic profiles for undistorted amide **31a** and distorted bicyclic amides **Ia-IV** are all shown in Figure 13 (see pg 55), it is convenient to make a comparison. Each of these amides shows at least two domains which are first order in $[OH^-]$ and first order in $[H_3O^+]$. Only amide **Ia** shows a water reaction between pH 7 and 9 which is pH independent. This may due to H_2O attack on the neutral form of amide **Ia** or its kinetic equivalent, OH^- attack on protonated amide **Ia**. Also for amide **Ia**, and two other less distorted amides **II** and **III**, there are plateau regions appearing at low pH which are attributable to H_2O attack on protonated form of the amides. The least distorted bicyclic anilide **IV** gives no evidence of a plateau at low pH.

The appearance of the profiles of amides **Ia**-**IV** and **31a** in Figure 13 (see pg 55) are consistent with a general hydrolytic mechanism in equation 12, which is an expanded form of equation 9, where P represents the product amino acid or amine + acid and **A**-H^+ represents the protonated amide without designation of the site.

$$\mathrm{P} \xleftarrow{k_1} \mathbf{A}\text{-}\mathrm{H}^+ + \mathrm{H_2O} \overset{K_a'}{\rightleftharpoons} \mathbf{A} + \mathrm{H_3O}^+ \left\{ \begin{array}{c} \xrightarrow{k_2[\mathrm{H_2O}]} \\ \\ \xrightarrow{k_3[\mathrm{OH}^-]} \end{array} \right. \mathrm{P} \qquad (12)$$

$$k_{hyd} = \frac{k_1[\mathrm{H_3O}^+]^2 + k_2K_a'[\mathrm{H_3O}^+] + k_3K_a'K_w}{[\mathrm{H_3O}^+]^2 + K_a'[\mathrm{H_3O}^+]} \qquad (13)$$

Corresponding to this mechanism, the observed k_{hyd} vs $[H_3O^+]$ expression can be deduced as shown in equation 13. For less distorted amides **II** and **III** which show no evidence of a water reaction, the rate expression can be simplified to the form given in equation 10 (see pg 56). For the least reactive amides **IV** and **31a**, which show no evidence for a kinetic pK_a' at low pH or a water reaction, the rate expression further simplifies into equation 11a (see pg 58).

Fitting the k_{hyd} vs $[H_3O^+]$ data for various amides to their corresponding equations generates the various rate and dissociation constants summarized in Table XV, the quoted errors being obtained from the standard deviations of the fit parameters.

Table XV. Rate and dissociation constants for the hydrolysis of amides **Ia**-**IV** and **31a** in H_2O, T = 25 ^{0}C, μ = 1.0(KCl)

	k_1(s^{-1})	pKa'	k_2×10^3(s^{-1})	k_3×10^4($M^{-1}s^{-1}$)	k_1/K'_a ($M^{-1}s^{-1}$)
Ia[a]	4.5(0.2)	3.71(0.05)	2.0(0.1)	2.6(0.2)×10^6 [b]2.39(0.05)×10^6	2.3(0.2)×10^4
II[a]	101(7)	-0.28(0.03)	-	60(1)×10^4 [b]62(2)×10^4	56(3)[c] 87(2)[e]
III	8(2)	0.56(0.05)	-	17(2)×10^4 [b]13.1(0.2)×10^4	30(2)[c] 33(2)[e]
IV	-	-	-	5.12(0.02) [b]5.26(0.04)	1.21(0.02)×10^{-4} [e]2.81(0.06)×10^{-4}
31a	-	-	-	0.22(0.01)[d]	[d]2.2(0.2)×10^{-7}

a. Reference 28.
b. in D_2O/OD^-.
c. Errors on k_1 and pK_a' are obtained from the fits of the k_{obsd} vs [H_3O^+] data to equation 13. Errors on k_1/K_a' obtained from linear least squares analysis of the first order section of the k_{obsd} vs [H_3O^+] plot.
d. Extrapolated to 25 ^{0}C from activation parameters in Table XVII.
e. Determined in D_2O/D_3O^+ media with pD = 2.18, then converted to 1 M [D_3O^+].

As shown in Table XV, k_3 (column 4), which represents the rate constant of base catalyzed hydrolysis for these amides, is changed by about 7 orders of magnitude when passing from the most distorted amide **Ia** to the undistorted amide **31a**.[50] The ratio k_1/K_a' (column 5), which represents the rate constant of acid catalyzed hydrolysis for these amides, differs by about 11 orders of magnitude when passing through the series **Ia→IV→31a**. Also it is of note that the acid term contains two factors: k_1 and K_a'. If the comparison is made directly on the k_1 term, then the fully protonated amide **Ia** is less reactive toward H_2O attack than are protonated amides **II** and **III** (see Table XV, column 1). However, in passing through the series **III≈II→Ia**, the corresponding kinetic pK_a' values of conjugated acid are increased (see Table XV, column 2) so that the protonated forms become more stable as distortion increases.

In D_2O media k_3 and (k_1/K_a') data were also obtained and the results are included in Table XV. From these data, the solvent kinetic isotope effects in base and acid can be derived and are shown in Table XVI.

Table XVI. Solvent kinetic isotope effects for hydrolysis of amides **Ia-IV**[a,b]

compounds	$k_3^{OH^-} / k_3^{OD^-}$	$(k_1/K_a')^{H_2O}/(k_1/K_a')^{D_2O}$ [d]
Ia	1.1(0.1)[c]	——
II	0.97(0.04)[c]	0.75(0.08)
III	1.3(0.2)	0.72(0.03)
IV	1.0(0.1)	0.89(0.02)

a. The experiments were performed at 25 °C.
b. Errors were obtained from standard deviation of individual rate constants.
c. The hydrolyses of amides **Ia** and **II** in OD^-/D_2O media were performed by Dr. A.J. Bennet and J. Kellor.
d. Comparison was made on rate constants of hydrolysis at pL = 2.18 (L H, or D).

2). Activation parameters for hydrolysis of distorted amides **Ia-IV** and N-methylacetanilide **31a**

For amides **III,IV** and **31a** the hydrolyses were carried out under both acidic and basic conditions at 5-6 different

Table XVII. Activation parameters for the hydrolysis of **Ia-IV** and **31a** in aqueous acid and base, μ = 1.0(KCl)[a]

Acid

Amide	$\Delta H^{\ddagger}$ (kcal/mol)	$\Delta S^{\ddagger}$ (e.u.)	$\Delta G^{\ddagger}_{25\,^{\circ}C}$ (kcal/mol)
Ia[b]	10.3(0.6)[c]	-22(2)	17(2)
II	6.6(0.5)[d]	-28(2)[d]	15(1)
III	6.3(0.5)[d]	-32(2)[d]	16(1)[d]
	8.0(0.5)[f]	-28(2)[f]	16(2)[f]
IV	15.96(0.08)[g]	-22.5(0.3)[g]	22.7(0.3)[g]
31a	19.7(0.4)[f]	-22.8(0.8)[f]	23(1)[f]

Base

Amide	$\Delta H^{\ddagger}$(kcal/mol)	$\Delta S^{\ddagger}$(e.u.)	$\Delta G^{\ddagger}_{25\,^{\circ}C}$ (kcal/mol)
Ia[b]	7.6(0.7)	-22(3)	14(2)
II	7(1)[e]	-26(5)[e]	15(4)[e]
III	9.1(0.4)	-23(1)	16(1)
IV	13.2(0.2)	-29.2(0.7)	21.9(0.6)
31a	11.9(0.2)	-39.8(0.5)	23.8(0.5)

---

a. 5-6 temperatures; activation parameters calculated according to Eyring equation from second order rate constants. Error limits computed according to the method described by Wiberg,K.B in reference 52.

b. Reference 53a.

c. Data of compound **31a** re-evaluated according to Eyring equation from pseudo first order rate constants at pH 3.2-three temperatures.

d. pH 2.0

e. Reference 53b.

f. pH 0.0

g. pH 1.5

temperatures. The obtained pseudo-first order rate constants (see supplementary material, Tables S1-S7, p143-145) were converted to second order ones and plotted as ln (k_2h/k_BT) vs 1/T according to the Eyring equation[51] to yield the $\Delta H^{\ddagger}$ and $\Delta S^{\ddagger}$ values. Given in Table XVII is the summary of the activation parameters for the hydrolysis of **Ia-IV** and **31a** in H_2O, $\mu = 1.0$(KCl).

D. Effects of Acetate Buffer on the Hydrolysis of **II,III** in H_2O and D_2O, T = 25 ^{0}C, $\mu = 1.0$(KCl)

It was observed that acetate buffer catalyzed the hydrolysis of **II** and **III** in both H_2O and D_2O media from pH 4-6. In order to study the effect of acetate buffer on the hydrolysis of amides **II** and **III**, acetate buffer solutions were prepared for pL (L=H,D) 3.5-6.7, $\mu = 1.0$(KCl). At each pL value, pseudo first order rate constants were evaluated in duplicate at 4 different acetate buffer concentrations (0.05-0.20 M). Listed in Table XVIII and Table XIX are experimental results for amides **II** and **III**, respectively, in which the buffer component k_{OAc} (apparent) was obtained from the slope of the plots of k_{hyd} vs $[\text{acetate}]_{total}$, and the intercept is $k_1[H_3O^+]/K_a'$, corresponding to the $[H_3{}^+O]$ catalyzed hydrolysis at [buffer] = 0.

The plots of log k_{OAc} (apparent) vs pL for acetate catalyzed hydrolysis of amide **III** in H_2O (open circle) and D_2O (closed circle), and amide **II** in H_2O (open triangle) and D_2O (closed triangle) are shown in Figure 14.

Correspondingly, the plots of log k_{hyd} (=log k_1/K_a') vs pL for amide **III** in H_2O (open circle) and D_2O (closed circle) and amide **II** in H_2O (open triangle) and D_2O (closed triangle) are shown in Figure 15.

Table XVIII. Acetate buffer catalysis of the hydrolysis of amide **II** in H_2O and D_2O, T = 25 ^{0}C, μ = 1.0(KCl).

pH[a]	k_{hyd}(s^{-1})	k_{OAc}($M^{-1}s^{-1}$)
3.75	[c]$1.05(0.01)\times10^{-2}$	$5.2(0.5)\times10^{-3}$
4.00	$7.20(0.06)\times10^{-3}$	$5.7(0.5)\times10^{-3}$
4.20	$4.33(0.06)\times10^{-3}$	$5.0(0.5)\times10^{-3}$
4.40	$2.28(0.04)\times10^{-3}$	$3.5(0.3)\times10^{-3}$
4.68	$1.40(0.05)\times10-3$	$2.9(0.3)\times10^{-3}$
4.98	$7.28(0.05)\times10^{-4}$	$1.48(0.04)\times10^{-3}$
5.30	$3.70(0.05)\times10^{-4}$	$8.8(0.4)\times10^{-4}$
5.50	$2.04(0.02)\times10^{-4}$	$5.7(0.2)\times10^{-4}$
5.72	$1.18(0.01)\times10^{-4}$	$3.25(0.06)\times10^{-4}$
6.35[d]	[e]$4.57(0.03)\times10^{-5}$	$6.6(0.2)\times10^{-5}$

pD[b]	k_{hyd}(s^{-1})	k_{OAc}($M^{-1}s^{-1}$)
3.94	$7.52(0.05)\times10^{-3}$	$1.52(0.03)\times10^{-2}$
4.70	$1.79(0.03)\times10^{-3}$	$8.5(0.3)\times10^{-3}$
4.90	$1.36(0.04)\times10^{-3}$	$3.7(0.3)\times10^{-3}$
5.12	$8.6(0.2)\times10^{-4}$	$1.8(0.2)\times10^{-3}$
5.40	$4.58(0.04)\times10^{-4}$	$1.14(0.03)\times10^{-3}$
5.70	$2.50(0.05)\times10^{-4}$	$7.1(0.5)\times10^{-4}$
5.90	$1.50(0.05)\times10^{-4}$	$5.1(0.3)\times10^{-4}$
6.70[d]	[e]$2.7(0.1)\times10^{-5}$	$1.01(0.08)\times10^{-4}$

---

a. pH was measured before and after reaction and did not deviate by more than 0.03 pH unit.

b. pD = pH (meter reading) + 0.4 unit.[54]

c. Numbers in parentheses are standard deviations of the mean of at least three separate determinations.

d. The buffer of pH > 6 was prepared by adding 5 mM of MES.

e. The data were obtained in MES buffers and extrapolated to zero [MES].

Table XIX. Acetate buffer catalysis of the hydrolysis of amide **III** in H_2O and D_2O, T = 25 ^{0}C, $\mu = 1.0$(KCl).

pH[a]	$k_{hyd}(s^{-1})$	$k_{OAc}(M^{-1}s^{-1})$
3.58	[d]$7.93(0.05)\times10^{-3}$	$4.4(0.4)\times10^{-3}$
3.84	$4.54(0.04)\times10^{-3}$	$3.9(0.3)\times10^{-3}$
4.20	$2.44(0.03)\times10^{-3}$	$2.6(0.2)\times10^{-3}$
4.40	$1.19(0.01)\times10^{-3}$	$2.40(0.08)\times10^{-3}$
4.68	$8.21(0.05)\times10^{-4}$	$1.90(0.03)\times10^{-3}$
4.98	$3.48(0.04)\times10^{-4}$	$1.12(0.03)\times10^{-3}$
5.30	$1.69(0.04)\times10^{-4}$	$7.3(0.2)\times10^{-4}$
5.58	$8.5(0.1)\times10^{-5}$	$3.99(0.09)\times10^{-4}$
6.35[c]	[f]1.44×10^{-5}	[e]5.20×10^{-5}

pD[b]	$k_{hyd}(s^{-1})$	$k_{OAc}(M^{-1}s^{-1})$
3.94	$5.44(0.04)\times10^{-3}$	$4.7(0.3)\times10^{-3}$
4.35	$2.21(0.02)\times10^{-3}$	$2.9(0.2)\times10^{-3}$
4.70	$1.00(0.01)\times10^{-3}$	$1.61(0.04)\times10^{-3}$
4.90	$7.2(0.1)\times10^{-4}$	$1.37(0.07)\times10^{-3}$
5.12	$4.03(0.04)\times10^{-4}$	$1.19(0.03)\times10^{-3}$
5.40	$2.12(0.02)\times10^{-4}$	$8.0(0.2)\times10^{-4}$
5.70	$1.12(0.01)\times10^{-4}$	$5.61(0.07)\times10^{-4}$
5.90	$7.1(0.1)\times10^{-5}$	$3.59(0.01)\times10^{-4}$
6.70[c]	$1.31(0.03)\times10^{-5}$	[e]$7.0(0.2)\times10^{-5}$

---

a. pH was measured before and after reaction and did not deviate by more than 0.03 pH units

b. pD = pH (meter reading) + 0.4 unit.[54]

c. The buffer of pH > 6 was prepared by adding 5 mM of MES.

d. Numbers in parentheses are standard deviations of the mean of at least three separate determinations.

e. The data were obtained in MES buffers and extrapolated to zero [MES].

f. Calculated data from pH rate profile.

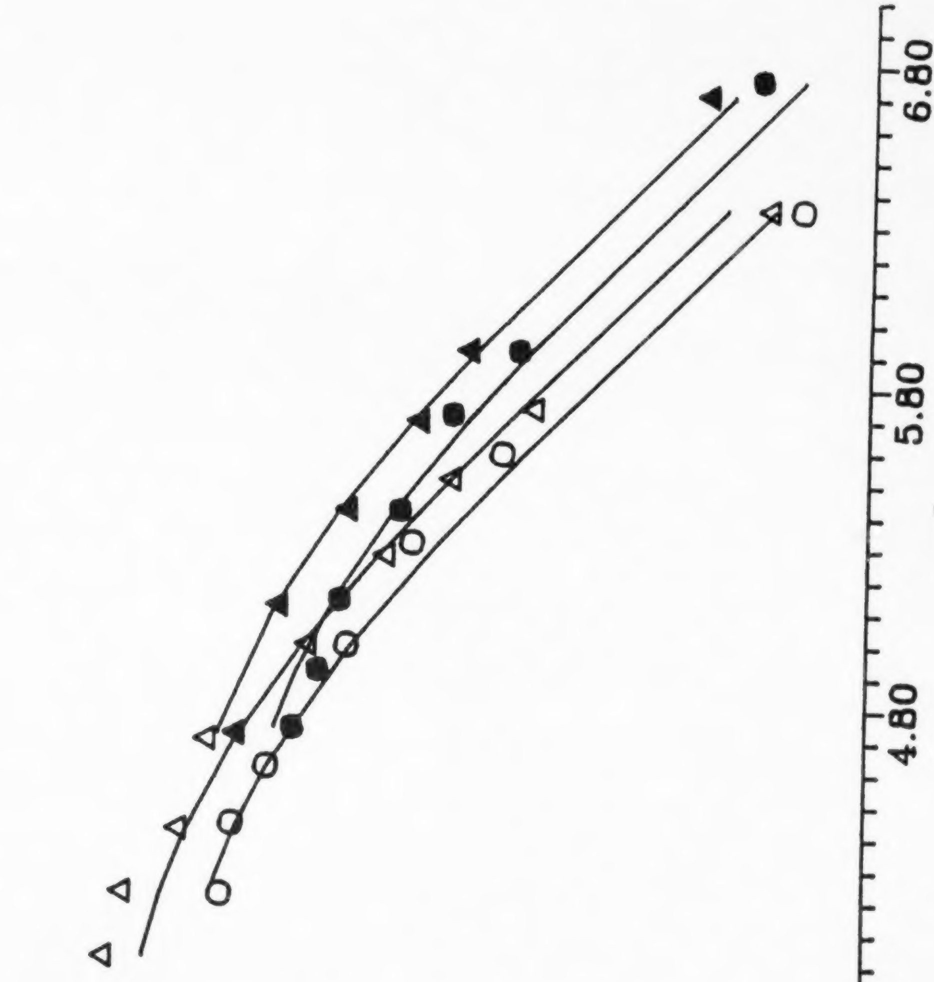

Figure 14. Plots of log k_{OAc} (apparent) vs pL for the hydrolysis of **II** (Δ) and **III** (O) in H_2O and D_2O media T = 25 ^{0}C, μ = 1 (KCl) closed symbols, D_2O.

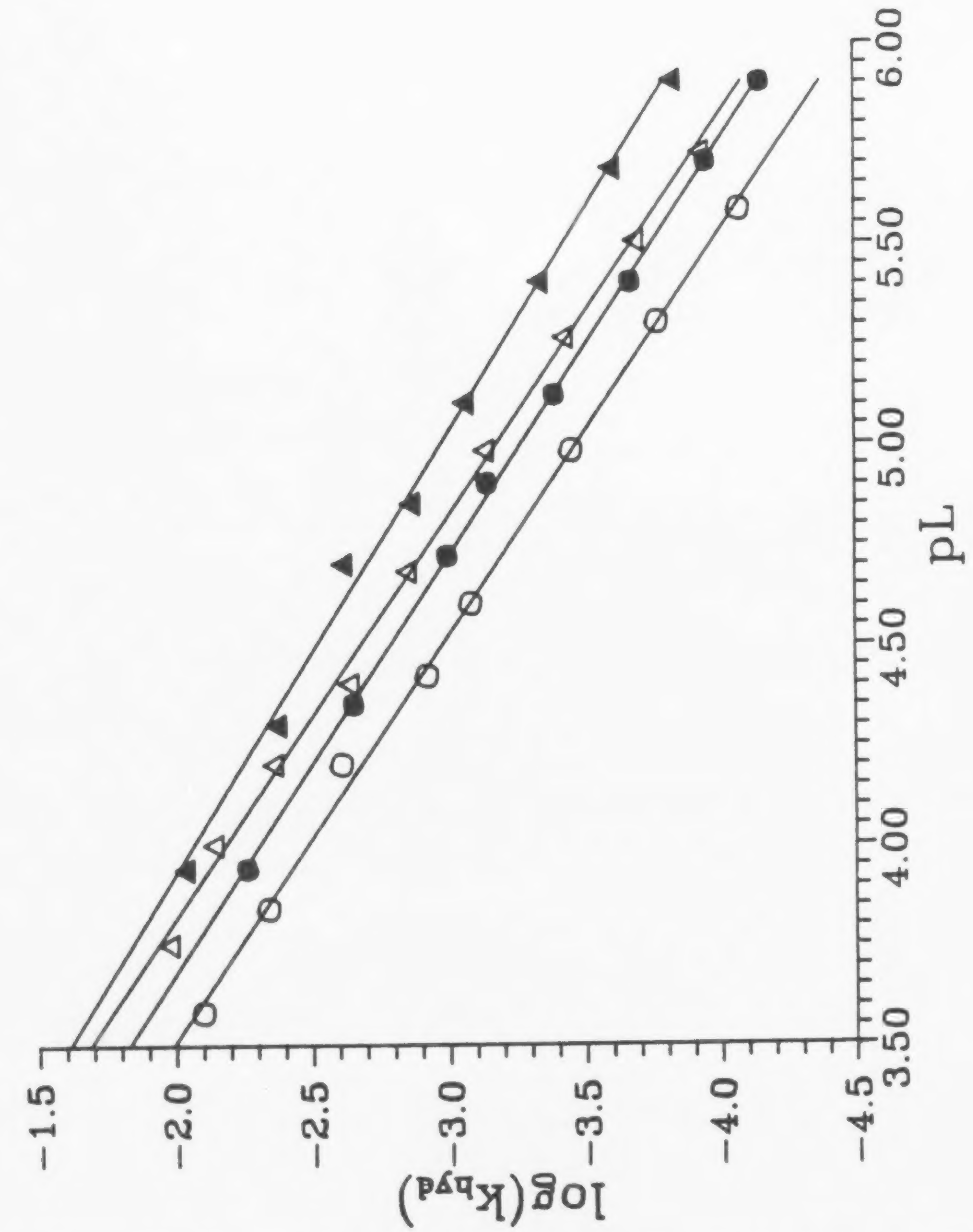

Figure 15. Plots of log k_{hyd} vs pL for the hydrolysis of II (Δ) and III (O) derived from the intercepts of plots of k_{hyd} vs $[acetate]_{total}$ at various pL values in H_2O and D_2O media T = 25 ^{0}C, $\mu = 1$ (KCl) closed symbols, D_2O.

From Figure 14, it appears that log k_{OAc} plateaus when pL is below the pK_a of LOAc (L=H,D) and in this region the reactivities of both **II** and **III** in H_2O are greater than those in D_2O. The results shown in Figure 15 indicate an inverse solvent isotope effect for both amides when no buffer is present.

The data shown in Figures 14 and 15 suggest that both acetate and water acts as general bases in deprotonating L_2O for attack on **A**-L^+. The corresponding mechanism is shown in equation 14. From equation 14 the kinetic expression as shown in equation 15 can be derived. In equation 15, K_a and

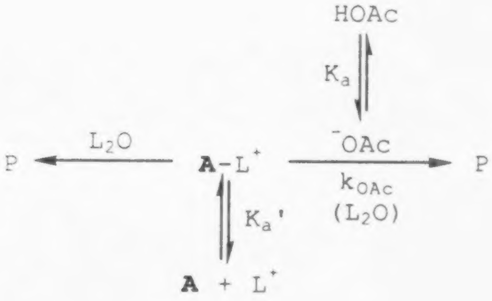

(14)

$$k_{hyd} = \frac{k_1}{K_a'}[L^+] + \frac{k_{OAc}}{K_a'}\left(\frac{K_a[L^+]}{[L^+] + K_a}\right)[\text{acetate}]_{total} \qquad (15)$$

K_a' are the acid dissociation constants for LOAc and **A**-L^+ respectively.

Non-linear least squares fitting of the data of k_{OAc} (apparent) shown in Tables XVIII,XIX to the second term of equation 15 gives the constants of $k_{OAc}K_a/K_a'$ and K_a. Since the dissociation constant of LOAc (K_a) is known[55] at $\mu = 0$ and can be corrected[55] to an ionic strength of 1.0($K_a[H_2O] = 2.818\times10^{-5}$; $K_a[D_2O] = 8.913\times10^{-6}$), the constant k_{OAc}/K_a' can be calculated, the results being shown in Table XX. For the zero [acetate], k_1/K_a' corresponds to the slope of the log k_{hyd} vs pL plot (Figure 15). The solvent KIE values on k_1/K_a' at pL 4.8 are calculated and also included in Table XX.

Table XX. Rate constant data for the effect of acetate on the hydrolysis of **II** and **III** in H_2O and D_2O, T = 25.0 ^{0}C, μ = 1.0(KCl)

Amide	$k_{OAc}/K_a'^{a}$		$(k_{OAc}/K_a')^{H_2O}/(k_{OAc}/K_a')^{D_2O}$	$(k_1/K_a')^{H_2O}/(k_1/K_a')^{D_2O}$
	H_2O	D_2O		
II	143±7	298±18	0.48±0.08	0.63±0.05
III	197±11	429±45	0.5±0.1	0.62±0.03

a. Evaluated from non-linear squares fitting of the data used to construct Figure 14 to the second term of equation 15. K_a fixed at the apparent values for LOAc, $\mu = 1.0$; pK_a (H_2O) = 4.55; $pK_a(D_2O)$ = 5.05. Errors quoted from the NLLSQ fits.

b. Evaluated at pL = 4.8 from data used to construct Figure 15.

E. The Study of the Position of Kinetic Methylation of Distorted Amides III and IV with MeOTf

The methylation of distorted amide **III** by methyl trifluoromethanesulfonate was monitored by ^1H-NMR spectrometry. The process is shown in equation 16.

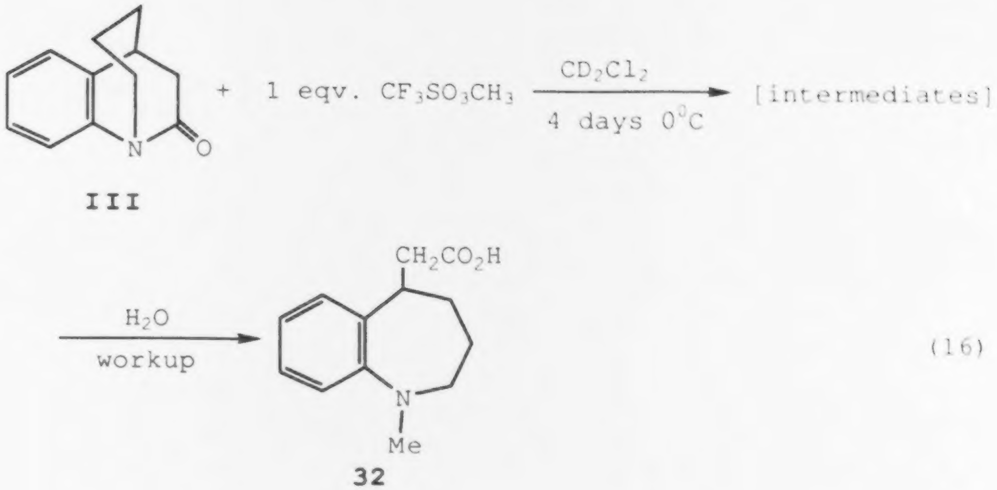

(16)

During the reaction, a new singlet peak at δ 3.65 ppm in the ^{1}H-NMR spectrum appears, which corresponds to a methyl group on a nitrogen or an oxygen. After workup, the product shows $M^{+\cdot}$ 219.1255 in the mass spectrum corresponding to formula $C_{13}H_{17}NO_2$ and a singlet at δ2.82 in the ^{1}H-NMR spectrum, which may be attributable to the N-methyl product.

Also, there is a small amount of N-methyl-5-(methoxycarbonylmethyl)benzazepine as shown by ^{1}H-NMR and mass spectroscopy ($M^{+\cdot}$ 233 for $C_{14}H_{19}NO_2$), which might result from the esterification of the formed product **32** by MeOH which produced by hydrolysis of methyl trifluoromethanesulfonate.

The identity of the methylation product was further confirmed by synthesizing the authentic compound N-methyl-5-(hydroxycarbonylmethyl)benzazepine **32** as shown in equation 17. The comparison was based on ^{1}H-NMR and mass spectra.

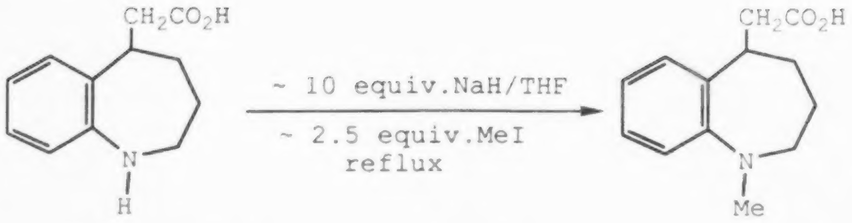

26 **32**

(17)

The methylated product **32** had the same pattern in the NMR spectrum as that of the authentic sample of **32**. The mass spectrum of **32** had the same molecular mass peak and relative intensity of fragments as that of the authentic sample. Therefore, for amide **III**, the kinetic methylation position must be on nitrogen.

The reaction of distorted amide **IV** with methyl trifluoromethanesulfonate was also studied. Two new singlet peaks appeared at 4.56 and 3.50 ppm in the ^{1}H NMR spectrum during the reaction with the former having a 15 times larger intensity than the latter. After all of the methyl trifluoromethanesulfonate was consumed, the reaction was terminated by the addition of water. The process is shown in equation 18.

The product was isolated by the addition of water and saturated $NaHCO_3$ and extracted with 3×5 mL of CH_2Cl_2. The obtained product was confirmed by ^{1}H NMR and mass spectra to be 5-(methoxycarbonylethyl)-2,3,4,5-tetrahydrobenzazepine **33**

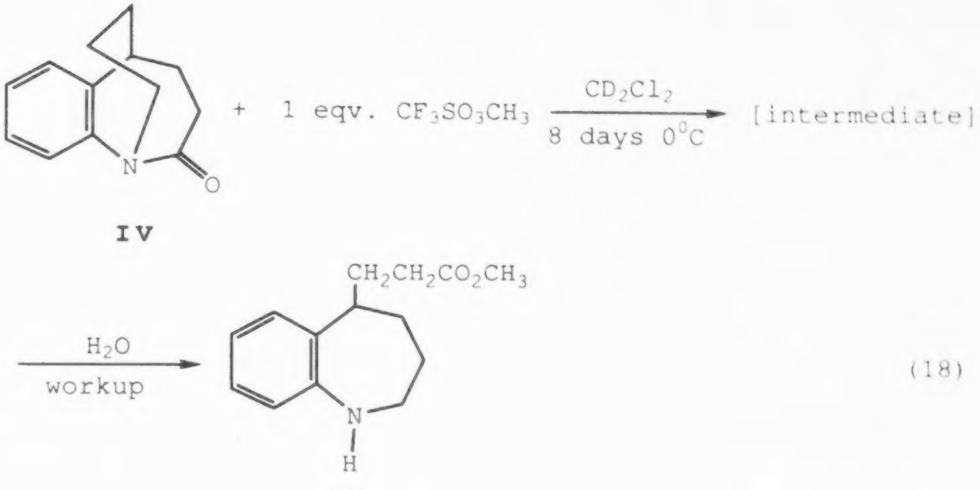

IV

33

(18)

(δ OCH_3 = 3.62). The remaining aqueous layer was then neutralized with dilute HCl and the pH of the solution was adjusted to 5, but no product was obtained after further extraction with 3×5 mL of CH_2Cl_2. Since two new peaks in the ^1H-NMR spectrum (δ 4.56 and 3.50) appear during the reaction course, two products were expected. However, after workup, only product **33** was isolated, which arises from the intermediate having the peak of δ 4.56. Therefore, the peak at δ 3.50 might come from methanol which is formed from the reaction of MeOTf with adventitious H_2O in the solution.

Also as in the case of amide **III**, a small amount of methylation on both nitrogen and oxygen was observed from ^1H-NMR and mass spectrum ($M^{+\cdot}$ 247 for $C_{15}H_{21}NO_2$).

In order to further confirm the product obtained by the methylation of distorted amide **IV**, the authentic ester **33** was prepared as shown in equation 19. The authentic sample shows an identical ^{1}H-NMR spectrum and the same pattern and relative intensities in the mass spectrum as the kinetic methylation product. Thus, the kinetic methylation position for amide **IV** is on oxygen.

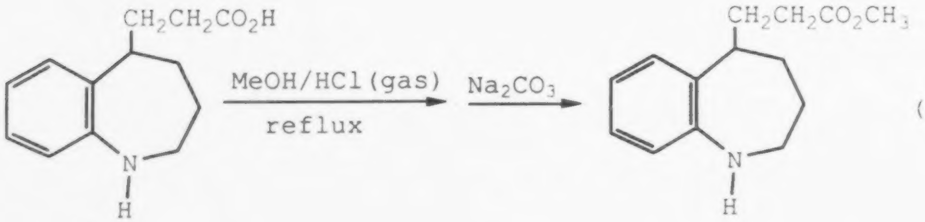

28 **33** (19)

F. Preparation of the Optically Active Amide 1,4-propano-3,4-dihydro-2-oxoquinoline III

Encouraged by H.C.Brown's successful addition of a chiral borane compound to an alkene,[56] an attempt was made to prepare the chiral amide **III** by the reaction of **23a** or **b** with the chiral borane which would produce the chiral saturated ester as shown in equations 20 and 21.

However, all such efforts were unsuccessful. Only the starting material and a mixture of double bond isomerized compounds were recovered.

We also tried to resolve the enantiomers of precursors for chiral amide **III** by using a column containing a chiral

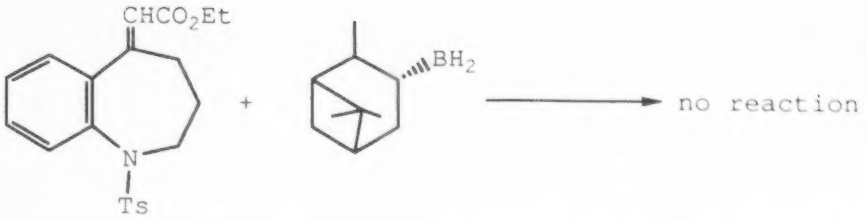
CHCO$_2$Et
N
Ts
BH$_2$
+
no reaction

23a(E-)

(20)

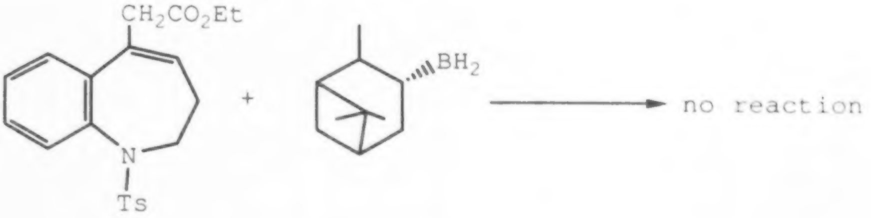
CH$_2$CO$_2$Et
N
Ts
BH$_2$
+
no reaction

23b

(21)

packing material. A 10μ 25×21.1 mm id chiral DPG (dinitrophenylglycine) HPLC column[57] was used to attempt to resolve the racemic compounds. The active component of the chiral DPG HPLC column is shown in structure **34**. The experiments were performed with a Hewlett Packard 1081A High Performance Liquid Chromatography system. With several selected derivatives (see the experimental section, Table XXVII), no separation was achieved under these conditions.

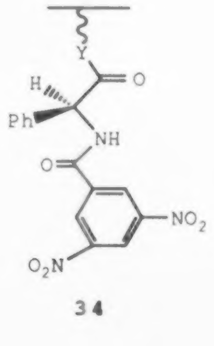
Y
O
H
Ph
NH
O
NO$_2$
O$_2$N

34

The reason for the lack of separation is probably that there is not enough interaction occurring between the chiral DPG column material and the system of interest to obtain chiral recognition.

Finally, the optically active amide **III** was prepared as shown in Scheme 4.

Carboxylic acid **25** was converted to acyl chloride **35**, which was directly reacted with anhydrous quinine (dried by heating at 80 ^{0}C under vacuum for 24 h) in benzene/Et_3N. Two diastereoisomers **36a** and **36b** were produced. Attempts were made to separate these two diastereoisomers on a MPLC (medium pressure liquid chromatography) RP-8 column with different solvent ratios of methanol and water, but no separation was achieved. However, these two isomers can be separated by a KC8F octyl reverse phase preparative TLC (200μ, 20×20 cm) using 60% ethanol as an eluant. The high R_f isomer **36b** was obtained pure; rechromatography of this material by reversed phase TLC gave only one spot.

The high R_f isomer **36b** was hydrolyzed to give chiral acid **37**. The specific rotation of the optically pure acid **37** was determined to be $[\alpha]_{Hg}^{25} = -0.300$ (c = 0.069 g/mL, $CHCl_3$, 365 nm).

From this chiral acid **37** was prepared chiral amide **III** by the removal of the tosyl group followed by the same cyclization method as used for the preparation of the racemic amide (see Scheme 2, pg 35).

Scheme 4

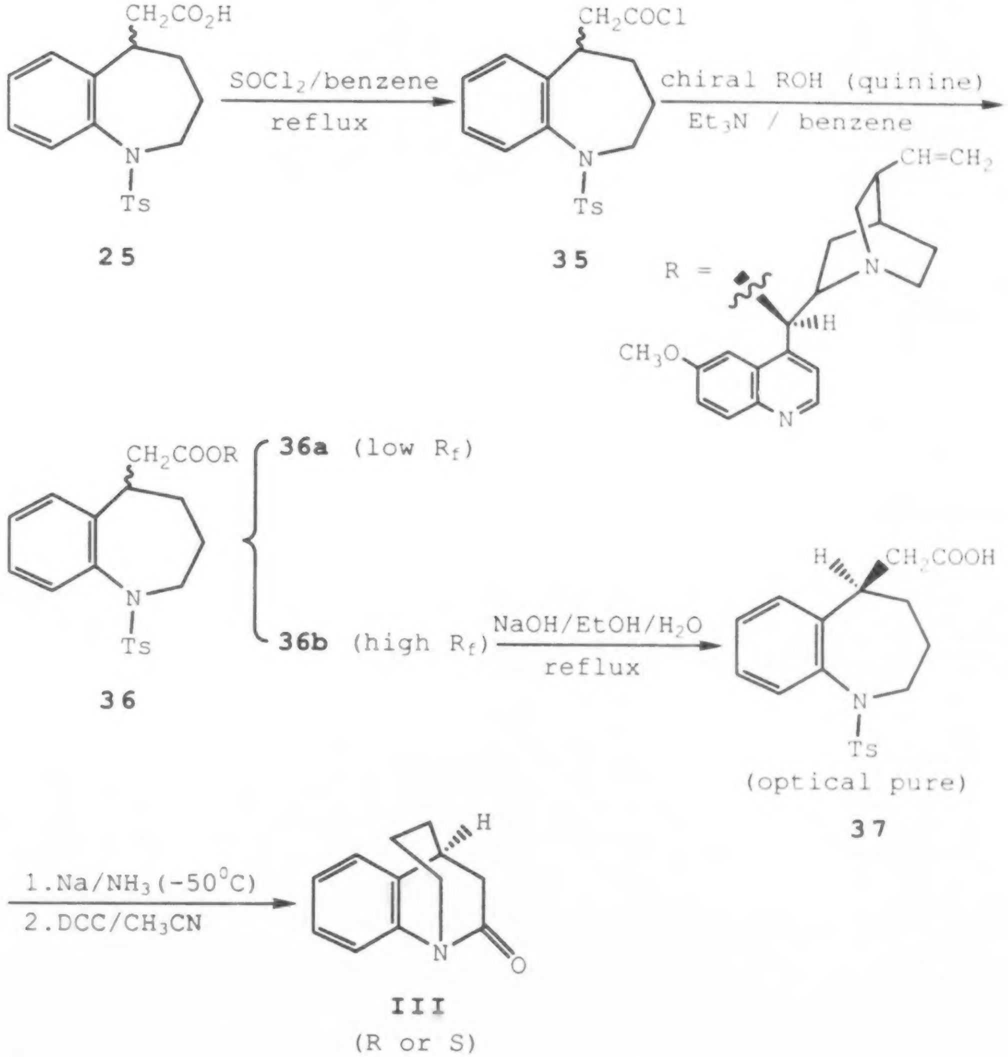
CH_2CO_2H
N
Ts
25
$SOCl_2$/benzene
reflux
CH_2COCl
N
Ts
35
chiral ROH (quinine)
Et_3N / benzene
R =
$CH=CH_2$
N
H
CH_3O
N
CH_2COOR
N
Ts
36
36a (low R_f)
36b (high R_f)
NaOH/EtOH/H_2O
reflux
H
CH_2COOH
N
Ts
(optical pure)
37
1.Na/NH_3(-50°C)
2.DCC/CH_3CN
H
N
O
III
(R or S)

No attempt was made to determine the absolute configuration of chiral amide **III** by x-ray diffraction determination.

In order to determine the enantiomeric purity of chiral amide **III**, the NMR spectrum of racemic amide **III** with the chiral lanthanide shift reagent (+)-Eu(facam)$_3$ **38** was tried.

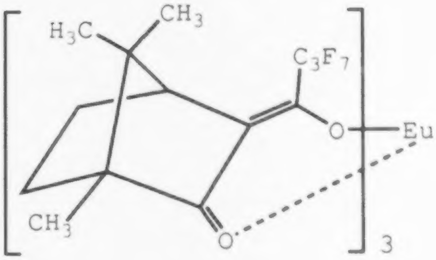

38

The chemical shifts of various protons of amide **III** were tracked through a series of 200 MHz ^{1}H NMR spectra of 10-20 mg of **III** in $CDCl_3$ containing successive additions of shift reagent dissolved in $CDCl_3$. The only useful proton signals for integration were those at δ 3.92 for the CH_2 attached to nitrogen since these are well separated from other signals. Unfortunately, no significant separation was observed in the ^{1}H-NMR spectrum after the addition. No attempt was made to try other chiral shift reagents. It was felt that rather than invest more time in determining the absolute configuration, the kinetic study would be initiated in order to determine whether chiral **III** exhibited different reaction rates with the two enantiomers of a nucleophile.

G. Kinetic Studies of Chiral Amide **III** with Various Ephedrines

The reaction rates were followed spectrophotometrically at λ = 285 nm. All the buffers with ephedrine diastereoisomers (the structures of which are shown below) were prepared at different concentrations, μ = 1.0 M(KCl) in 2% ethanol aqueous solutions using triply distilled water. The ethanol was required to increase the solubility of ψ-ephedrine in water. The results are listed in Tables XXI, and XXII.

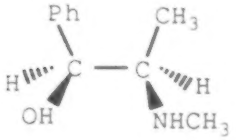
(1S 2R)-(+)-ephedrine

39

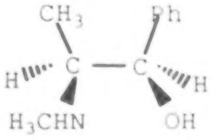
(1R 2S)-(-)-ephedrine

40

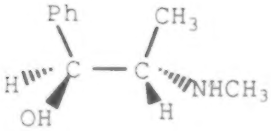
(1S 2S)-(+)-ψ-ephedrine

41

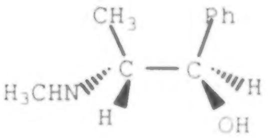
(1R 2R)-(-)-ψ-ephedrine

42

The second order rate constants for reaction of chiral amide **III** with various ephedrine diastereoisomers can be calculated by linear least squares treatment of the slopes

Table XXI. Pseudo first-order rate constants for the reaction of chiral amide **III** with (+)-ephedrine and (-) ephedrine (**39,40**)[a]

Buffer[b] (M)	pH[c]	$k_{obsd}(s^{-1})$
0.075 (+)-ephedrine	9.55	$8.93(0.07)\times10^{-4}$
0.050 (+)-ephedrine	9.54	$6.8(0.2)\times10^{-4}$
0.025 (+)-ephedrine	9.54	$5.6(0.2)\times10^{-4}$
0.075 (-)-ephedrine	9.56	$8.7(0.1)\times10^{-4}$
0.050 (-)-ephedrine	9.54	$6.93(0.06)\times10^{-4}$
0.025 (-)-ephedrine	9.54	$5.40(0.01)\times10^{-4}$

a. Reactions were conducted at 25.0±0.2 °C. The concentration of **III** was 2.67×10^{-4} M.
b. buffers were made up in 2% (98%) ethanol in triply distilled water, $\mu = 1.0$(KCl).
c. pH was measured before and after reaction and did not deviate by more than 0.03 pH unit.

Table XXII. Pseudo first-order rate constants for the reaction of chiral amide **III** with (+)-ψ-ephedrine and (-)-ψ-ephedrine (**41,42**)[a]

buffer[b] (M)	pH[c]	$k_{obsd}(s^{-1})$
0.1 (+)-ψ-ephedrine	9.67	$1.69(0.05)\times10^{-3}$
0.075 (+)-ψ-ephedrine	9.67	$1.47(0.03)\times10^{-3}$
0.050 (+)-ψ-ephedrine	9.66	$1.29(0.06)\times10^{-3}$
0.025 (+)-ψ-ephedrine	9.65	$9.76(0.08)\times10^{-4}$
0.1 (-)-ψ-ephedrine	9.67	$1.67(0.02)\times10^{-3}$
0.075 (-)-ψ-ephedrine	9.67	$1.43(0.03)\times10^{-3}$
0.050 (-)-ψ-ephedrine	9.66	$1.14(0.06)\times10^{-3}$
0.025 (-)-ψ-ephedrine	9.65	$9.50(0.08)\times10^{-4}$

a. Reaction conducted at 25.0±0.2 °C. The concentration of **III** was 2.67×10^{-4} M.
b. buffers were made up in 2% (98%) ethanol in triply distilled water, $\mu = 1.0$(KCl).
c. pH was measured before and after reaction and did not deviate by more than 0.03 pH unit.

of the plots of k_{obsd} vs [ephedrine]. Table XXIII contains the summary of these results.

From the data shown in Table XXIII, there is no difference in the rate constants between the two sets of enantiomers (e.g.**39,40**; or **41,42**) reacting with chiral amide **III** within experimental error. For (+)-ψ-ephedrine (**41**) and (-)-ψ-ephedrine (**42**), the extrapolated rate constant k_1 for water attack on chiral amide **III** is slightly out of the error range for some unknown reason. Since it is not associated with an effect of ephedrine, we need not to consider it here. However, there is a difference in the k_2 rate constants when chiral amide **III** was reacted with different diastereoisomers (e.g. **39,41**; or **40,42**). From the data of dissociation constants of ψ-ephedrine and

Table XXIII. Rate constant data for the reactions of ephedrine diastereoisomers with chiral amide **III**[a]

Buffer[b]	pH[c]	k_1 (s^{-1})[d]	k_2 ($M^{-1}s^{-1}$)[e]
(+)-ephedrine	9.55	$3.9(0.3)\times10^{-4}$	$6.2(0.5)\times10^{-3}$
(-)-ephedrine	9.55	$3.74(0.08)\times10^{-4}$	$6.5(0.2)\times10^{-3}$
(+)-ψ-ephedrine	9.67	$7.7(0.4)\times10^{-4}$	$9.3(0.5)\times10^{-3}$
(-)-ψ-ephedrine	9.67	$6.8(0.3)\times10^{-4}$	$9.8(0.4)\times10^{-3}$

---

a. Reaction conducted at 25.0±0.2 °C. The concentration of **III** was 2.67×10^{-4} M.

b. All the buffers were prepared in the same way.

c. pH was measured before and after reaction and did not deviate by more than 0.03 pH unit.

d. Calculated by linear least squares treatment as the intercept of the plots of k_{obs} vs [ephedrine].

e. Calculated by linear least squares treatment as the slope of k_{obs} vs [ephedrine].

ephedrine,[58] it is found that the pK_a of ψ-ephedrine (10.14 at 10 °C) is 0.18 unit higher than that of ephedrine (9.96 at 10 °C). Therefore, one might expect that some of the difference in the rate constants for both diastereoisomers of ephedrines (**39** or **40** vs **41** or **42**) might result from the ΔpK_a. Somayaji et al[30] determined a Bronsted constant of $\beta = 0.720 \pm 0.008$ for reactions of β-aminoalcohols with distorted amide **II**. If we assume this β for amide **III**, then a difference of ~ $\beta \times \Delta pH = 0.72 \times 0.12 = 0.09$ in log k_2 should be obtained, which contributes ~ 23% ($\Delta k_2/k_2 = 10^{0.09} - 1 = 0.23$) difference in rate constants. Therefore, the remaining ~ 25% difference in k_2 might result from diastereomeric preference.

3. DISCUSSION

A. Molecular Structures of **Ia-IV** and **29**

The structures of the bicyclic amides **Ia-IV** give continuous changes in the degree of distortion about the amide (N-C=O) linkage. As seen from Table XI (pg 52), when compared with undistorted amide **29**, the distortion in bicyclic amides **IV-Ia** manifests itself in lengthening of the N-C(O) bond, increasing N pyramidalization (χ_N[47], tilt angle[31]) and twisting about the N-C(O) bond (τ'[47], twist angle[31]). However, accompanying the molecular deformation is a slight change in the C=O bond length and small amount of pyramidalization of the carbonyl carbon.

In the conventional view of amide resonance shown in equation 22, charge is transferred from nitrogen to oxygen, reducing the C=O bond order, and increasing the C-N bond order. The calculated data for formamide presented by Wiberg and Laidig[48] (see Table XII, pg 54) shows that the C-N bond length increases 0.08 Å on going from a planar conformer **30a** to an orthogonal conformer **30b**, suggesting that there is some C-N double bond character in the planar conformer.

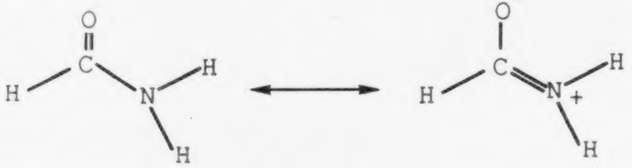

(22)

However, the C=O bond length decreases only 0.01 Å. This suggests that the carbonyl is relatively unaffected by the rotation. Based on the atomic population analysis of Bader,[49] Wiberg and Laidig[48] have provided the atomic charge density data for formamide **30**. It was calculated that the electron population at N in **30a** is larger than in **30b**, just the opposite of what would be expected on the basis of a simple resonance model. The population at oxygen is only slightly affected, and most of the charge transfer occurs between carbon and nitrogen instead of nitrogen to oxygen as would be predicted by the resonance model. Also of note is a marked change in geometry at the nitrogen between the two conformers.[48] In the planar conformer **30a**, the bond angles about the nitrogen are all ~120°, corresponding to sp^2 hybridization. In the orthogonal conformer **30b**, the angles are ~105°, corresponding roughly to sp^3 hybridization. Wiberg and Laidig[48] concluded that amidic resonance which involves N→O charge transfer does not exist, and the structural properties stem from N rehybridization that accompanies rotation about the N-C(O) bond.

Although the experimental structural data for **II-IV** and **29** (see Table XI, pg 52) compare favorably with that predicted[48,49] for planar and orthogonal formamide, they provide no information concerning the changes in electronic distribution accompanying N-C(O) bond rotation.

B. Hydrolysis of **Ia-IV** and **31a**

The enhancement of hydrolysis of **Ia-IV** in both acid and base (see Table XV, pg 61) is attributed to the structural distortion. Under acidic conditions, passing from undistorted amide **31a** to distorted amides **IV→III→II→Ia**, there is roughly an 11 orders of magnitude enhancement in the complex rate constant k_1/K_a' (Table XV). It is obvious that this kind of acceleration consists of two factors. One is the rate constant of water attack on **A**-H^+ (k_1), and another the extent to which the amide is protonated at a given $[H_3O^+]$ (K_a'). The more distorted amides (**Ia-III**) show evidence of a kinetic pK_a' for **A**-H^+ which has been interpreted as coming from on an N-protonated form (the rationale for this will be given later in section D). Also from Table XV, it is found that the most distorted amide **Ia** has a higher kinetic pK_a' (3.71) than the less distorted amides **II** ($pK_a' = -0.28$) and **III** ($pK_a' = 0.56$). Therefore at a given $[H_3O^+]$, the distorted amides are more extensively protonated than are less distorted or undistorted amides. If one compares the rate constant of H_2O attack on **A**-H^+ (k_1) for distorted amides **Ia-III**, it is noticed that when fully protonated, the most distorted amide **Ia** is more stable and less reactive toward H_2O attack than are fully protonated amides **II** or **III**.

The solvent kinetic isotope effects (SKIE) on k_1/K_a' for amides **II-IV** are 0.75, 0.72, 0.89, respectively, indicating an inverse kinetic isotope effect. This is consistent with the mechanism shown in equation 12 (see pg 60) and also suggests amides **II** and **III** have earlier transition states for H_2O attack than does amide **IV**, since the latter is less distorted and more stable in its ground state than are amides **II** and **III**.

In base, all the anilides **Ia**-**IV** and **31a** are hydrolyzed by pathways that are first order in $[OH^-]$ (as shown in equation 12, pg 60). As judged from the second order rate constant k_3 (see Table XV), there is roughly 7 orders of magnitude difference in the rate constants passing from **31a** to **Ia**. In an earlier study, Somayaji and Brown[28] failed to detect any ^{18}O=C carbonyl exchange in base. Therefore they interpreted the mechanism of hydrolysis in basic media as shown in equation 23 where the rate limiting step is the irreversible attack of OH^-. However, such ^{18}O-exchange data should be interpreted very cautiously for these bicyclic anilides because their structures do not allow symmetrization of the two oxygen even if there is rapid ^{16}O/ O^{18} proton transfer. Nevertheless, all these distorted amides **Ia**-**IV** have ground-state destabilization, so the rate

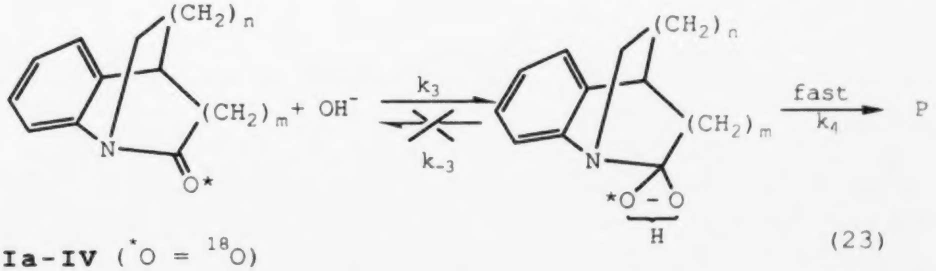

(23)

Ia-IV ($^*O$ = ^{18}O)

limiting step for their hydrolysis in base is probably OH^- attack (see equation 23).

Additional information related to the mechanism of hydrolysis comes from the solvent kinetic isotope effects (SKIE). Anilides **Ia-IV** show SKIE for OL^- attack ranging from 0.97-1.31 (see Table XVI, pg 62, no ordering in the series), which is consistent with a rate-limiting OH^- attack step. The SKIE calculated by fractionation factor analysis for this mechanism is close to unity as shown in Scheme 5.[60]

Scheme 5[a]

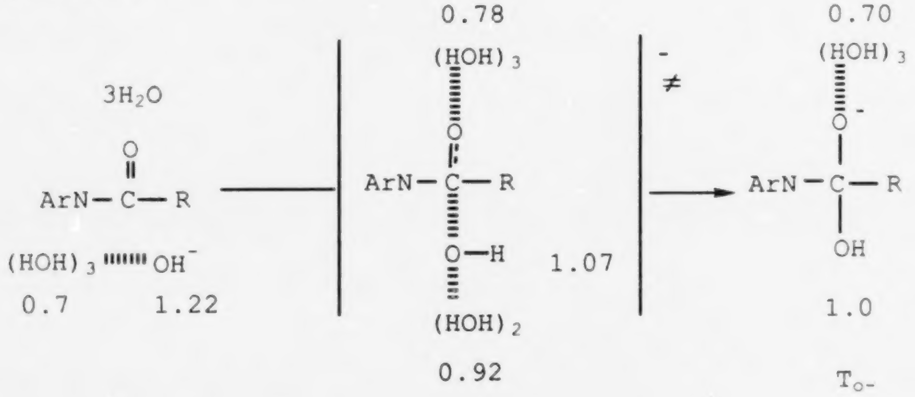

$k_D/k_H = \Pi_{\phi j}{}^{TS}/\Pi_{\phi i}{}^{GS}$ where ϕ = fractionation factor for various species.

Therefore, calculated value: SKIE $\cong$ 0.98

a. The numerical data shown in Scheme 5 are fractionation factors (ϕ),[59] which are defined as below:

$$MH + SD \xrightleftharpoons{K} MD + SH$$

$$K = \phi = (X_{MD}/X_{MH})/(X_{SD}/X_{SH})$$

T.S. is assumed to be 70% along reaction coordinate, and at T.S. one solvating L_2O is removed from OL^- to allow attach.

Therefore, the near-unity value of SKIE for amides **Ia-IV** is due to desolvation of the attacking lyoxide which is compensated by solvation of developing alkoxy anion at the transition state as shown in Scheme 5. There are other examples of base catalyzed amide hydrolysis with similar SKIE's that suggest a commonality of mechanism. For example, toluamides **43a,b**[60] and **c**,[34] each have SKIE's for the OL^- attack rate constants near unity, the respective values being 0.90±0.15; 0.92±0.05; and 0.90±0.08.

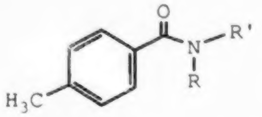

43a $R=R'=CH_3$
b $R,R'=(CH_2)_4$
c $R=Et; R'=CH_2CF_3$

The SKIE reported by Gani and Viout[61] for OL^- attack on **31a** is $k_{OH^-}/k_{OD^-} = 1.16$ in L_2O at 76.7 °C in the presence of 1 M NaOL. They suggested that the rate limiting step for base catalyzed hydrolysis is the decomposition of the anionic tetrahedral intermediate. If the hydrolysis of **31a** in base follows this mechanism, an ^{18}O-isotopically substituted **31a** should show a large amount of ^{18}O-exchange accompanying of its hydrolysis. Deslongchamps et al[62] have reported that **31a** shows a considerable amount of ^{18}O-exchange when it is submitted to hydrolysis in base at temperatures between 27 and 90 °C. Although the Deslongchamps' study provides adequate evidence of ^{18}O-exchange for **31a**, there were not sufficient data presented to determine a k_{ex} value accurately. Therefore we repeated an ^{18}O-exchange experiment with ~50% ^{18}O-labelled **31a**. The experimental results are listed in supplementary material (Table S8) in detail; the final results are given in Table XXIV.

Table XXIV. ^{18}O-exchange results for amide **31a**[a,b]

t (min)	0	12	24	48
%^{18}O-content (recovered)	48.4(0.4)	42.1(0.3)	36.4(0.4)	28.1(0.5)

a. The experiment was performed at 74.0(0.5) ^{0}C, $[OH^{-}]=1.077$ M.
b. k_{hyd} at 74.0 ^{0}C is $4.81(0.03)\times10^{-4}$ s^{-1} at $[OH^{-}]=1.077$ M.

From Table XXIV, we can obtain $k_{ex} = 1.89(0.05)\times10^{-4}$ s^{-1}; thus $k_{ex}/k_{hyd} = 0.39 \pm 0.01$. Therefore, the tetrahedral intermediate formed from **31a** during base catalyzed hydrolysis is reversibly formed, and the rate-limiting step is not OH^{-} attack on the amide such as is the probable case for amides **Ia-IV**. One must also conclude that the reported[61] SKIE of 1.16 for **31a** does not corresponded to one kinetic step, but to those of an anionic tetrahedral intermediate[63] that has almost the same energy to go back to the starting material and go forward to the product (a "virtual transition state"). Thus, the data for **31a** cannot be compared to the SKIE data for **Ia-IV**, which probably pertain exclusively to the k_3 step (see the explanation above).

C. Activation Parameters for the Hydrolysis of **Ia**-**IV** and **31a**

In order to more fully understand the factors which are responsible for the rate enhancement caused by distortion, the activation parameters for the hydrolysis of **Ia**-**IV** and **31a** in both acid and base were obtained and are listed in Table XVII (see pg 63).

In acid, comparing a general domain for all amides which is first order in $[H_3O^+]$, the rate constants manifest themselves in terms of k_1/K_a', and thus the apparent activation parameters pertain to two components: those of the rate constant for H_2O attack on **A**-H^+ and those involved in determining K_a'. In our current studies, undistorted amide **31a** has the highest $\Delta G^{\ddagger}{}_{25^0C}$, which decreases in the series of **IV**→**III**→**II**. It is obvious that distortion causes a marked reduction in the apparent $\Delta H^{\ddagger}$ in passing from **31a** to **IV**→**III**→**II**, but there is no general trend in $\Delta S^{\ddagger}$, probably because of the differential entropic terms in K_a'. For amide **Ia** at pH = 3.2, and amide **III** at pH = 0, the major species in solution will be the protonated forms (**Ia**-H^+ and **III**-H^+). The activation parameters in these cases refer principally to k_1, which is H_2O attack on the protonated amide. The data (see Table XVII, pg 63) show a smaller $\Delta H^{\ddagger}$ and more negative $\Delta S^{\ddagger}$ for amide **III** than amide **Ia**. This suggests that when fully protonated, **III**-H^+ is less stable than **Ia**-H^+, as expected since its pK_a is lower, and that at the transition state for H_2O attack on **III**-H^+, there is a greater restriction of waters of solvation. Another comparison of activation parameters can be made for amide **III** at pH = 2 and at pH = 0, the former corresponding to k_1/K_a' (first order in $[H^+]$) and the latter to k_1 (H_2O attack on **III**-H^+). The data (Table XVII, pg 63) shows a higher $\Delta H^\ddagger$ and less negative $\Delta S^\ddagger$ at pH = 0 than is observed at pH = 2. This probably results from restricted waters of solvation of **III**-H^+ that are in place prior to the transition state for nucleophilic attack. However, this suggestion must be tentatively offered since the $\Delta S^\ddagger$ values are nearly the same within experimental error.

In basic media, since all bicyclic anilides **Ia**-**IV** show terms first order in $[OH^-]$, the activation parameters refer to k_3 (see equation 12, pg 60) with the rate-limiting step being $[OH^-]$ attack on amide. From the data (see Table XVII, pg 63), the least reactive amide **IV** has the largest $\Delta G^\ddagger_{25^0C}$, and the most distorted amide **Ia** has the smallest $\Delta G^\ddagger_{25^0C}$. The analysis of activation free energy $\Delta G^\ddagger_{25^0C}$ in terms of $\Delta H^\ddagger$ and $\Delta S^\ddagger$ indicates that the increase in reactivities produced by distortion through the series of **IV**→**Ia** is manifested in a reduction of $\Delta H^\ddagger$, and a less negative $\Delta S^\ddagger$. We propose that by increasing the distortion of the amides **IV**→**III**≈**II**→**I**, the transition state for OH^- attack on amides becomes increasingly earlier in accordance with the Hammond postulate,[64,65] which means less $^-OH\cdots$**A** (amide) bond making and less restriction of solvent. However, for amide **31a**, since the rate-determining step is not the same as that for amides **Ia-IV**, the activation parameters of **31a** (see Table XVII, pg 63) refer to a virtual transition state and cannot be directly compared to those of these bicyclic anilides.

D. Effect of Acetate on the Hydrolysis of **II,III** in H_2O and D_2O

Since acetate buffer has a marked catalytic effect on the hydrolyses of amides **II** and **III**, the effects of [acetate] in both H_2O and D_2O media were investigated. The plots of log k_{OAc} (apparent) vs pL for both amides **II** and **III** are shown in Figure 14 (see pg 67). It is noticeable that the curves tend to plateau at pL values < pK_a of LOAc. This requires a pL independent domain which must be due to a neutral transition state. Thus a general acid catalyzed process (**A** + L_2O + LOAc) or its more likely kinetically equivalent process, a specific acid followed by a general base process (**A**-L^+ + L_2O + $^-$OAc) are both consistent with the reaction of amides **II** and **III** with acetate. Although there is evidence[28] that $^-$OAc is capable of nucleophilically attacking **II**-H^+ in CD_3CN to yield an open anhydride **44** (see equation 24), **44** has also been shown[33] to rapidly reform **II** + $^-$OAc while in aqueous acetate buffer. Therefore the observed accelerated hydrolysis in acetate buffers probably does not come from direct nucleophilic attack.

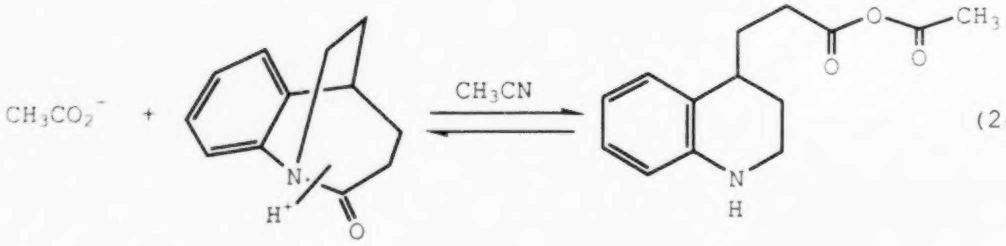

44

(24)

The mechanism for this process is believed to be a specific acid followed by a general base process as shown in equation 25. The SKIE consists of D_2O perturbation of three individual processes, namely the equilibrium constant of LOAc (K_a), the equilibrium constant of **A**-H^+ (K_a') and the kinetic isotope effects involved in the catalyzed delivery of LOL to **II**-L^+ or **III**-L^+ to yield the corresponding neutral (**45b**) or zwitterionic (**45a**) tetrahedral intermediates. The pK_a values of LOAc[66] in H_2O and D_2O at μ = 1.0 are 4.55 and 5.05, respectively. Thus the k_{OAc}/K_a' values in H_2O and D_2O for both amides **II** and **III** can be evaluated, and the results are listed in Table XX (see pg 70). If K_a' of **II**-L^+ and **III**-L^+ are changed by the same amount as those of LOAc from H_2O to D_2O, then K_a' should be a factor of ~3[67] larger in H_2O than D_2O. Therefore the change from H_2O to D_2O will lead to a counterbalancing of two components **II** + HOAc and **II**-L^+ and $^-$OAc. The obtained data $(k_{OAc}/K_a')^{H_2O}/(k_{OAc}/K_a')^{D_2O}$ of 0.46 and 0.48 for **II** and **III** yields a small SKIE of 1.38 and 1.44 on the k_{OAc} term for amide **II** and **III** respectively when modified by the anticipated $K_a'(H_2O) \approx 3K_a'(D_2O)$. This is consistent with the mechanism given in equation 25.

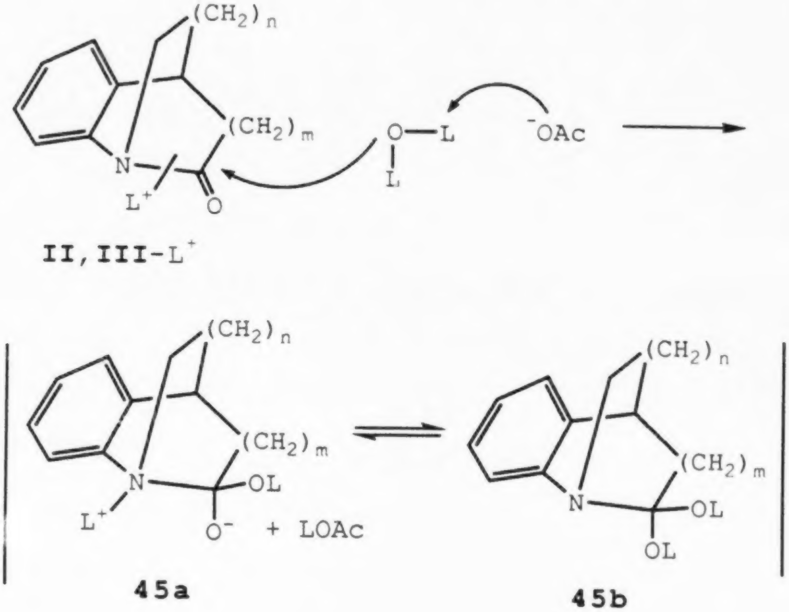

II,III-L$^+$

45a **45b** (25)

The plots of log k_{hyd} vs pL for both amides **II** and **III** (shown in Figure 15, pg 68) suggest the rates of uncatalyzed L_2O attack on **II**-L^+ or **III**-L^+ in H_2O are smaller than those in D_2O. The computed data $(k_1/K_a')^{H_2O}/(k_1/K_a')^{D_2O}$ of 0.63 and 0.62 respectively for amide **II** and **III** (see Table XX, p 70) can be analyzed in the same way as was done for the acetate buffer effect. Thus a normal primary isotope effect of ~1.86 can be obtained for L_2O attack on **II**-L^+ or **III**-L^+ when modified by the $K_a'(H_2O) \approx 3K_a'(D_2O)$. This isotope effect is consistent with the process shown in equation 26, in which L_2O functions as a general base in deprotonating a second

L_2O during attack on the protonated amide to yield **45a** and **45b**.

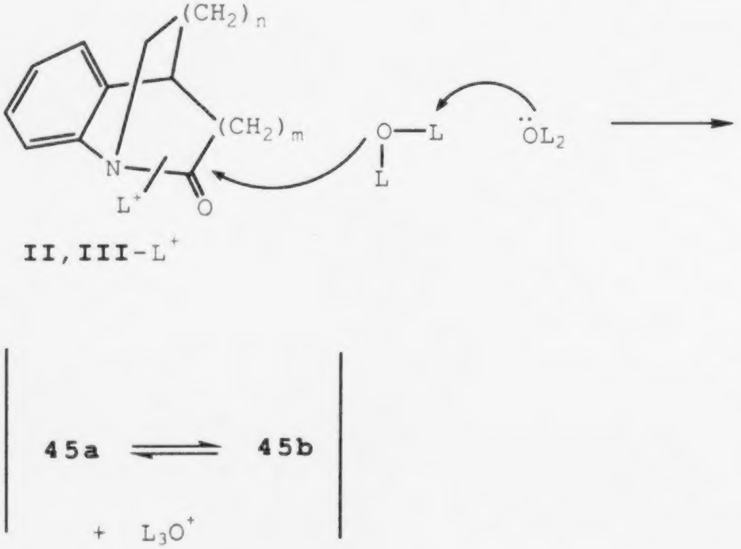

(26)

The evaluation of the expected SKIE can be also made on the basis of fraction factor analysis.[68,69] In the case of the acetate promoted delivery of L_2O, if in the plateau region the ground state consists of **II,III** + LOAc + L_2O, and the transition state resembles that for the process in equation 25, then the SKIE is determined by a single proton in flight having a fractionation factor of 0.65-0.70 (SKIE = $k_{OAc}{}^{H}/k_{OAc}{}^{D}$ = 1.54-1.42). In the case of water promoted delivery of L_2O, if the ground state consists of **II,III** + L_3O^+ + L_2O and the fractionation factor for L_3O^+ 0.69[3], the SKIE is determined by a single proton in flight (0.5) [SKIE = $(k_1)^{H_2O}/(k_1/)^{D_2O}$ = 1.8~2.0]. That the fractionation factors for a proton in flight from acetate + L_2O, and L_2O + L_2O are slightly different is attributable to an earlier transition state for the acetate promoted reaction.

E. Kinetic Methylation Position (N or O)

The determination of whether the site of protonation is N or O for these distorted amides can be attempted by comparison of the kinetic pK_a's of distorted amides with the pK_a's of normal amides. Typical amides have $N-H^+$ and $O-H^+$ pK_a values of -6 to -8[70] and 0 to -2[70] respectively. In amide **Ia**, and to a lesser extent **II** and **III**, favorable resonance effects that stabilize the O-protonation of amides are precluded. Thus, the N and C=O units in **Ia** should tend to behave independently, as amino and ketonic units that can exert mutual inductive effects that destabilize the other's protonated form. Thus, the pK_a of the $C=O^+-H$ unit in amide **Ia** is anticipated to be even lower than that of a ketone (normally -7 to -5 for acetone, cyclohexanone, etc[70c]) so that the observed kinetic pK_a (3.71) must be attributable to the $N-H^+$ form. By way of comparison, the pK_a of 3.71 for the conjugated acid of **Ia**[28] is ~4 units lower than the pK_a of benzoquinolidine 7.79,[71] in line with the inductive destabilization of $N-H^+$ by an adjacent orthogonal C=O.

As pointed out above, the structures of amide **II** and **III** do not completely inhibit N-C=O delocalization, and this leads to a drop in the $N-H^+$ pK_a relative to **Ia**. Correspondingly, the $N-C=OH^+$ forms of **II**,**III** are more stable than the O-protonated form of **Ia**, but they cannot be as stable as that of a normal amide where full delocalization is permitted. Also the kinetic methylation of amide **III** by methyltrifluoromethane sulfonate gives only a N-methylated product. Therefore, the observed kinetic pK_a values of -0.28 for **II** and 0.58 for **III** are most consistent with the $N-H^+$ forms. However, the structure of amide **IV** is more like a normal amide and allows more delocalization in the N-C=O unit and from the hydrolysis data, the pK_a is < 0. The kinetic methylation position of **IV** is on the oxygen, giving an ester as the final product. This is consistent with an O-protonated amide as being the kinetically important form for acid hydrolysis of **IV**.

Some relationship between the twist angle (Φ) and kinetic pK_a's for distorted amides is anticipated. Shown in Figure 16 is a plot of the pK_a's vs the $\cos^2\Phi$, the latter value being some measurement of the overlap between the N lone pair and C=O π bond. In the Figure, one dashed line arbitrarily represents the $N-H^+$ pK_a passing from an independent amino-ketone to a normal amide, and the other dashed line represents the $O-H^+$ pK_a passing from an independent amino-ketone to a normal amide. Placed on the graph are the kinetic pK_a's for the amides **Ia-IV**, the latter three being above the $N-H^+$ dashed line. Although we are confident that **Ia-III** show kinetic pK_a's that are consistent with an $N-H^+$ form, they need not react exclusively via that form. Shown in Scheme 5 is a tentative process that explains the situation.

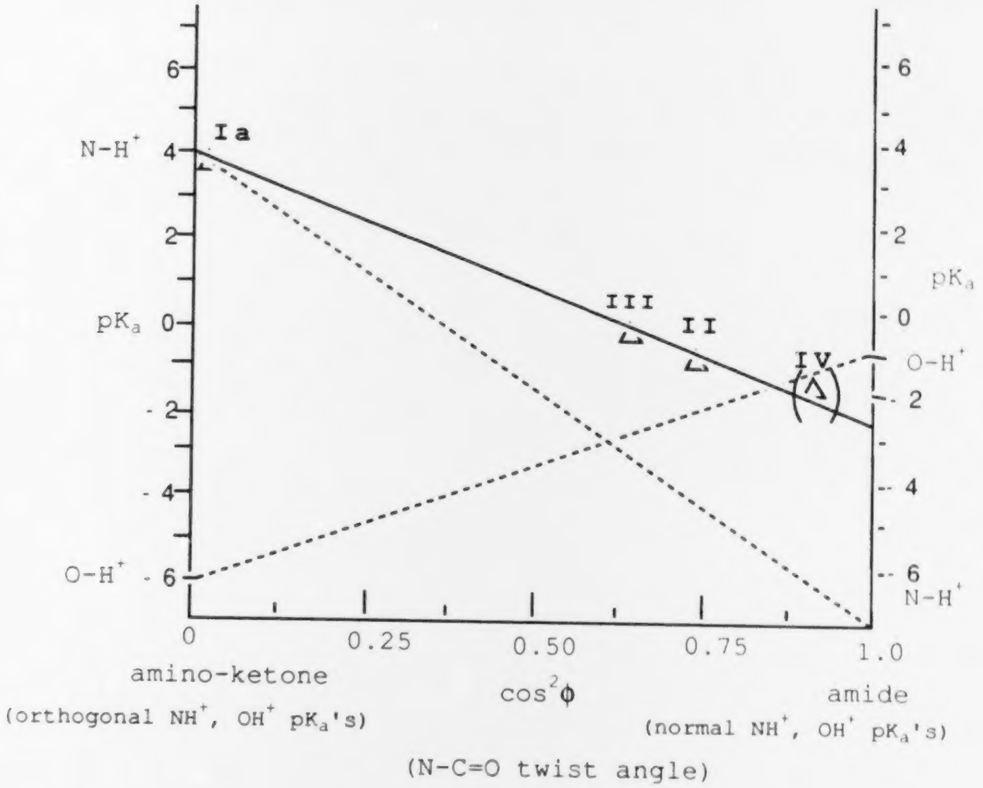

Figure 16. Kinetic pK_a of distorted amides.

For **Ia**, kinetic pK_a for $N-H^+$ is 3.71, and the corresponding pK_a of $O-H^+$ is -6, therefore $N-H^+$ form is favored by 10^{10} fold. Even if the water attack constant k_1' is much slower than k_1 (see Scheme 5), most of the reaction will go through a N protonated form. However, when the pK_a of $N-H^+$ is close to the value of the pK_a of $O-H^+$ form, both protonated forms may exist in equilibrium. Although distorted amides **II,III** might contain more of the $N-H^+$ forms than $O-H^+$, if k_1' is slower than k_1, the reaction will involve H_2O attack on both protonated forms. The exact situation is uncertain at present, but is controlled by the relative rate constants for water attack on the protonated forms, and on the respective pK_a's. Such an explanation may account for distorted amides **II-IV** deviating from the arbitrary dashed line.

Scheme 5

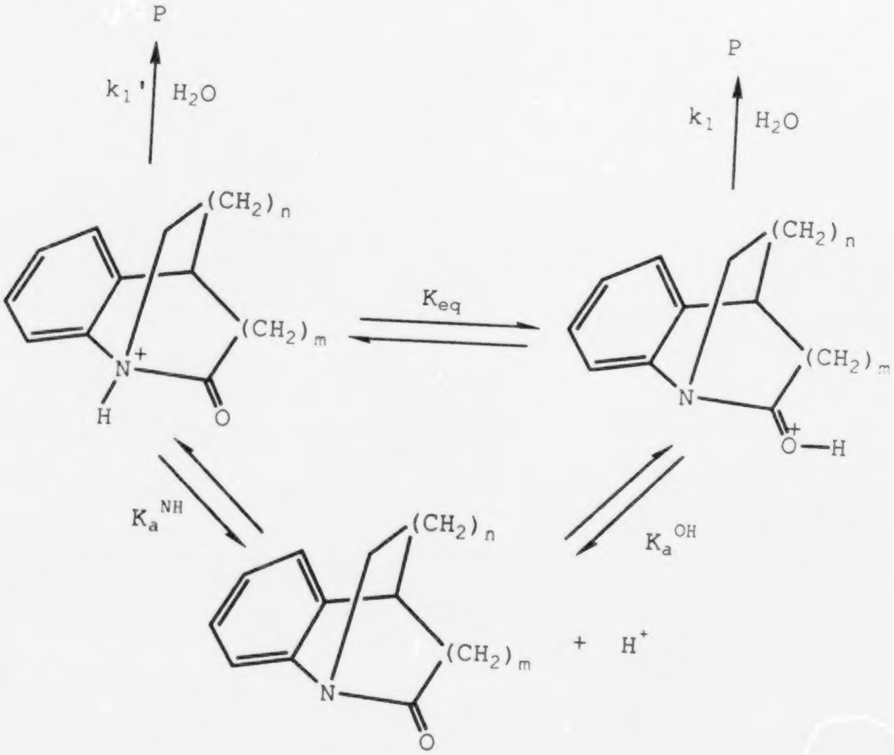
P
k_1'
H_2O
P
k_1
H_2O
$(CH_2)_n$
$(CH_2)_m$
N^+
H
O
K_{eq}
N
O^+—H
K_a^{NH}
K_a^{OH}
+ H^+

F. The Attempted Establishment of Kinetic Discrimination of Chirality

The analysis of the reaction k_{obsd} vs $[\text{ephedrine}]_{total}$ plots at pH 9.55 and 9.67 allows one to derive the constants given in Table XXIII (see pg 81). The results shown in Table XXIII indicate no discrimination between enantiomers when reacted with chiral amide **III**.

The difference in rate constant (~50%) for the reaction of the chiral amide **III** with ψ-ephedrine compared with the rate reacted with ephedrine is not entirely due to the diastereoisomeric preference, since the pK_a of both diastereoisomers is different by ~0.18 unit.[58] Using a Bronsted constant of β of 0.72,[28] the ΔpK_a of 0.18 (pK_a ψ-ephedrine - pK_a ephedrine) would account for ~23% difference in rate constants for reactions with the chiral amide **III**. Nevertheless, when corrected for the basicity difference, that the remaining of ~25% more reactive of ψ-ephedrine than ephedrine suggests some diastereomeric preference in the reactions.

Many factors influence the binding of a substrate to an enzyme, a drug to a receptor, and other similar processes. It appears that in all cases where the biological differentiation of the enantiomeric forms of a chiral ligand occurs, the fundamental stereochemical basis is diastereoisomeric in nature. The enzyme, receptor, membrane, etc. will be a chiral molecule —— most usually a chiral macromolecule. For example, Bergmann and his colleagues[72] discussed the "antipodal specifity of papain peptidase 1". This enzyme hydrolyzed only (-)-L-benzoylleucineamide and not the D-enantiomer. They stated that the enzyme must contain at least three different atoms or atomic groups which are fixed in space with respect to one another, these groups entering during the catalysis into relation with a similar number of different atoms or atomic groups of the substrate.

However, if the differentiation of enantiomers and diastereoisomers by a chiral reagent is a "one-point approach" rather than "three-point attachment" or "polyaffinity relationship", there are about 0.2-0.5 kcal/mol difference in energy for enantiomers and 0.6-1.2 kcal/mol for diastereoisomers.[73] For example, for the neutralization of various ephedrines with (R)- or (S)-mandelic acid, the heats of formation of ion pairs are listed in Table XXV[74].

Table XXV. Heats of neutralization at 25 °C in DMSO for various ephedrines and mandelic acid

Base	Acid	$-\Delta H$ (kcal/mol)
Ephedrine	Mandelic acid	
1R,2S	R	7.29(0.02)
1S,2R	S	7.33(0.03)
1R,2S	S	7.55(0.03)
1S,2R	R	7.61(0.03)
ψ-ephedrine	mandelic acid	
1R,2R	R	6.67(0.03)
1S,2S	S	6.66(0.02)
1R,2R	S	6.40(0.02)
1S,2S	R	6.38(0.02)

Such an energy difference of 0.2-0.5 kcal/mol can account for the difference between reaction yields or rates of 1:1 and 6:4.

In our investigated system, there are probably two main reasons for not observing a rate discrimination between the enantiomers. There was not enough interaction between chiral amide **III** and ephedrine enantiomers since the site of chiral discrimination is relatively far away from the site of reaction. Also the reactions were performed in aqueous solution, and solvation effects might disturb the stereochemical interaction between reactants. However, if there is a greater stereochemical difference in structure for the reactants such as with the diastereoisomers ψ-ephedrine vs ephedrine, the chiral amide **III** does show some kinetic discrimination.

G. Conclusions:

1). The comparison of x-ray crystal structures for distorted amides **II-IV** with the structure of undistorted amide **29** indicates the distortion in amides **II-IV** manifests itself in a lengthening of the N-C(O) bond with only a slight shortening of the C=O bond, along with a pyramidalization of the N from sp^2 to sp^3 hybridization that accompanies rotation around the C-N bond.

2). The markedly enhanced hydrolytic reactivities of distorted amides **Ia-IV** in both acid and base when compared with an undistorted amide **31a** are due to the progressive structural distortion of the anilides. The pH-rate profiles for distorted amides **Ia**-**IV** and **31a** show two general domains: first order in [H_3O^+] and [OH^-]. The more distorted amides **Ia**-**III**, show a domain of H_2O attack on the protonated amide with an increasing kinetic pK_a for the fully protonated amides as the distortion increases in the order **III**$\approx$**II**$\rightarrow$**Ia**. The most distorted amide **Ia**, shows an additional domain of H_2O attack on a neutral form of amide or its kinetic equivalent, OH^- attack on **Ia**-H^+. Solvent kinetic isotope effects (SKIE) in base for the hydrolysis of all distorted amides **Ia**-**IV** are close to unity, and are consistent with the rate determining attack of OH^-. The inverse solvent kinetic isotope effects (0.75 for **II**, 0.77 for **III**, 0.89 for **IV**) for acid catalyzed hydrolysis of amides **II**-**IV** indicate that amides **II** and **III** have earlier transition states for the process of H_2O nucleophilic attack on the protonated form than does amide **IV**.

3). The activation parameters for the hydrolysis of **Ia**-**IV** in base indicate that the enhanced hydrolytic reactivities produced by distortion result from a reduction of $\Delta H^\ddagger$ with less negative $\Delta S^\ddagger$. In acid, the activation parameters (corresponding to k_1/K_a') for the hydrolysis of **II**-**IV** show a reduction of $\Delta H^\ddagger$ and no general trend in $\Delta S^\ddagger$. If one compares the activation parameters in terms of k_1 only, then the fully protonated form of the more distorted amide **Ia** has a higher $\Delta H^\ddagger$ and less negative $\Delta S^\ddagger$ than the fully protonated form of the less distorted amide **III**, which indicates that the ground state of **Ia**-H^+ is more stable than **III**-H^+, and H_2O attack on **Ia**-H^+ involves less restriction of waters of solvation at the transition state.

4). The solvent kinetic isotope effects obtained by analyzing the log k_2 vs pL data from the study of acetate catalyzed hydrolysis of amides **II** and **III** are consistent with a specific acid followed by a general base process. In the case of L_2O acting as a general base, the data were analyzed in terms of log k_{hyd} vs pL and a similar mechanism to that above is implied.

5). Kinetic methylation of amide **III** gives a N-methyl acid (**32**) as the final product, and amide **IV** gives an ester (**33**). This implies that the kinetic pK_a's of the protonated amides **III-Ia** might arise from an N-H^+ form and the kinetic pK_a of **IV** might be attributed to an O-H^+ form. For nucleophilic attack of H_2O on the protonated amide, if the kinetic pK_a of both N-H^+ and O-H^+ are close, H_2O might attack both protonated forms.

6). Chiral amide **III** does not show a kinetic discrimination for ephedrine enantiomers (**39,40**) nor for ψ-ephedrine enantiomers (**41,42**). Chiral amide **III** exhibits ~50% difference in the rate constants for attack of the diastereoisomers of ψ-ephedrine (**41** or **42**) vs ephedrine (**39** or **40**). Although the pK_a of both diastereoisomers differs by 0.18 unit(at 10 °C), this ΔpK_a only corresponds to ~20% different in rate. Therefore, chiral amide **III** has a slight kinetic diastereomeric discrimination.

4. EXPERIMENTAL

Routine ^{1}H-NMR spectra were recorded with a Bruker WP-200 spectrometer. ^{13}C NMR spectra were recorded at 85 MHz with a Bruker WP-200 spectrometer. Routine IR spectra were recorded with a Nicolet 7000 FT-IR spectrophotometer. Mass spectral analyses were performed with an AEI MS-50 high-resolution mass spectrometer and an AEI MS-12 low resolution mass spectrometer (CI).

Elemental analyses were carried out in the Microanalytical Laboratory of the Department of Chemistry, University of Alberta.

X-ray structures were determined on an Enraf-Nonius CAD4 automated diffractometer by B.D. Santarsiero in the Department of Chemistry, University of Alberta.

Optical rotations were determined on a Perkin-Elmer 241 polarimeter.

Medium performance liquid chromatographic (MPLC) separations were accomplished with an FMI LAB pump Model RP-SY, RP-8 reverse phase column and Isco 254nm UV detector.

High performance liquid chromatographic (HPLC) separations were done using a HP 1081A Liquid Chromatography system consisting of a 10μ 25cm × 21.1mm id 20 micron chiral DPG (dinitrophenylglycine) HPLC column and a 254nm UV detector.

A.Syntheses

1). The compound 3,4-dihydro-2-oxo-1,4-propano quinoline (**III**) was synthesized starting with a known ketone **21**.[39]

5-(Ethoxycarbonylmethyl)-5-hydroxy-N-tosyl-2,3,4,5-tetrahydrobenzazepine (**22**)

To a 500 mL 3-necked flask equipped with a 250 mL dropping funnel (charged with 16.6 g (0.053 mol) of 5-oxo-N-tosylbenzazepine **21** and 6.45 mL (0.058 mol, d = 1.506) of ethyl α-bromoacetate and 210 mL of dry benzene), a reflux condenser and magnetic stirring bar, were added 4.56 g (0.070 mol) of zinc powder and 210 mL of dry ether. The contents of the dropping funnel were added dropwise to the stirred Zn suspension, after which the mixture was heated at reflux overnight under an argon atmosphere. By morning a white suspension had formed and the mixture was cooled (ice bath) and treated with 210 mL of 10% H_2SO_4. The phases were separated and the organic phase washed with 5×140 mL of 10% H_2SO_4, the combined extracts being saved. The organic layer was then extracted with 5×100 mL of 5% KOH, and 5×100 mL of saturated NaCl, and subsequently dried ($MgSO_4$), filtered and stripped of volatiles to give crude **22**. The combined acid extracts were reextracted with 3×100 mL of $CHCl_3$, these extracts being combined, dried ($MgSO_4$), filtered and stripped of volatiles. The crude product thus obtained was combined with that above, and recrystallized from 95%

ethanol to yield 18.3 g (86.3%) of pure **22**, mp 149-150 ^{0}C; ^{1}H-NMR (200 MHz, $CDCl_3$) δ 7.80 (2 H, m), 6.90-7.35 (6 H, m), 4.08 (4 H, m), 3.15 (2 H, s), 2.90 (1 H, br.t), 2.45 (3 H, s), 2.15 (2 H, br), 1.80 (2 H, br.t), 1.20 (3 H, t, J = 7 Hz). Exact Mass cacld for $C_{21}H_{25}NO_5S$: 403.1453; found: 403.1445. Anal calcd for $C_{21}H_{25}NO_5S$: C, 62.51; H, 6.25; N, 3.47. Found: C, 62.24; H, 6.44; N, 3.44.

5-(Ethoxycarbonylmethyl)-2,3-dihydro-N-tosylbenzazepine (**23a**) and 5-(Ethoxycarbonylmethylidene)-2,3,4,5,-tetrahydro-N-tosylbenzazepine (**23b**).

Into a 500 mL rb flask was placed 250 mL of benzene, 0.7 g of *p*-toluenesulfonic acid and 36.0 g (0.0892 mol) of the alcohol **22**. The mixture was heated at reflux for 16 h and 1.5 mL of H_2O was removed using a Dean-Stark apparatus. The benzene was extracted with 2×200mL of saturated $NaHCO_3$ and 2×200 mL of water after which it was dried ($MgSO_4$), filtered, and the volatiles removed by rotary evaporation. The crude residue was recrystallized from 95% ethanol after it had been decolorized with charcoal to yield 33.0 g (96%) of **23a** and **23b** as a mixture of isomers, mp 126.5-128.5 ^{0}C; ^{1}H-NMR (200 MHz, $CDCl_3$) of the exo methylene derivative, δ 7.64-7.40 (8 H, m), 5.28 (1 H, s), 4.06 (2 H, q, J = 7 Hz), 3.77 (2 H, t, J = 7 Hz), 2.75 (2 H, br.t), 2.35 (3 H, s), 1.80 (2 H, m), 1.28 (3 H, t, J = 7 Hz); of the ethoxycarbonylmethyl isomer, δ 7.64- 7.12 (8 H, m), 5.75 (1 H,t, J = 6 Hz), 4.08 (2 H, q, J = 7 Hz), 3.93 (2 H, m), 2.78

(2 H, s), 2.35 (3 H, s), 2.20 (2 H, m), 1.22 (3 H, t, J = 7 Hz). Exact Mass cacld for $C_{21}H_{23}NO_4S$: 385.1348; found: 385.1351. Anal calcd for $C_{21}H_{23}NO_4S$: C, 65.43; H, 6.01; N, 3.63. Found: C, 65.39; H, 6.22; N, 3.58.

5-(Ethoxycarbonylmethyl)-2,3,4,5-tetrahydrobenzazepine (**24**)

Produced by catalytic hydrogenation (30 psi) of 17.4 g (0.045 mol) of **23** in 150 mL THF containing 0.5 g of PtO_2. After 36 h, the mixture was filtered and the volatiles were removed to yield 17.4 g (100%) of the hydrogenated product, mp 97.5-98.5 ^{0}C; ^{1}H-NMR (200 MHz, $CDCl_3$) δ 7.65 (2 H, m), 7.10 (6 H, m), 4.05 (2 H, q, J = 7 Hz), 3.86-3.54 (1 H, br), 3.20-3.00 (2 H, br), 2.64 (2 H, br), 2.34 (3 H, s), 1.40-1.80 (4 H, br.m), 1.18 (3 H, t, J = 7 Hz). Exact Mass cacld for $C_{21}H_{25}NO_4S$: 387.1504; found: 387.1504. Anal calcd for $C_{21}H_{25}NO_4S$: C, 65.09; H, 6.50; N, 3.62. Found: C, 65.12; H, 6.51; N, 3.65.

2-[5-(2,3,4,5-tetrahydrobenzazepinyl)]acetic acid (**26**)

To a 100 mL rb flask containing 16 mL of 20% KOH, and 24 mL of 95% ethanol was added 3.61 g (9.33 mmol) of the ester **24**. The contents were heated at reflux for 5 h, and then the mixture was poured into an ice-HCl mixture at pH 1. The mixture was then extracted with 3×50 mL of $CHCl_3$, and the combined extracts dried ($MgSO_4$), filtered, and the volatiles were removed. The resulting acid **25** was not purified further, but taken immediately on to the next step. Removal of the N-tosyl protecting group was effected by a modification of a reported[40] procedure. Into a 500 mL 3-necked rb flask equipped with serum stoppers, magnetic stirring bar, and Ar inlet was placed the crude acid **25**, 10 mL of dry DME and 720 mg (30 mmol) of NaH (prepared from 1.2 g of 60% NaH in oil, which was freed from the oil by washing with heptane).

In a separate 200 mL 3-necked rb flask equipped with serum stoppers, magnetic stirring bar and argon inlet, was placed 16.8 g (0.13 mol) of naphthalene and 40 mL of dry DME. To this solution was added 2.7 g (0.12 mol) of Na^0 upon which the solution turned deep green. This was allowed to stir at room temperature for 15 min and then it was taken up via syringe, and injected into the first flask. As the $Na/C_{10}H_8$ solution was injected, the green color immediately disappeared, and enough was added so that the color persisted. This resulting mixture was allowed to stir at room temperature overnight. In the morning, the DME was removed by rotary evaporator, and ~100 mL H_2O and ~100 mL benzene were added to the residue. The water layer was extracted with 3×100 mL of benzene and then the pH of the aqueous layer was adjusted to 1 by addition of conc. HCl. Solid Na_3PO_4 was added to adjust the pH to 5-6, and then the solution was extracted with 50 mL of ethyl acetate, followed by 2×25 mL of CH_2Cl_2. The organic layers were combined, dried ($MgSO_4$), filtered, and the volatiles removed to yield

1.5 g of the crude product **26**. Purification was effected by dissolving this material in a small amount of 95% ethanol containing a few drops of conc. HCl and adding ether to turbidity. After refrigeration, a yellow crystalline material was obtained by filtration. This was dissolved in water, treated with charcoal to decolorize it, filtered, and the water removed to give a solid. The solid was dissolved again in the above EtOH/HCl solution and ether added to turbidity. Refrigeration yielded 1.1 g (50%) of the HCl salt of **26**, mp > 200 ^{0}C (decomp.); ^{1}H NMR (200 MHz, DMSO-d_6) δ 6.75 (1H, m), 6.30-6.40 (3 H, m), 3.70 (1 H, m), 3.50 (1 H, m), 2.70-3.10 (3 H, m), 2.55 (2 H, m), 1.90-2.22 (3 H, br.m), 1.4-1.6 (1 H, br). Exact Mass calcd for $C_{12}H_{15}NO_2$: 205.1103; found: 205.1099. Anal calcd for $C_{12}H_{15}NO_2 \cdot HCl$: C, 59.63; H, 6.67; N, 5.79; Cl, 14.67. Found: C, 59.53; H, 6.66; N, 5.76; Cl, 14.76.

3,4-Dihydro-2-oxo-1,4-propanoquinoline (**III**)

To a 500 mL 3-necked rb flask was added 220 mL of dry acetonitrile (distilled from P_2O_5), 1.0 g of the HCl salt of **26** (4.14 mmol), and 0.58 mL (d = 0.726, 4.17 mmol) of triethylamine. The mixture was stirred under argon until everything dissolved, and then 0.86 g (4.17 mmol) of dicyclohexylcarbodiimide (DCC) in 4.2 mL of dry acetonitrile was added via syringe. The solution was periodically monitored by ir to observe the reaction progress by the appearance of a 1720 cm^{-1} C=O band. The mixture was allowed to stand overnight, filtered and the volatiles were removed by rotary evaporation. The solid residue was redissolved in dry benzene, filtered to remove traces of the dicyclohexylurea, and evaporated to dryness with a vacuum pump. The solid so obtained was recrystallized from octane to give 0.45 g (58%) of **III** which was filtered in a cold room (4 ^{0}C); mp 36.0-37.0 ^{0}C; ^{1}H-NMR (200 MHz, $CDCl_3$) δ 7.15 (4 H, m), 3.90 (1 H, m), 3.25 (1 H, m), 3.15 (1 H, m), 2.68 (2 H, d, J = 3 Hz), 2.05 (1 H, br), 1.23-1.72 (3 H, m) (for assignments see Table V, Pg 37); ^{13}C-NMR (85 MHz, $CDCl_3$) δ 200.5, 129.7, 128.7, 127.8, 126.9, 125.4, 54.9, 44.6, 33.7, 28.4, 24.8; ir (FT-IR, $CHCl_3$, cast) 1722.23 cm^{-1}. Exact Mass calcd for $C_{12}H_{13}NO$: 187.0997; found: 187.1001. Anal calcd for $C_{12}H_{13}NO$: C, 76.98; N, 7.48; H, 7.00. Found: C, 76.62; N, 7.37; H, 6.99.

2). The synthesis of 2,3,4,5-tetrahydro-2-oxo-1,5-propanobenzazepine (**IV**):

5-(2-Hydroxycarbonylethyl)-N-tosyl-2,3,4,5-tetrahydrobenzazepine (**27**)

To a 200mL rb flask was added 8.6 g (24mmol) of the acid **25**, 17.5 mL (240mmol) of thionyl chloride and 50 mL of dry benzene. The mixture was heated at reflux overnight, and in the morning an additional 5 mL of $SOCl_2$ was added, followed by heating at reflux for 1 h. The volatiles were removed by rotary evaporation and then 50 mL of benzene was added and evaporated. The latter process was repeated to removed traces of $SOCl_2$. The resulting acid chloride exhibited an ir absorbance at 1802cm^{-1} (film).

The acyl chloride was immediately placed in a 250 mL dropping funnel along with 200 mL of dry ether. It was then added dropwise to a solution of ~ 3 g of diazomethane in 130 mL of ether (prepared from Diazald® as reported[43]) that had been cooled to 0 ^{0}C in an ice bath. After complete addition, the mixture was allowed to stand for 2 h. The excess CH_2N_2 was removed by distilling (bath temp. 50-60 ^{0}C) an amount of ether sufficient to afford a colorless distillate after which the remaining volatiles were removed by rotary evaporation to yield an oil: ir (film) 2120 cm^{-1}.

The rearrangement of the adducts above to give **27** was effected by the procedure reported by Hudlicky and Sheth.[42] The diazomethane addition product from above was immediately placed into a dropping funnel containing 40 mL of 1,4-dioxane. The contents were then added over a 20 min period to a 500 mL flask containing a stirred mixture of 0.28 g of silver oxide, 0.70 g of anhydrous sodium carbonate, 0.42 g of sodium thiosulfate and 30 mL of water at 60-65 ^{0}C. Following the addition, the contents of the flask were heated at 90 ^{0}C for 5 h during which time a mixture of silver oxide (0.28 g), sodium carbonate (0.7 g), sodium thiosulfate (0.42 g), 30 mL of water and 15 mL of dioxane was added after each hour.

The pH of the reaction mixture was then adjusted to ~1.0 with 1.0 N HNO_3, and the resulting mixture was then extracted with 3×100 mL of $CHCl_3$. The combined organic layers were dried ($MgSO_4$), filtered and the volatiles removed by rotary evaporation to yield 8.0 g of crude **27**. It was purified by dissolution in 200 mL of 1 N NaOH after which the basic solution was extracted with 3×100 mL of CH_2Cl_2, and the aqueous base layer decolorized with charcoal. The solution was made acidic by addition of conc. HCl which induced precipitation. The solid was collected, dissolved in a minimum amount of 95% EtOH and then water was added to turbidity. After refrigeration, a white solid was collected and dried to yield 4.36 g of pure **27** (49% based on **25**): mp 152.2-153.3 ^{0}C; ^{1}H-NMR (200 MHz, $CDCl_3$) δ 7.1-7.8(8 H, br), 3.3-4.1 (2 H, br), 2.5 (5 H, br), 2.2 (3 H, s), 2.0-1.2 (4 H, br); NH_4^+ chemical ionization mass (m/z) 391 (100%, $M^{+\cdot}$ + 18). Anal cacld for $C_{20}H_{23}NO_4S$: C,64.33; H,6.21; N,3.75. Found: C,63.90; H,6.20; N,3.76.

5-(2-Carboxyethyl)-2,3,4,5-tetrahydrobenzazepine (**28**)

To a 500 mL rb flask fitted with a dry ice condenser and gas inlet tube was added 2.0 g (5.36 mmol) of **27** and 50 mL of dry THF and the solution was then cooled to -50 ^{0}C. Into this was condensed ~200 mL of NH_3. Sodium metal was added portionwise until a persistent blue color was obtained. The mixture was stirred for an additional 5 min after which solid NH_4Cl was added in small portions until the mixture was colorless. After evaporation of the NH_3 (ambient conditions), the solution was acidified with 1 N HCl and then extracted with 3×50 mL of benzene to remove reduction byproducts. The remaining aqueous layer was neutralized by K_3PO_4 to pH ~ 5, and extracted with 3×50 mL CH_2Cl_2. The CH_2Cl_2 extracts were combined, dried ($MgSO_4$), filtered, and the volatiles removed to yield 1.1 g of crude **28**. It was purified by recrystallization from 95% EtOH/H_2O to yield 0.61 g (52%) of pure **28**; mp 129-130 ^{0}C; ^{1}H-NMR (200 MHz, $CDCl_3$) δ 7.32(2 H, br), 7.03(2 H, dd, J_1 = 5 Hz, J_2 = 7 Hz), 6.84 (1 H, dd, J_1 = 7 Hz, J_2 = 2 Hz), 6.70 (1 H, d, J=7 Hz), 3.26 (1 H, m), 2.83(2 H, m), 2.10-2.40 (3 H, m), 1.60-2.00(5 H, m). Exact Mass calcd for $C_{13}H_{17}NO_2$, 219.1259; found: 219.1258. Anal calcd for $C_{13}H_{17}NO_2$: C,71.21; H,7.81; N,6.39. Found: C,71.32; H,7.84; N,6.30.

2,3,4,5-Tetrahydro-2-oxo-1,5-propanobenzazepine (**IV**)

To a 500 mL 3-necked rb flask was added 200 mL of dry CH_3CN (distilled from P_2O_5) and 0.50 g (2.28 mmol) of amino acid **28**. The mixture was stirred until all solids dissolved after which 0.50 g (2.42 mmol) of dicyclohexylcarbodiimide in 2.5 mL of dry CH_3CN was added by syringe. The solution was allowed to stand overnight and periodically monitored by ir spectroscopy to observe the appearance of a C=O band at ~1680cm^{-1}. The mixture was filtered and the volatiles were removed by rotary evaporation. The solid residue was redissolved in a small amount of dry benzene, filtered to remove the last traces of dicyclohexylurea, and then stripped of benzene. The so-obtained solid was recrystallized from octane to yield 0.41 g (89%) of the pure amide **IV**: mp 82.3-83.3 ^{0}C; ^{1}H-NMR (200 MHz, $CDCl_3$) δ 7.32(2 H, m), 7.18(2 H, m), 4.53(1 H, m), 3.10-3.24(1 H, m), 2.92(1 H, m), 2.26(2 H, m), 2.10(3 H, m), 1.52-1.68(2 H, m), 1.20-1.34(1 H, m) (for assignments see Table VI, Pg 41); ^{13}C-NMR (85 MHz, $CDCl_3$) δ 180.39, 142.24, 139.37, 128.38, 127.97, 127.72, 126.29, 47.67, 38.44, 38.26, 32.23, 28.96, 25.44; ir (FTIR, $CHCl_3$ cast) 1676.58cm^{-1}. Exact mass calcd for $C_{13}H_{15}NO$: 201.1154; found: 201.1146. Anal calcd for $C_{13}H_{15}NO$: C,77.58; H,7.51; N,6.96. Found: C,77.76; H,7.77; N,6.74.

B. Kinetics

1). General procedure

Triply distilled water was used throughout. Kinetic data at 25.0 ^{0}C were obtained by monitoring the rate of change of absorbance of a 2.67×10^{-4} M aqueous solution of amide at the wavelength of maximum change, (**III**, 260nm, pH < 5.0, 280nm, pH > 5.0; **IV**, 230nm, pH <3.0, 240nm, pH > 12), with a Hewlett Packard 8451A Diode Array U.V.-vis spectrophotometer. Temperature was maintained at 25.0±0.2 ^{0}C by means of an external Colora Model NB-ELE circulating water bath.

Buffered solutions at 4 concentrations from 0.05-0.20 M were employed, μ = 1.0 (KCl). The buffers used were HCl (pH

$\leq$ 2); formate (3.0-4.0); acetate (4.0-5.0); MES (2-[N-morpholino]ethanesulphonic acid) (5.1-6.5); MOPS (3-[N-morpholino]propanesulfonic acid) (6.7-7.6); EPPS (N-[2-hydroxyethyl]-piperazine-N'-[3-propanesulfonic acid] (8.0-8.7); CHES (2-[N-cyclohexylamino]-ethanesulfonic acid) (9.0-9.8); CAPS (3-[cyclohexylamino]propanesulfonic acid) (9.8-11.1); NaOH (> 11).

Slower reactions were initiated by injection 10 µL of a stock solution of **III** or **IV** (80 mM in CH_3CN) into 3.0 mL of the buffer in a 1.0 cm quartz cuvette that had thermally equilibrated in the spectrophotometer cell holder for 20 min at 25.0±0.2 ^{0}C. All reactions were followed in triplicate and monitored for at least three half-lives.

Because of its slow hydrolysis, amide **IV** at pH 2.7 and 3.0 was only followed to 2 $t_{1/2}$. The end points for the two slow reactions were determined by measuring the absorbance at 230 nm of a 2.67×10^{-4} M aqueous solution of the authentic amino acid **28** in the same medium.

Pseudo first order rate constants were evaluated by non-linear least squares fitting of the Abs vs time data to a standard exponential model[75] $(Abs)_t = (Abs)_{inf} + [(Abs)_0 - (Abs)_{inf}]\times e^{-kt}$. Plots of k_{obsd} data vs [buffer] for a given pH were extrapolated back to zero [buffer] in order to yield the k_{hyd} values given in the text.

Faster reactions ($k_{obsd} > 0.1$ s^{-1}) for amide **III** were obtained using a Durrum-Gibson 115 Stopped-Flow kinetics system thermostated at 25 ^{0}C. Into one drive syringe was placed the main buffer solution, $\mu = 1.0$ (KCl), while the second syringe contained a 2.7×10^{-4} M solution of **III** in 10 mL of 1 M KCl along with 1 drop of a MOPS buffer (0.05 M) to set the pH at the value corresponding to the slowest hydrolysis. Both solutions were thermostated at 25 ^{0}C for 20 min, and then rapidly mixed. Four runs were made at each pH. pH measurements were made on the effluent from the mixing chamber and it was assumed that the pH was instantly equilibrated on mixing. pH measurements were made with a Radiometer TTT2 titration unit in conjunction with a Radiometer GK-2321C combination electrode. The electrode was standardized prior to use with Fisher Certified pH 4.00, 7.00 and 10.00 buffers. $[H^+]$ at pH values less than 2 or greater than 12 were determined by titration with standardized NaOH or HCl respectively using bromothymol blue as an indicator.

2). Product analysis

For amide **III**, into 3.0 mL of sample of pH 7.93 CHES buffer was injected 20 µL of 20 mM **III** in CH_3CN. The U.V.-vis spectrum (330-250 nm) was continuously scanned using a Cary 210 U.V.-vis Spectrophotometer. An isobestic point at $\lambda = 265$ nm was observed during the run. At the completion of the kinetic event the spectrum indicated a λ_{max} of 278 nm ($\varepsilon = 1015\ M^{-1}cm^{-1}$) which was superimposable upon the spectrum of a solution containing an equivalent concentration of the authentic amino acid **26** at same concentration in pH 7.93 CHES buffer.

For amide **IV**, into 3.0 mL of pH 0.0 HCl buffer was injected 10 μL of 80 mM **IV** in CH_3CN. The U.V. spectrum was monitored from 220-300 nm continuously for the time course of the reaction using a Cary 210 U.V.-vis spectrophotometer. An isobestic point at λ = 250 nm was observed. At the completion of the run, the λ_{max} at 230 nm had an ε = 2820 $M^{-1}cm^{-1}$ and the overall spectrum was superimposable upon that of an authentic 2.67×10^{-4} M solution of the authentic amino acid **28** in 1.0 N HCl.

3). D_2O Studies

Solvent kinetic isotope studies for amides **Ia-III** were conducted at 25.0 ^{0}C at their λ_{max} of 291nm, 291nm, 280nm respectively in basic media and 260nm for both amides **II** , **III** under acidic conditions using a Durrum-Gibson Stopped Flow spectrophotometer. Into one drive syringe was placed an 0.2 M NaOD solution (μ = 1.0 KCl) or 2×10^{-2} M DCl (μ = 1.0 KCl) solution. The second syringe contained D_2O (μ = 1.0 KCl) along with ~ 3×10^{-4} M of amides **Ia-III**. Reactions were monitored to completion in triplicate. The final $[OD^-]$ or $[D_3O^+]$ was determined by titration of the effluent from the spectrophotometer cell using standardized HCl or NaOH titrants and bromothymol blue as an indicator. For **IV**, which reacts more slowly than any of **Ia-III**, the solvent isotope effects were determined using a Cary 210 U.V.-vis spectrophotometer at 25.0 ^{0}C, λ = 240 nm (1.06 M NaOD) or λ = 230 nm (pD = 2.18).

4). Acetate buffer effects on the hydrolysis of Amides **II**, **III** in H_2O and D_2O at 25.0 ^{0}C

Anhydrous NaOAc (GIC), MES (2-[N-morpholino]ethane sulfonic acid) and D_2O (Merck) were used without further purification. Throughout its useful buffering range (pL values between pK_a+1 and pK_a-1, L = H, D) acetate was used as the buffer. Above pL readings of pK_a+1, the pL was controlled by 0.005 M MES to which was added acetate. pL readings of the solution before and after the kinetic determinations indicated no changes in excess of 0.02 units. pD values were determined by adding 0.4 units[54] to the pH meter reading. Pseudo-first order rate constants k_{obsd} for the disappearance of amide **II** (291 nm) and **III** (260 nm) were determined in triplicate at each pL as a function of total acetate concentrations varying between 50 and 200 mM (μ = 1.0 KCl). Second order rate constants were evaluated from the slopes of the k_{obsd} values vs [acetate total]. The pK_a^D for DOAc was taken from a literature value (5.25, μ = 0, 25 ^{0}C) and corrected[55] to a value of 5.05 (25 ^{0}C) at μ = 1.0.

5). ^{18}O-exchange experiment for 50% ^{18}O labelled N-methylacetanilide **31a**.[76]

The rates of ^{18}O-exchange were determined using methodologies and mass spectrometric instrumentation previously described by Brown et al[34] at 74.0 ^0C with $[OH^-]$ 1.077M. All base solutions were CO_2 free and manipulations were performed in an Ar-filled drybox. Exchange rate constants (k_{ex}) were evaluated from the slopes of the plots of $\ln(I_{M^+}+2)/(I_{M^+}+2 + I_{M^+})$ vs time where I represents the intensity of parent and parent + 2 mass ions. Eight points up to at least 2 $t_{1/2}$ were taken for each plot, and errors in the quoted k_{ex} values were determined as the standard deviation of the linear regression lines. The results of ^{18}O-exchange experiment is shown on supplementary material (S8).

6). The determination of activation energies for the hydrolysis of amides **Ia-IV** and **31a** in acid and base.

A Durrum-Gibson 115 Stopped-Flow kinetic system interfaced to a microcomputer was used to determine the activation energy for the hydrolysis of amide **III** in both acidic and basic media. In basic media, $[OH^-] = 0.087M$, $\mu = 1.0(KCl)$, the data were obtained at $\lambda = 280$ nm and seven different temperatures (5.0, 10.3, 17.8, 25.7, 33.4, 40.2, 48.9 ^0C). The effluent from the mixing chamber was collected, and then titrated with standard 0.10 N HCl by using bromothymol blue as an indicator. Under acidic conditions, the data were obtained at $\lambda = 260$ nm and seven different temperatures [(7.2, 13.6, 18.8, 25.8, 32.1, 39.5, 47.3 ^{0}C for pH = 2.0 μ = 1.0 KCl) and (6.7, 12.4, 18.5, 25.4, 32.4, 40.0, 48.4 ^{0}C for pH = 0.0)]. The effluent from the mixing chamber was collected and then titrated with 0.318 N NaOH or 0.891 N NaOH respectively by using bromothymol blue as an indicator.

A Cary 210 U.V.-vis spectrophotometer equipped with a cell programmer, a wavelength programmer and a timer accessory, also interfaced to a computer for data collection and processing was used to determine the activation energy for amide **IV** and amide **31a** in both acidic and basic media.

For amide **IV** in base with $[OH^-]$ = 0.01M μ = 1.0 (KCl), the data were obtained at four different temperatures (25.0, 39.0, 54.3, 75.3 ^{0}C) and the absorbance change was measured at λ = 240 nm. The product solutions were titrated with standard 0.10 N HCl by using bromothymol blue as an indicator. In acid with pH = 1.5, μ = 1.0 (KCl), the data were obtained at six different temperatures (16.1, 30.6, 37.6, 53.2, 63.0, 76.2 ^{0}C) and the absorbance change was measured at λ = 230 nm. The product solutions were titrated with 0.102 N NaOH by using bromothymol blue as an indicator.

For amide **31a** (N-methylacetanilide), under basic conditions $[OH^-]$ = 0.834M, the data were obtained at λ = 255 nm and five different temperatures (47.7, 56.8, 65.4, 74.0, 82.6 ^{0}C). The product solutions were titrated with 1 N HCl by using bromothymol blue as an indicator. In acid, the data were obtained at λ = 240 nm and four different temperatures (56.6, 65.5, 73.8, 82.6 ^{0}C) at pH = 0 (standard 1 N HCl).

The results are all listed in S1-S7 in supplementary material.

C. Crystal and Molecular Structures of Amides **III** and **IV**

A crystal of **III** suitable for X-ray diffraction studies was grown by dissolving the amide in a small amount of pentane, and placing the solution in a sealed disposable pipette in the freezer compartment of a refrigerator. Suitable crystals of **IV** were grown from a saturated 50:50 ethanol/H_2O solution that was allowed to stand overnight at room temperature. The structures were determined by Dr. B.D. Santarsiero of the X-ray Structure Determination Laboratory of the Department of Chemistry, University of Alberta.

Given in Table XXV are experimental details for the structure determinations of amides **III** and **IV** respectively.

Table XXVI. Experimental Details of Data Collection and Structure Refinement of Amides **III, IV**

	Crystal Data	
Formula	$C_{12}H_{13}NO$	$C_{13}H_{15}NO$
Formula Weight	187.24	210.27
Crystal Dimensions,mm	0.13,0.13,0.35	0.3,0.3,0.3
Space Group	$P2_1/c$	$P2_1/n$
a, Å	6.686(4)	9.020(3)
b, Å	10.508(4)	10.177(4)
c, Å	28.397(9)	22.663(10)
β, deg	102.80(5)	93.72(3)

V, Å^3	1945	2075
Z	8	8
D_c, g cm^{-3}	1.278	1.285
μ, cm^{-1}	0.50	0.76

Data collection

Radiation	MoK$_\alpha$	MoK$_\alpha$
Wavelength	0.7101	0.7107
Monochromator	graphite	graphite
Scan-type	θ-2θ	θ-2θ
Scan rate, deg min^{-1}	5.0	1.0-2.0
Scan width, deg	0.800+tanθ	0.40-0.60+tanθ
2θ(max), deg	50	40
Index range	*h, ±k, ±l*	*h, ±k, ±l*
Reflections, averaged	8277	3877

Refinement

Observations:Variables	1212:253	1434:271
Discrimination criteria	$I>3\sigma(I)$	$I>2\sigma(I)$
absorption	empirical	empirical
R_1	0.065	0.055
R_2	0.070	0.055
Goodness-of-fit	1.66	1.29

D. Methylation of 3,4-dihydro-2-oxo-1,4-propanoquinoline **III** and 2,3,4,5-tetrahydro-2-oxo-1,5-propano- benzazepine **IV**

1). Methylation of 2,3-dihydro-2-oxo-1,4-propano quinoline (**III**)

Amide **III** (15.16 mg, 0.081 mmol) was dissolved in 0.5 mL of CD_2Cl_2 in a NMR tube. In a dry box, methyl trifluoromethane sulfonate (9.17 μL, 0.081 mmol) was injected into the solution. After mixing, the reaction was monitored periodically by ^1H-NMR spectroscopy. ^1H-NMR (200 MHz, CD_2Cl_2) of amide **III** δ 7.12-7.45 (4 H, m), 3.75-3.91 (1 H, m), 3.04-3.22 (2 H, m), 2.62 (2 H, d, J = 2 Hz), 1.12-2.12 (4 H, m). The methyl protons of $CF_3SO_3CH_3$ appear as a singlet at δ 4.21 ppm.

During the reaction, a new peak at δ 3.65 ppm appeared. The relative intensities of the methyl groups for $CF_3SO_3CH_3$ at δ 4.21 ppm and that of the product at δ 3.65 ppm vs time are listed below:

time (h)	peak ratio(δ 4.21:3.65)
0.5	1:1
1	1:1.6
20	1:20
96	1:200

After the methyl trifluoromethane sulfonate was almost consumed, the reaction was terminated by the addition of 2 mL of water. The organic layer was extracted with 3×20 mL of dichloromethane, and the combined organic layers were dried with $MgSO_4$. The residue which was obtained after the volatiles were removed was dried *in vacuo* and analyzed without further purification. Exact mass calcd for $C_{13}H_{17}NO_2$: 219.1259; found: 219.1255; m/e (relative intensity) 219 ($M^{+\cdot}$ 69%), 174 ($M^{+\cdot}$-CO_2 38%), 160 ($M^{+\cdot}$-CH_2COOH 100%), 146 (16%), 132 (31%). ^{1}H-NMR (200 MHz, $CDCl_3$) δ 6.92-7.22 (4 H, m), 3.45-4.00 (2 H, m), 2.88 (3 H, m), 2.82 (3 H, s), 1.48-1.95 (4 H, m).

The preparation of an authentic compound of N-methyl-5-(2-hydroxycarbonylmethyl)-2,3,4,5-tetrahydrobenzazepine (**32**)

To a flask was added NaH (60% dispersion, 0.546 g, 13.6 mmol washed with hexane 3 times), 5-(hydroxycarbonylmethyl)-2,3,4,5-tetrahydrobenzazepine **26** (0.30 g, 1.46 mmol) and 20 mL of THF. To this was added MeI (0.23 mL, 3.7 mmol), after which the suspension was heated at reflux overnight. The reaction was worked up by the addition of 20 mL of water and extraction with 3×25 mL of diethyl ether. The aqueous layer was adjusted to pH 2 and extracted with 3×25 mL of $CHCl_3$. The combined $CHCl_3$ layers were dried over $MgSO_4$ and the volatiles were removed to yield the crude product. Purification was effected by column chromatography (SiO_2 column, ethyl acetate eluant). The final product was a light yellow oil. Exact mass calcd for $C_{13}H_{17}NO_2$: 219.1259; found: 219.1257; m/e (relative intensity) 219 ($M^{+\cdot}$ 66%), 174 ($M^{+\cdot}$-CO_2 32%), 160 ($M^{+\cdot}$-CH_2COOH 100%), 146 (20%), 132 (38%).

^{1}H-NMR (200 MHz, $CDCl_3$) δ 6.84-7.20 (4 H, m), 3.45-3.82 (2 H, m), 2.90 (3 H, m), 2.82 (3 H, s), 1.52-1.90 (4 H, m).

2) Methylation of 2,3,4,5-tetrahydro-2-oxo-1,5-propanobenzazepine (**IV**)

In a dry box, 5.89 µL of methyl trifluoromethane sulfonate (0.052 mmol) was injected into a solution of amide **IV** (10.46 mg, 0.052 mmol) in 0.5 mL of CD_2Cl_2. The reaction was monitored by NMR spectroscopy. ^{1}H-NMR (200 MHz, CD_2Cl_2) of amide **IV** δ 7.25-7.38 (2 H, m), 7.12-7.24 (2 H, m), 4.36-4.52 (1 H, m), 3.08-3.21 (1 H, m), 2.81-2.94 (1 H, m), 2.02-2.32 (5 H, m), 1.20-1.68 (3 H, m).

Over the course of the reaction, there appeared two singlets at δ 4.45 and 3.50 ppm respectively. The relative intensities of the methyl groups of $CF_3SO_3CH_3$ at δ 4.21 ppm and those for the new species at δ 4.45,3.50 vs time are listed below:

time	peak ratio δ 4.45:4.21:3.50
0.5 h.	7:1:0.5
21 h.	11:1:1
4 days	17:1:4
6 days	21:1:6
9 days	21:1:7

After 9 days, the reaction was worked up by addition of 2 mL of water and 2 mL of saturated Na_2CO_3. The product was extracted with 3×20 mL of CH_2Cl_2. The combined CH_2Cl_2 layers were dried over Na_2SO_4 and the volatiles removed to yield the crude product (51% yield). It was analyzed without further purification. Exact mass calcd for $C_{14}H_{19}NO_2$: 233.1416; found: 233.1414; m/e (relative intensity) 233 ($M^{+\cdot}$ 41%), 202 ($M^{+\cdot}$-OCH_3 12%), 174 ($M^{+\cdot}$-CO_2Me 5%) 160 ($M^{+\cdot}$-CH_2CO_2Me 76%), 146 ($M^{+\cdot}$-$CH_2CH_2CO_2Me$ 100%), 132 (11%). ^{1}H-NMR (200 MHz, $CDCl_3$) δ 6.68-7.09 (4 H, m), 3.65 (3 H, s), 3.18-3.32 (1 H, m), 2.72-2.88 (2 H, m), 1.58-2.38 (8 H, m).

Since the new peak at δ 3.50 might correspond to the N-methyl compound analogous to that of amide **III**, the remaining aqueous layer was neutralized with dilute HCl to pH 4.0. The solution was extracted with 3×20 mL of CH_2Cl_2. The combined CH_2Cl_2 layers were dried over Na_2SO_4 and the volatiles removed. However, no product was found in the residue.

The preparation of an authentic compound of 5-(2-methoxycarbonylethyl)-2,3,4,5-tetrahydrobenzazepine (**33**)

HCl gas was bubbled through a solution of amino acid **28** (0.0734 mg, 0.33 mmol) in 10 mL of methanol for 30 min. The solution was then heated at reflux overnight. The solvent was removed by rotary evaporation and then 5 mL of water was added to the residue. A few drops of NaOH solution was used to adjust the pH to 10. The product was extracted with 3×10 mL of CH_2Cl_2. The combined organic layers were washed with water and dried (Na_2SO_4). The crude product (~50 mg) was obtained after the volatiles were removed. Purification by column chromatography (SiO_2, eluant petroleum ether:EtOAc 75:15) gave an oil. Further purification was made by dissolving the product in diethyl ether and bubbling HCl through the solution. After refrigeration, The HCl salt of **33** formed as white crystals. The crystals were dissolved in 10 mL of saturated Na_2CO_3 and the free amine was extracted with 3×20 mL of CH_2Cl_2. The CH_2Cl_2 layers were combined and dried (Na_2SO_4) and the volatiles were evaporated to give a solid. Exact mass calcd for $C_{14}H_{19}NO_2$: 233.1416; found: 233.1410; m/e (relative intensity) 233 ($M^{+\cdot}$ 46%), 202 ($M^{+\cdot}$-OCH_3 12%), 174 ($M^{+\cdot}$-CO_2Me 2%), 160 ($M^{+\cdot}$-CH_2CO_2Me 71%), 146 ($M^{+\cdot}$-$CH_2CH_2CO_2Me$ 100%), 132 (9%). ^1H-NMR (200 MHz, $CDCl_3$) δ 6.62-7.08 (4 H,m), 3.65 (3 H, s), 3.18 (1 H, m), 2.72-2.90 (2 H, m), 1.58-2.38 (8 H, m).

E. Resolution of Chiral Amide 3,4-dihydro-2-oxo-1,4-propanoquinoline **III**

1) Attempted separation of diastereoisomers by MPLC

The diastereoisomers **36** (14 mg in 1.0 mL of CH_2Cl_2) were injected into a 24×10 cm Lichroprep RP-8 column (40-63 µm). Elution with methanol/water in ratios between 100:0, 90:10 was attempted, but no apparent separation was found. The eluant, EtOH/water, in a ratio of 40:60 was also used, but still no separation was found.

2).Attempted separations of racemic compounds on HPLC with a column containing chiral packing material

The separation of different compounds was attempted with a 10m 25cm ×21.1 mm i.d. chiral dinitrophenylglycine HPLC column. The results are shown in Table XXVI.

3). The quinine ester of 2-(N-tosyl-2,3,4,5-tetrahydrobenzazepinyl)acetic acid (**36**)

Acid **25** (0.36 g, 1mmol) and 6.0 mL of thionyl chloride in 5.0 mL of benzene were heated at reflux overnight. The next morning the volatiles were removed by rotary evaporation. Dry benzene (10 mL) was added to the residue and evaporated. The process was repeated three times to remove traces of $SOCl_2$.

The so-formed acyl chloride was immediately dissolved in 20 mL of dry benzene. To this solution was added 1.0 mL of dry Et_3N and 0.324 g of anhydrous quinine (1 mmol). This mixture was heated at reflux overnight. The reaction was worked up by washing with 3×50 mL of water. The organic layer was dried ($MgSO_4$) and the solvent was removed to yield 0.76 g of the crude product **36**. Further purification was accomplished by column chromatography (silica gel, eluant 5% MeOH in EtOAc). The product was obtained as a light yellow solid (0.27 g, 41%); mp 90-94 ^{0}C. MS (FAB) m/e = 666 ($M^{+\cdot}+1$ calcd. for $C_{39}H_{43}N_3O_5S$).

Table XXVII. Conditions for the attempted separation of various compounds using a chiral HPLC column

compounds	solvent system	separation
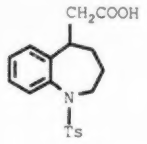	20% isopropanol in hexane	no
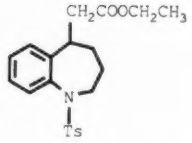	20% isopropanol in hexane	no
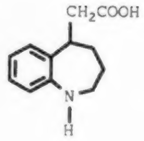	30% isopropanol in hexane	no
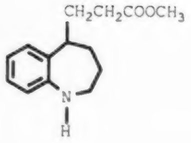	20% isopropanol in hexane	no
	30% isopropanol in hexane	no
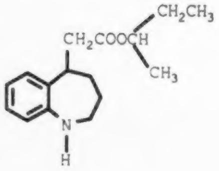	30% isopropanol in hexane	no
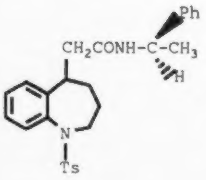	30% isopropanol in hexane	no

4). Separation of the diastereoisomers **36** by reverse phase preparative thin layer chromatography (TLC)

A reverse phase preparative TLC plate (20×20 cm) was prepared with 0.152 g of diastereoisomers **36**. After being developed 6 times with water/98%EtOH eluant (ratio 2:3), two isomers were separated. The high R_f and low R_f isomers were individually extracted using a soxlet extractor with ethyl acetate as a solvent. The extraction was continued for two days. After the solvent was removed, the residue was checked again by reverse phase TLC. Only one spot was found for the high R_f isomer. A smaller amount of the low R_f material was obtained. Thus the high R_f portion was used for the next reaction. No attempt was made to calculate the yield. The ester (high R_f portion) is a white solid: m.p. 93-94 ^{0}C; ^{1}H-NMR (200 MHz, $CDCl_3$) δ 8.50-7.56 (4 H, m), 7.56-6.85 (8 H, m), 6.62 (1 H, br), 5.70 (1 H, m), 4.95 (2 H, m), 3.95 (3 H, s), 3.78-2.55 (9 H, br), 2.46 (3 H, s), 2.20-1.18 (12 H, br). MS (FAB) m/e =666 ($M^{+\cdot}$+1 calcd for $C_{39}H_{43}N_3O_5S$).

5) Preparation of chiral 2-(N-tosyl-2,3,4,5-tetrahydro benzazepinyl)acetic acid **37**

The mixture of 0.8 g (obtained after repeating the steps above) of the high R_f ester **36b**, 50 mL of 95% EtOH and 1.8 g of NaOH in 50 mL of water was heated at reflux overnight. In the morning, EtOH was removed by rotary evaporation. The aqueous solution was extracted with Et_2O to remove quinine and then was acidified with HCl. The product was extracted with 3×30 mL of CH_2Cl_2. The combined CH_2Cl_2 layers were washed with water and saturated NaCl and then dried ($MgSO_4$). The crude product (0.40 g) was obtained after the solvent was removed. Recrystallization from 50% EtOH gave 0.263 g of white needles (yield 61%), mp 158-159 ^{0}C; $[\alpha]_{Hg}^{25} = -0.30^0$ (365nm, c = 0.069 g/mL). ^{1}H-NMR (200 MHz, $CDCl_3$) δ 7.52-8.00 (2 H, br), 7.00-7.45 (6 H, br), 3.90-4.30 (1 H, br), 2.55-3.60 (3 H, br), 2.42 (3 H, s), 1.10-2.08 (4 H, br).

6).Preparation of chiral 3,4-dihydro-1,4-propano-2-oxo quinoline **III**

Pure chiral amide **III** was obtained according to the identical procedure for the racemic amide by the reaction of chiral amino acid **37** with DCC in CH_3CN. The product identity was confirmed by ^{1}H-NMR and MS spectra, which were identical to those of the racemic isomer.

5. REFERENCES

1. Florkin, M.; Stotz, E.H. "Comprehensive Biochemistry", Elsevier: New York, 1972; vol.30, p267.

2. Liener, I.E. "Organic and Biological Chemistry", The Ronald Press: New York, 1966; p179.

3. Fersht, A. "Enzyme Structure and Mechanism" Freeman, W.H. Company: New York, 2nd Ed.; 1985; p335.

4. Walsh, C. "Enzymatic Reaction Mechanisms" Freeman, W.H.: San Francisco, 1979; p24-207.

5. Jencks, W.P. "Catalysis in Chemistry and Enzymology" Dover publications, Inc.: New York, 2nd Ed.; 1987; p1-322.

6.(a) Koshland, D.E.Jr. *Advan. Enzymol.* **1960**, *22*, 45.

(b) Koshland, D.E.Jr.; Neet, K.E. *Ann. Rev. Biochem.* **1968**, *37*, 359.

(c) Koshland, D.E.Jr. *Proc. Natl. Acad. Sci. U.S.* **1958**, *44*, 98.

7.(a) Bernhard, S.A. and Gutfreund, H. *Proc. Intern. Symp. Enzyme. Chem. Tokyo. Kyoto.* **1958**, 124.

(b) Bernhard, S.A. *J. Cellular Comp. Physiol.* (suppl. 1) **1959**, *54*, 256.

(c) Huang, H.T.; Niemann, C. *J. Am. Chem. Soc.* **1952**, *74*, 4634.

(d) Niemann, C. *Science*, **1964**, *143*, 1287.

(e) Hamilton, C.L.; Niemann, C.; Hammond, G.S. *Proc. Natl. Acad. Sci. U.S.* **1966**, *55*, 664.

8. (a) The "Circe effect" refers to the utilization of strong attractive forces to lure a substrate into a site which it undergoes an extraordinary transformation of form and structure.[8b]

(b) Jencks, W.P. *Advan. Enzymol.* **1975**, *43*, 219.

9. Van Eikeren, P.; Chipman, D.M. *J. Am. Chem. Soc.* **1972**, *94*, 4788.

10. Philips, D.C. *Proc. Natl. Acad. Sci. U.S.* **1967**, *57*, 484.

11. Ford, L.O.; Johnson, L.N.; Machin, P.A.; Philips, D.C.; Tjian, R. *J. Mol. Biol.* **1974**, *88*, 349.

12. Wolfenden, R. *Acc. Chem. Res.* **1972**, *5*, 10.

13. Lienhard. G.E. *Science* **1973**, *180*, 149.

14. Secemski, I.I.; Lehrer, S.S.; Lienhard, G.E. *J. Biol. Chem.* **1972**, *247*, 4740.

15.(a) Hofstee, H. *J. Biochim. Biophys. Acta* **1957**, *24*, 211.

(b) Hofstee, H. *J. Biochim. Biophys. Acta* **1959**, *32*, 182.

(c) Hofstee, H. *J. Biol. chem.* **1954**, *207*, 219.

16. Pearl, L. "Aspartic Proteinases and Their Inhibitors" Kostka, V. Ed.; Walter de Gruyer: Berlin, 1985; p189.

17.(a) Young, J.K.; Pazhanisamy, S.; Schowen, R.L. *J. Org. Chem.* **1984**, *49*, 4148.

(b) Pollack, R.M.; Bender, M.L. *J. Am. Chem. Soc.* **1970**, *92*, 7190.

(c) Bender, M.L.; Thomas, R.J. *J. Am. Chem. Soc.* **1961**, *83*, 4183.

(d) Bender, M.L. *Chem. Rev.* **1960**, *60*, 53 and references therein.

(e) O'Connor, C.O. *Q. Rev. Chem. Soc.* **1970**, *24*, 553-564 and references therein.

(f) Menger, F.M.; Donohue, J.A. *J. Am. Chem. Soc.* **1973**, *95*, 432.

(g) Kershner, L.D.; Schowen, R.L. *J. Am. Chem. Soc.* **1971**, *93*, 2014.

(h) Schowen, R.L.; Jayaraman, H; Kershner, L.; Zuorick, G.W. *J. Am. Chem. Soc.* **1966**, *88*, 4008.

(i) Schowen, R.L.; Jayaraman, H; Kershner, L. *J. Am. Chem. Soc.* **1966**, *88*, 3373.

(j) Drake, D.; Schowen, R.L.; Jayaraman, H. *J. Am. Chem. Soc.* **1973**, *95*, 454.

(k) Deslongchamps, P.; Barlet, R.; Taillefer, R.J. *Can J. Chem.* **1980**, *58*, 2167.

(l) Eriksson, S.O.; Bratt, L. *Acta. Chem. Scand.* **1967**, *21*, 1812.

(m) Bunton, C.A.; Nayak, B.; O'Connor, C.J. *J. Org. Chem.* **1968**, *33*, 572.

(n) Bender, M.L.; Ginger, R.D.; Kemp, K.C. *J. Am. Chem. Soc.* **1954**, *76*, 3350.

(o) Bender, M.L.; Ginger, R.D. *J. Am. Chem. Soc.* **1955**, *77*, 348.

(p) Beichler, S.S.; Taft, R.W. *J. Am. Chem. Soc.* **1957**, *79*, 4927.

18.(a) Komiyama, M.; Bender, M.L. *J. Am. Chem. Soc.* **1978**, *100*, 5977.

(b) Komiyama, M.; Bender, M.L. *Bioorg. Chem.* **1978**, *7*, 133.

(c) Shaskus, J.; Haake, P. *J. Org. Chem.* **1983**, *48*, 2036 and references therein.

(d) Pollack, R.M.; Dumsha, T.C. *J. Am. Chem. Soc.* **1975**, *97*, 377.

19.(a) Oakenfull, D.G.; Jencks, W.P. *J. Am. Chem. Soc.* **1971**, *93*, 178.

(b) Oakenfull, D.G.; Salvesen, K.; Jencks, W.P. *J. Am. Chem. Soc.* **1971**, *93*, 188.

(c) Jencks, W.P.; Carriuolo, J. *J. Biol. Chem.* **1959**, *239*, 1272-1279, 1280-1285.

(d) Gopalakrishnan, G.; Hogg, J.L. *J. Org. Chem.* **1983**, *48*, 2038 and references therein.

(e) Gour-Salin, B.J. *Can. J. Chem.* **1983**, *61*. 2059.

(f) Wolfenden, R.; Jencks, W.P. *J. Am. Chem. Soc.* **1961**, *83*, 4390.

20. Holley, R.W. *Science* **1957**, *117*, 23.

21. Sweet, R.M.; Dahl, L.F. *J. Am. Chem. Soc.* **1970**, *92*, 5489.

22. Earle, R.H. Jr.; Hurst, D.T.; Viney, M. *J. Chem. Soc.(C)* **1969**, 2093.

23.(a) Pracejus, H. *Chem. Ber.* **1959**, *92*, 988.

(b) Pracejus, H.; Kehlen, M.; Kehlen, H.; Matschiner, H. *Tetrahedron* **1965**, *21*, 2257.

24. Albertson, N.F. *J. Am. Chem. Soc.* **1950**, *72*, 2594.

25.(a) Blackburn, G.M.; Plackett, J.D. *J. Chem. Soc. Perkin Trans. II* **1972**, 1366.

(b) Blackburn, G.M.; Plackett, J.D. *J. Chem. Soc. Perkin Trans. II* **1973**, 981.

26.(a) Luche, J.L.; Kagan, H.B.; Parthasarathy, R.; Tsoucaris, G.; DeRango, C.; Zeliver, C. *Tetrahedron* **1968**, *24*, 1275.

(b) Manhas, M.S.; Jeng, S.; Bose, A.K. *Tetrahedron* **1968**, *24*, 1237.

27. Blackburn, G.M.; Skaife, C.J.; Kay, I.T. *J. Chem. Res. (Miniprint)* **1980**, No 9, 3650.

28. Somayaji, V. and Brown, R.S. *J. Org. Chem.* **1986**, *51*, 2676.

29. Dr. Bennet, A.J.(Dept. of Chem., U of Alberta) performed the hydrolysis of amide **II** at high $[H_3O^+]$ (from $[H_3O^+]$ 1.0 M to 5.0 M). The hydrolysis profile plateaus at low pH.

30. Somayaji, V.; Skorey, K.I.; Brown, R.S.; Ball, R.G. *J. Org. Chem.* **1986**, *51*, 4866.

31. For a planar amidic unit lying in the X-Z plane with N-C along the X-axis, the twist and tilt angles are respectively defined as the rotaion angle of the N-lone pair out of optimum conjugation with the C=O π system (e.g. rotation about the X-axis), and the tilt of the lone pair away from

the Y-axis. Lone pair position is defined by a perpendicular drawn through N, normal to the plane defined by the three attached C's.

32. Wang, Q; Bennet, A.J.; Brown, R.S.; Santarsiero, B.D. *J. Am. Chem. Soc.* **1991**, *113*, 5757.

33.(a) Somayaji, V.; Brown, R.S. *J. Am. Chem. Soc.* **1987**, *109*, 4738.

(b) Somayaji, V.; Keillor, J.; Brown, R.S. *J. Am. Chem. Soc.* **1988**, *110*, 2625.

34.(a) Slebocka-Tilk, H. Brown, R.S. *J. Org. Chem.* **1987**, *52*, 805.

(b) Slebocka-Tilk, H.; Brown, R.S. *J. Org. Chem.* **1988**, *53*, 1153.

(c) Slebocka-Tilk, H.; Bennet, A.J.; Keillor, J.W.; Brown, R.S.; Guthrie, J.P.; Jodhan, A. *J. Am. Chem. Soc.* **1990**, *112*, 8507.

35. Shibaeva, R.P.; Atovmyan, L.O.; Kostyanovskii, R.G. *Dokl. Akad. Nauk. USSR* **1968**, *12*, 669.

36. Zacharis, H.M.; Trefonas, L.M. *J. Heterocycl. Chem.* **1968**,*5*, 343.

37. Bennet, A.J.; Wang, Q.-P.; Slebocka-Tilk, H; Somayaji, V.; Brown, R.S.; Santarsiero, B.D. *J. Am. Chem. Soc.* **1990**, *112*, 6383 and references therein.

38. Bennet, A.J.; Somayaji, V.; Brown, R.S.; Santarsiero, B.D. *J. Am. Chem. Soc.* **1991** (in press).

39.(a) Proctor, G.P. *J. Chem. Soc.* **1961**, 3989.

(b) McCall, I.; Proctor, G.P.; Purdie, L. *J. Chem. Soc. (C)*. **1970**, 1126.

40. Ji, S.; Gortler, L.B.; Waring, A.; Battisti, A.; Bank, S. Closson, W.D.; Wriede, P. *J. Am. Chem. Soc.* **1967**, *89*, 5311.

41. Lennon, M.; McLean, A.; McWatt, I.; Proctor, G.R. *J. Chem. Soc. Perkin Trans. I* **1974**, 1828.

42. Hudlicky, T.; Sheth, J.P. *Tetra. Lett.* **1979**, No 29, 2667.

43. Fieser, L.F.; Fieser, M. "Reagents for Organic Synthesis" J. Wiley and Sons: New York, 1967; vol.1 p191-192.

44. Schneider, F. *Physiol. Chem.* **1967**, *348*, 1034.

45. (a) The crystal was grown from a 95% ethanol/water solution by Dr X. Huang (Dept. of Chem., Univ. of Alberta).

(b) This crystal was made by Dr. A.J. Bennet (Dept. of Chem., Univ. of Alberta).

46. Santarsiero, B.D.; Huang, X.; Brown, R.S. unpublished results.

47. Dunitz, J.D.; Winkler, F.K. *Acta. Crystallogr.* **1975**, *B31*, 251.

48. Wiberg, K.B.; Laidig, K.E. *J. Am. Chem. Soc.* **1987**, *109*, 5935.

49. Bader, R.F.W.; Nguyen-Dang, T.T. *Adv. Quantum Chem.* **1981**, *14*, 63.

50. The deemed rate acceleration depends upon the comparison material. Probably 2,N-dimethylacetanilide **31b** is a more appropriate reference, but no detectable hydrolysis of this was observed after 50 h. T = 100 ^{0}C, 0.2 M OD^{-}/D_2O.

51. Glasstone, S.; Laidler, K.J.; Eyring, H. "The Theory of Rate Processes" McGraw-Hill: New York, 1941.

52. Wiberg, K.B. "Physical Organic Chemistry" Wiley and Sons: New York, 2nd Ed.; 1966; p379.

53.(a) This experiment was done by Dr. A.J. Bennet (Dept. of Chem., Univ. of Alberta)

(b) This experiment was done by Mr. J. Keillor (Dept. of Chem., Univ. of Alberta)

54. Fife, T.H.; Bruice, T.C. *J. Phys. Chem.* **1961**, *65*, 1079.

55. Alberts, A.; Seargent, E.P. "The Determination of Ionization Constants" 3rd Ed.; 1984; p50.

56.(a) Brown, H.C.; Schwier, J.R.; Singaram, B. *J. Org. Chem.* **1978**, *43*, 4395.

(b) Brown. H.C.; Singaram, B. *J. Org. Chem.* **1984**, *49*, 945.

57. Dr. R.J.Crawford (Dept. of Chem., Univ. of Alberta) generously provided the use of this chiral column.

58. CRC press "Handbook of Chemistry and Physics" 54th edition, Weast, R.C. Ed; 1973-1974, D126.

59. Alvarez, F.J.; Schowen, R.L. "Isotopes in Organic Chemistry" 7 Buncel, E.; Lee, C.C. Eds.; Elsevier: Amsterdam 1987; p1-60.

60. Slebocka-Tilk, H.; Bennet, A.J.; Hogg, H.J.; Brown, R.S. *J. Am. Chem. Soc.* **1991**, *113*, 1288.

61. Gani, V.; Viout, P. *Tetrahedron* **1976**, *32*, 1669.

62. Deslongchamps, P.; Gerval, P.; Cheriyan, U.O.; Guida, A.; Taillefer, R.J. *Nouv. J. Chimie* **1978**, *2*, 631.

63. It is possible that SKIE data reported for **31a**[60] refer to a more complicated situation than a reversible addition to produce T_o- where k_{-3} and k_4 steps are nearly isoenergetic. Under comparable conditions (0.2 M OD^-/D_2O, 100 ^0C) we have observed that N,2-dimethylacetanilide undergoes complete exchange of the $C(O)CH_3$ group within 30 min. (Bennet, A.J.; Brown, R.S. unpublished result). A similar exchange should obtain with **31a** in OD^-/D_2O so that the actual SKIE refers to the reversible attack of OD^- on $C(O)CH_xD_{3-x}$ (x = 1,2,3).

64. Hammond, G.S. *J. Am. Chem. Soc.* **1955**, *77*, 334.

65. Farcasiu, D. *J. Chem. Educ.* **1975**, *52*, 76.

66. Glasoe, P.K.; Long, F.A. *J. Phys. Chem.* **1960**, *64*, 188.

67. Gold, V. *Adv. Phys. Org. Chem.* **1969**, *7*, 259.

68. Schowen, R.L. in "Isotope Effects on Enzyme Catalyzed Reactions", Cleland, W.W.; O'Leary, M.H.; Northrup, D.B.; Eds: University Park press: Baltimore, 1977.

69. Schowen, R.L. *Prog. Phys. Org. Chem.* **1972**, *9*, 275.

70.(a) Arnett, E.M. *Prog. Phys. Org. Chem.* **1963**, *1*, 223.
 (b) Guthrie, J.P. *J. Am. Chem. Soc.* **1974**, *96*, 3608.
 (c) Arnett, E.M.; Quirk, R.P. and Larsen, J.W. *J. Am. Chem. soc.* **1970**, *92*, 3977.

(d) Williams, A. *J. Am. Chem. Soc.* **1976**, *98*, 5645.

71. Wepster, B.M. *Recl. Trav. Chim. Pays-Bas* **1952**, *71*, 1171.

72.(a) Bergmann, M.; Fruton, J.S. *J. Biol. Chem.* **1937**, *117*, 189.

(b) Bergmann, M.; Zervas, L.; Fruton, J.S. *J. Biol. Chem.* **1936**, *115*, 593.

(c) Bergmann, M.; Zervas, L.; Fruton, J.S.; Schneider, F.; Schleich, H. *J. Biol. Chem.* **1935**, *109*, 325.

73. Ch. Tamm " New Comprehensive Biochemistry" (stereochemistry) Elsevier; Biomedical Press: New York, 1982; vol.3 p56.

74. Arnett, E.M.; Zingg, S.P. *J. Am. Chem. Soc.* **1981**, *103*, 1221.

75. Brown, R.S.; Ulan, J.G. *J. Am. Chem. Soc.* **1983**, 105, 2382.

76. Preparation of ^{18}O-N-methylacetanilde was done by Dr. H. Slebocka-Tilk (Dept. of Chem., Univ. of Alberta).

SUPPLEMENTARY MATERIAL

S1. The rate constants for the hydrolysis of amide **III** in $[OH^-] = 0.087$ M, $\mu = 1.0$ (KCl) at different temperatures.

T (°C)	k_{obs} (s^{-1})	k_2 ($M^{-1}s^{-1}$)
5.0	0.33±0.02	3.8±0.2
10.3	0.48±0.01	5.6±0.1
17.8	0.70±0.01	8.0±0.1
25.7	1.06±0.01	12.2±0.1
33.4	1.61±0.02	18.5±0.2
40.2	2.42±0.04	27.8±0.5
48.9	3.7±0.2	43±2

S2. The rate constants for the hydrolysis of amide **III** in $[H^+] = 0.0113$ M, $\mu = 1.0$ (KCl) at different temperatures.

T (°C)	k_{obs} (s^{-1})	k_2 ($M^{-1}s^{-1}$)
7.2	0.11±0.01	9.7±0.4
13.6	0.14±0.01	12.12±0.09
18.8	0.18±0.01	15.6±0.3
25.8	0.25±0.01	21.7±0.6
32.1	0.30±0.01	26.1±0.3
39.5	0.40±0.01	35.8±0.3
47.3	0.48±0.02	42±2

S3. The rate constants for the hydrolysis of amide **III** in $[H^+] = 1.0$ M, $\mu = 1.0$ (KCl) at different temperatures.

T (°C)	k_{obs} (s^{-1})	k_2 ($M^{-1}s^{-1}$)
6.7	2.65±0.04	2.65±0.04
12.4	3.40±0.02	3.40±0.02
18.5	4.5±0.1	4.5±0.1
25.4	6.6±0.1	6.6±0.1
32.4	9.2±0.2	9.2±0.2
40.0	13.2±0.1	13.2±0.1
48.4	19±1	19±1

S4. The rate constants for the hydrolysis of amide **IV** in $[OH^-] = 0.01$ M, $\mu = 1.0$ (KCl) at different temperatures.

T (°C)	k_{obs} (s^{-1})	k_2 ($M^{-1}s^{-1}$)
25.0	$(5.3\pm0.1)\times10^{-6}$	$(5.3\pm0.1)\times10^{-4}$
39.0	$(1.64\pm0.02)\times10^{-5}$	$(1.64\pm0.02)\times10^{-3}$
54.3	$(4.45\pm0.07)\times10^{-5}$	$(4.45\pm0.07)\times10^{-3}$
75.3	$(1.57\pm0.01)\times10^{-4}$	$(1.57\pm0.01)\times10^{-2}$

S5. The rate constants for the hydrolysis of amide **IV** in $[H^+] = 0.0314$ M, $\mu = 1.0$ (KCl) at different temperatures.

T (°C)	k_{obs} (s^{-1})	k_2 ($M^{-1}s^{-1}$)
16.1	$(2.06\pm0.02)\times10^{-6}$	$(6.57\pm0.06)\times10^{-5}$
30.6	$(8.16\pm0.04)\times10^{-6}$	$(2.60\pm0.01)\times10^{-4}$
37.6	$(1.46\pm0.02)\times10^{-5}$	$(4.64\pm0.05)\times10^{-4}$
53.2	$(5.45\pm0.03)\times10^{-5}$	$(1.74\pm0.09)\times10^{-3}$
63.0	$(1.16\pm0.01)\times10^{-4}$	$(3.68\pm0.03)\times10^{-3}$
76.2	$(2.92\pm0.02)\times10^{-4}$	$(9.30\pm0.06)\times10^{-3}$

S6. The rate constants for the hydrolysis of amide **31a** in $[OH^-] = 0.834$ M at different temperatures.

T (°C)	k_{obs} (s^{-1})	k_2 ($M^{-1}s^{-1}$)
47.7	$(8.1\pm0.1)\times10^{-5}$	$(9.8\pm0.1)\times10^{-5}$
56.8	$(1.44\pm0.02)\times10^{-4}$	$(1.73\pm0.02)\times10^{-4}$
65.4	$(2.24\pm0.02)\times10^{-4}$	$(2.69\pm0.02)\times10^{-4}$
74.0	$(3.70\pm0.01)\times10^{-4}$	$(4.43\pm0.01)\times10^{-4}$
82.6	$(5.70\pm0.04)\times10^{-4}$	$(6.84\pm0.05)\times10^{-4}$

S7. The rate constants for the hydrolysis of amide **31a** in $[H^+] = 1.0$ M at different temperatures.

T (°C)	k_{obs} (s^{-1})	k_2 ($M^{-1}s^{-1}$)
56.6	$(5.91\pm0.03)\times10^{-6}$	$(5.91\pm0.03)\times10^{-6}$
65.5	$(1.36\pm0.02)\times10^{-5}$	$(1.36\pm0.02)\times10^{-5}$
73.8	$(2.92\pm0.03)\times10^{-5}$	$(2.92\pm0.03)\times10^{-5}$
82.6	$(5.70\pm0.04)\times10^{-5}$	$(5.70\pm0.04)\times10^{-5}$

S8. ^{18}O-exchange data for amide **31a** at 74.0 °C and $[OH^-] = 1.077$ M.

t (min)	$\%^{18}O$	$\%^{18}O_{ex}$[a]
0	47.7±0.8	0
12	43.8±0.6	8±1
24	38.1±0.6	20.26±0.02
48	29.2±0.6	39±2

a. $$\%^{18}O_{ex} = \frac{(\%^{18}O\text{ before hydrolysis} - \%^{18}O\text{ after hydrolysis})}{\%^{18}O\text{ before hydrolysis}}$$